THEORETICAL PERFORMANCE OPTIMIZATION OF SOLAR ABSORPTION CHILLER COUPLED TO UNDERGROUND COOLING TOWER

A Thesis Submitted to
the Graduate School of Engineering and Sciences of
İzmir Institute of Technology
in Partial Fulfillment of the Requirements for the Degree of

MASTER OF SCIENCE

in Energy Engineering

by

Kiswendsida Elias OUEDRAOGO

December 2018
İZMİR

We approve the thesis of **Kiswendsida Elias OUEDRAOGO**

Examining Committee Members:

Dr. Kasım TOPRAK
Department of Mechanical Engineering, İzmir Institute of Technology

Prof. Dr. Gülden GÖKÇEN AKKURT
Department of Energy Engineering, İzmir Institute of Technology

Prof. Dr. Mustafa Serhan KÜÇÜKA
Department of Mechanical Engineering, Dokuz Eylül University

26 December 2018

Dr. Kasım TOPRAK
Supervisor, Department of Mechanical Engineering, İzmir Institute of Technology

Assoc. Dr. Unver ÖZKOL
Co-Supervisor, Department of Mechanical Engineering, İzmir Institute of Technology

Prof. Dr. Gülden GÖKÇEN
Head of the Department of Energy System Engineering, İzmir Institute of Technology

Prof. Dr. Aysun SOFUOĞLU
Dean of the Graduate School of Engineering and Science

ABSTRACT

THEORETICAL PERFORMANCE OPTIMIZATION OF SOLAR ABSORPTION CHILLER COUPLED TO UNDERGROUND COOLING TOWER

The study aims to enhance the thermal/economic performance of a solar powered absorption heat pump used for the cooling/heating of a shopping center in Izmir. MATLAB and TRNSYS are used to simulate the system. First, borehole thermal energy storage is added to the system to store the heat rejected by the chiller condenser in summer for later use in winter. Secondly, cooling water out of a condenser is partially stored during an 8:00-16:00 working time, and cooled from 16:00 to 8:00 to take advantage of the lower ambient temperature at night. Lastly, chilled water storage is added to the system to level the cooling load. The study revealed that the borehole efficiency is 37%. Also, it enhanced the solar fraction in winter by 40% and increased the system cooling load to heat input ratio by 110%. The second study showed that operating a cooling tower at night can reduce cooling water temperature by 5°C. In the last study, producing chilled water 24h/day reduced the required cooling capacity of the chiller to 34% of its current capacity of 1020kW, thus increasing the capacity factor from 41% to 96%. A brief economic analysis showed that the levelized cost of cooling/heating is 0.034$/kWh and 0.049$/kWh for the system with chilled water storage and the system without chilled water storage respectively. This represented a cost reduction of 29%.

Keywords: Solar Collector, Absorption Chiller, Thermal Storage, Capacity Factor, BTES.

ÖZET

YERALTI SOĞUTMA KULESİ İLE BİRLEŞTİRİLMİŞ GÜNEŞ ENERJİLİ SOĞURMALİ SOĞUTMA SİSTEMİNİN PERFORMANSININ TEORİK OLARAK OPTİMİZASYONU

Bu çalışma, İzmir'deki bir alışveriş merkezinin soğutulması/ısıtılması için kullanılan güneş enerjisi ile çalışan absorbsiyonlu ısı pompası sisteminin termal/ekonomik performansını iyileştirmeyi amaçlamaktadır. İlk olarak, sonradan kışın kullanmak için, soğutma sistemi kondensatörü tarafından yaz aylarında geri çevrilen sıcaklığı korumak amacıyla sisteme sondaj deliği termal enerji deposu eklenmiştir. İkinci olarak ise, bir kondensatörden çıkan soğutma suyu, 8:00-16:00 çalışma saatlerinde kısmen depolanmış ve gece daha düşük seviyedeki ortam sıcaklığından faydalanmak amacıyla, 16:00'dan 8:00'a kadar soğutulmuştur. Son olarak da, sisteme soğutma yükünü seviyelemek amacıyla soğutulmuş su deposu eklenmiştir. Çalışma, sondaj deliği verimliliğinin %37 olduğunu açığa çıkarmıştır. Ayrıca kış aylarında güneş enerjisinden yararlanma oranını %40 oranında genişletmiş ve sistemin soğutma yükünü %110 oranındaki bir ısı girdisi oranına yükseltmiştir. İkinci çalışma, gece bir soğutma kulesi kullanmanın, soğutma suyu sıcaklığını 5°C kadar azaltabileceğini göstermiştir. Son çalışmada ise, günde 24 saat boyunca soğutulmuş su üretimi, soğutma sisteminin istenen soğutma kapasitesini 1020kW olan mevcut kapasitesinden %34 oranında azaltılmış ve böylece, kapasite faktörünü %41'den %96'ya artırmıştır. Küçük bir ekonomik analiz de, soğutmanın/ısıtmanın seviyelendirilmiş maliyetinin, sırasıyla soğutulmuş su deposu olan sistem ve soğutulmuş su deposu olmayan sistem için, 0.034$/kWh ve 0.049$/kWh olduğunu göstermiştir. Bu da maliyette %29 oranında bir düşüşü tasvir etmektedir.

Anahtar Sözcükler: Güneş Enerjisi Kolektörü, Absorbsiyonlu Soğutma Sistemi, Termal Depo, Kapasite faktörü, BTES (Sondaj Deliği Termal Enerji Deposu).

ACKNOWLEDGMENTS

I would like to express my gratitude to Dr. TOPRAK and Dr. OZKOL, my supervisors, for their guidance throughout my study. Thanks to their laboratories, I was able to spot quickly where I should focus my study to make it practically useful for my future career.

I would thank Prof. GULDEN for her constant help to fix my administrative problems and for her advices during the thesis review sessions. Thanks to the academic staff who helped me switch smoothly from electrical engineering to mechanical engineering. The new set of multi discipinary knowledge I acquiered will be useful in conducting commercial projects.

My gratitude also goes to LUCIDASOLAR, a company in Izmir Technopark, for the professional training I benefited from its team. Their assistance has been very useful in helping me understand the real technical problems, economic and social problems faced by sustainable energy businesses. I wish more companies will join the park to work in synergy with academicians in order to better train future generations.

Thanks to Turkish Government for their scholarship initiative which beyond the financial aid helps young people around the world to broaden their horizon, to build that connection essential for the creation of a peaceful world where knowledge is shared for the well-being of all. I wish one day my Country will be a technologically advanced country so young Turkish could learn back something from us.

Finally, I would thank my mum for her financial support, her encouragement, and her understanding of placing our education on her top priority. Being a single mum for almost two decades and still carry six children all to university is a remarkable achievement I can’t omit to appreciate. Mum my late dad and we are proud of your ACHIEVEMENT. THANK YOU! The Best Heritage is: Education

TABLE OF CONTENTS

LIST OF FIGURES

LIST OF TABLES

CHAPTER 1

INTRODUCTION

In this thesis, a building cooling system powered by the sun is being investigated. Rather than focusing on a specific component performance improvement, the overall system performance that is the deciding factor for market acceptance of the system is analyzed.

1.1. Background

Increasing Cooling/Heating Demand: The need for air conditioning (AC) has increased sharply in the last three decades. The industrialization of developing countries combined with the emergence of the middle classes worldwide is the main driver of air conditioning demand. For the period 2000-2100, the global residential air conditioning energy demand is forecasted to increase by 30% for heating and 70% for cooling [1]. Global warming contributes to the increase in cooling demand but only slightly reduces the heating demand. AC is an energy-intensive process which accounts for 40% to 50% of building energy consumption [2–4]. In hot region countries such as Saudi Arabia, AC consumes up to 70% of the electricity in summer [5].

High AC Cost: The satisfaction of the cooling demand has major economic implications. In fact, summer peak demand has often been addressed by running less efficient power generators or by constructing low load factors power plants. In either case, the cost of the produced electricity is much higher than the baseload electricity cost. In the worst case that the utility fails to meet peak demand, load shedding is implemented to maintain the grid stability. Load sheeding impacts negatively all economic activities in the concerned zones. In 2005 the World Bank data showed that power shortage cost up to 10% of the GDP of East Asian countries, 7% of GDP in Africa and 2% of GDP in Europe.

Renewable Energy Opportunities & Challenges: In recent years, many countries have seen some opportunities in renewable energies systems (RES) to reach their

sustainable development goals as well as to gain energy independence. However, RES including energy harvesting equipment, storage, and others special application components are known for having a high initial cost, which constitute a market barrier for poor regions. Operating cost, on the other hand, is insignificant compared to fossil fuel energy system. Technically, the efficiencies of RES (solar, wind, geothermal) are still relatively low compared to that of fossil fuel powered energy systems (Thermal power plant, boiler, heat engine). Furthermore, RES suffer from a low capacity factor that is typically less than 30% for solar and less than 40% for wind [6,7]. Despite their cost decline, RES initial investment is still high because of the low efficiency and low capacity factors mentioned above. According to the International Renewable Energy Agency (IRENA), the cost of solar PV has fallen by 69% while that of wind has fallen by 18% from 2010 to 2016 [8]. However, for solar thermal system, the cost has almost stagnated in recent years and only 49% drop is expected by 2050 [9]. One way of improving the economic performance of RES is to study the overall system and its function rather than focusing on a single component performance. The low operating costs of RES combined with a better system technical/economic performance are the keys to make the technologies viable in a free market.

Renewable Energy Powered AC: Powering AC with RES is made using electricity (Solar PV, Wind, Hydro, geothermal) or heat (solar thermal, geothermal). Cooling technology has been dominated by vapor compression AC system due to their higher performance relative to heat driven AC. The weighted average coefficient of performance (COP) of electric AC is up to 6 while that of heat driven AC or absorption chiller (ACH) is up to 1.8. However, while ACH must have their power source generated on the place where it is used, (Boiler or Solar heater or hot spring), electrical AC often rely on power generated miles away. When the power plant electricity generation efficiency (15-18% for solar, 35-45% for the thermal plant), transmission and distribution losses are taken into account, the overall system performance of electric AC drops drastically to become similar to that of ACH. Rising electricity cost, the need to upgrade power system to cope with higher peak demand, together with climate change issues are redirecting people to think about alternative cooling technologies driven by heat. Solar thermal cooling/heating is a very old technology. However, other than domestic hot water production, it is not widespread for other applications because

of their low performance. The recent advances in electronic technology however brought in better control capabilities that improved the performance of solar ACH.

Solar Powered Absorption Chiller: Solar absorption chiller that converts directly heat into cold is becoming popular to replace or supplement electric AC for large-scale applications or remote applications. However, one of the biggest issues with these machines is their sensitivity to ambient temperature that can severely degrade performance for only little degree temperature fluctuation. Also, the cost is still high, reaching 600 USD/kW of installed capacity which is two-three times more expensive than their electric counterpart[10]. To reduce the absorption chiller required rated peak power for an application, Phase Change Material (PCM) has been proposed to serve as hot water/chilled water storage to level the load or to lower the condenser cooling water temperature which in turn reduce the required input power. Garcia et al. [11] reviewed 88 PCM and found that only 40 were potentially commercially viable. Long-term stability and cost remain some barriers for these technologies. In Helm et al. [12] study of PCM for condenser cooling, they reported a system efficiency increase of up to 64% compared to dry air cooling. From their findings, the PCM was able to stabilize cooling water temperature at 32°C versus 36°C for dry air cooling. They further reported that the lower ambient temperature below 25°C during the night was enough to regenerate the PCM in 7 hours.

Sensible Heat Storage with Water: PCM being costly and subject to properties degradation over time, sensible cold storage has been in use to level AC peak load. In Illinois University, a 24000 m^3 chilled water storage (CHWS) project in 2011 achieved 8.5 MW peak demand reductions [13]. Through multiple projects, it has already been demonstrated that ice storage is a good option for only small systems such as an office room, while CHWS is the most economical for large systems requiring chilled water up to 160,000 m^3 [14]. CHWS has been more successful as peak load leveling medium. As the cooling load becomes large such as in district cooling, storage volume becomes incredibly big to be done with liquid fluid. To meet these huge storage requirements, the earth itself has been used as a theoretically infinite storage medium, the only limit being cost

Ground Source Energy Storage: the volumetric heat capacity of the earth is nearly half that of water, meaning that for the same volume, water can store twice the thermal

energy the earth can. Insulated rock bed can serve as a storage medium. A fluid with a temperature much higher or much lower than the rock bed temperature is passed through a tube bundle dispersed in the rock, storing or extracting heat from it. As the earth is free and doesn't need any special container, high storage volume can be built cost-effectively. For high-temperature storage up to 600°C, bedrock storage has been reported to cost down to a third of the cost of molten salt PCM storage [15]. Another well-used earth energy storage technology is borehole thermal energy storage (BTES). Tubes in "U" shape are laid horizontally at 2-5m depth or vertically at 20-200m in the ground to use the earth as a heat source or a heat sink. This is due to the fact that as the deep increases, the earth temperature is becoming constant, close to the annual average ambient temperature. Solar powered chiller and storage system are a good combination to make RES as reliable as their counterpart fossil fuel energy system. Eventually, the combination may improve the cost and overall technical/economical figures of the system.

1.2. Scope of the study

In figure 1.1 is shown a general block diagram of solar ACH. It has a collector that harvests solar heat, a buffer tank that limits fluid temperature fluctuations, an ACH that converts heat to cold, a cooling tower that can reject heat into air or underground and the building that receives the cooling service. In this study, the effects of the addition of storage system (tank, ground) to solar absorption cooling/heating system on the overall system performance are analyzed. Tanks are used to store hot water for the chiller or to store chilled water to serve the building load. Also, cooling tower operating with storage tank will be added to the system to study the effect of night cooling on system performance. BTES is added to store heat rejected by the chiller in summer, for later use in winter. The study is limited to:

- Investigating the temperature at different nodes of the system
- Calculating the heat flow of each fluid stream
- Determining the performance of the system including collector efficiency, solar energy contribution ratio, and overall system performance cooling load to heat input ratio.
- Choosing the appropriate system for a brief economic analysis

What is not covered in the study are:

- Electrical performance of the heat driven machine. This is due to the fact that electrical energy consumption is negligible compared to heat consumption.
- Pressure drop analysis since pumps are not considered.
- Single component performance optimization. The whole system output to input ratio is sought.

The aims of this study are:

- To increase the cooling/heating output while minimizing the heat input.
- To increase the utilization ratio or capacity factor of the system especially the absorption chiller.
- To reduce the peak power of the absorption chiller
- To reduce the system cost in terms of capital expenditure (CAPEX) and operation expenditure (OPEX).

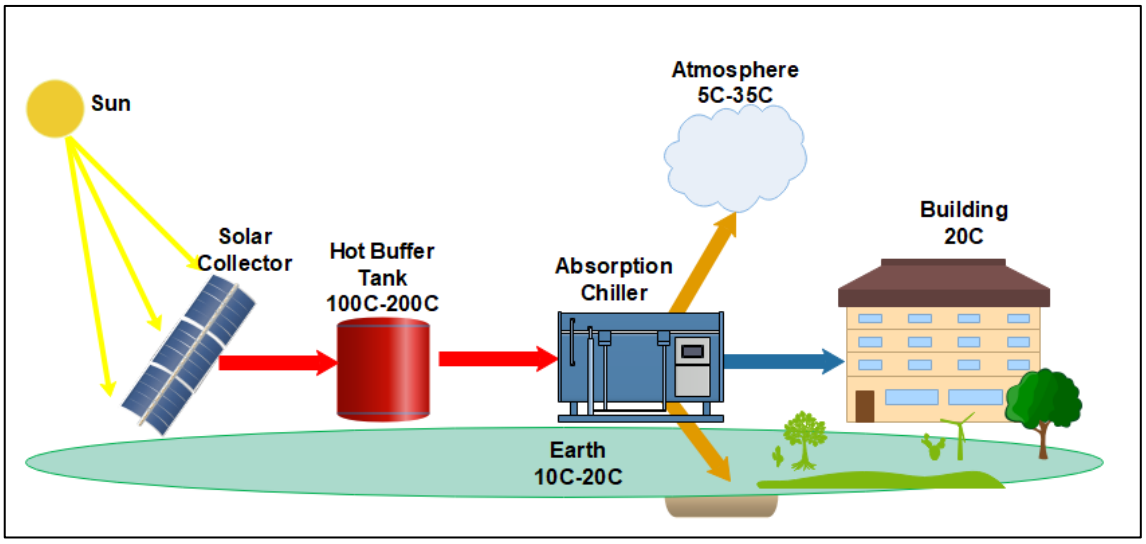

Figure 1.1. Solar Powered Absorption Chiller Cooling System

1.3. Thesis plan

In chapter 2, a literature review of the ACH system is done. Research on solar collector technologies is first presented. Secondly, heat driven machines development history, their performance status are explained. Thirdly sensible storage systems including water tanks and borehole storage are reviewed. Lastly, ACH systems using

more or less solar heater, absorption chiller in addition to the storage system are presented.

In chapter 3 and 4, deep explanations of the science behind each component used in the study systems are worked out. This includes the working principle of the components as well as their mathematicals models. The types of solar thermal collectors are discussed in details, showing the advantages and drawbacks of each technology. Absorption chiller and cooling tower are presented technically and the conditions most suitable for their use are discussed. Water storage tank along with borehole energy storage system is explained before case studies of systems proposed in the thesis are introduced.

In chapter 5, the methodology employed to obtain the study results is developed. First, the simulation tools are briefly introduced. Next, the meteorological data sources are compared to highlight the importance of getting good data in order to obtain accurate results especially if a commercial project is to be implemented. Lastly, the simulation flow of each case study is explained.

In chapter 6, the results of the three cases studies are presented and discussed. The merits of all systems are compared to each other in order to select the best system worth considering for an economic assessment. The economic parameters of interests are first explained, and then the calculations assumptions are given. The financial figures of the reference system versus the best proposed system are presented and discussed to conclude the chapter.

CHAPTER 2

LITERATURE REVIEW

The literature review presents the research findings about the main components used to build the cooling/heating systems. They are: the solar collector, the ACH, and storage systems including hot/cold water storage tanks and BTES. Entire solar cooling systems are also reviewed to serve as a reference for the proposed study.

2.1. Solar Thermal Energy

The use of solar heat for processes such as cooking, drying, space heating cannot be traced back with certainty. Hundreds of years BC in Africa, ancient black Egyptians were using solar heat for space heating at night. Buildings were constructed such that heat is stored in the wall on daytime and released at night in the living space. In the 15th century, water distillation and agriculture product drying were done using solar energy [16]. In modern time, in 1866, Augustin Mouchot developed the solar parabolic collector showed in figure 2.1 [17]. Sunray was concentrated on a metal tube or a boiler that contained water. Steam was then produced to drive a steam engine that in turn powered various applications such as water pumps, printing presses and ice making machine. There are mainly two types of solar collectors: Concentrating collectors and Non-Concentrating collectors. Each type uses sun energy differently. In the first one, only the sun ray falling normally to the collector aperture area or the Direct Normal Irradiation (DNI) can be converted to heat. This means that a tracking system is necessary to ensure DNI is always received normal to the aperture area. In the latest one, sun ray coming from all directions or the sum of DNI, diffuse radiation (DIF) and reflected radiation (REF) can be converted to heat which means that a tracker is not necessary for these collectors.

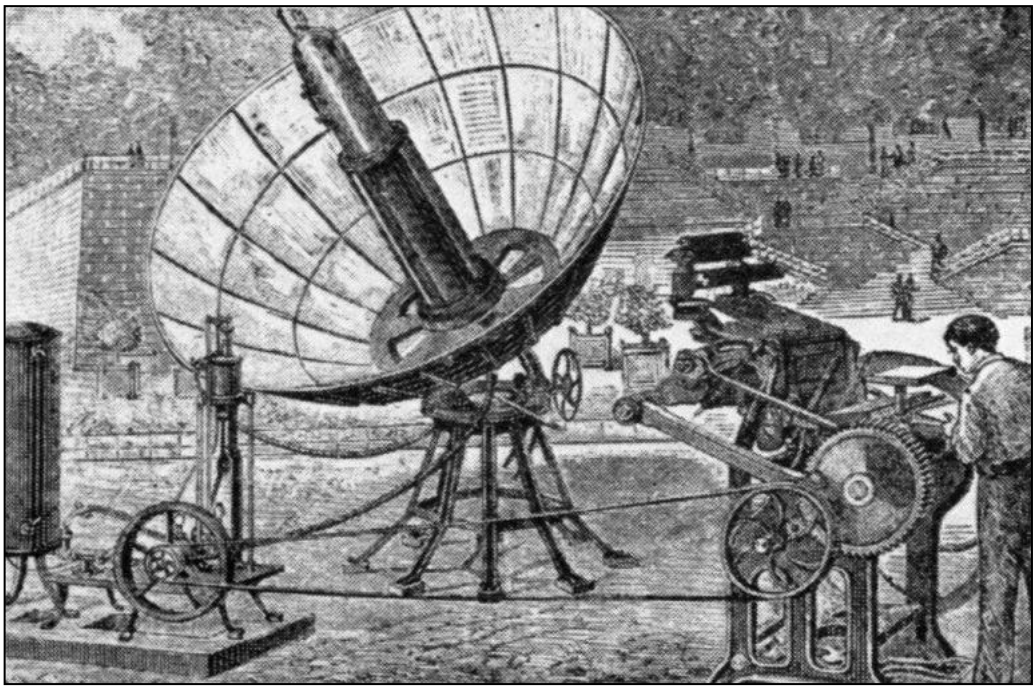

Figure 2.1. Parabolic Solar Concentrator by A. Mouchot [17]

For non-concentrated collectors such as flat plate collectors (FPC) are used for domestic hot water production. A study by Ming et al. [18] showed that when the diffuse radiation is varied from 20% to 50% of the total radiation, the collector peak efficiency decreased by less than 1.83%. However, the corresponding heat loss decreased up to 7.83%. The DNI which has more energy tends to heat at a faster rate the collector, increasing heat loss considerably as the receiver area is large. To overcome this issue, some researchers attempted to reduce the receiver area by using a "V" shape reflector to reflect sunlight onto a much smaller area at the bottom of the structure. Doing this, Ruhul et al. [19] obtained an efficiency increase by 10%. Collector Efficiency is also affected by the flow rate. At higher flow rate, the temperature difference between the inlet/outlet of the collect is reduced, which decrease the heat loss to the ambient [18,20,21]. However, higher flow rate increases pumping power which may cancel the efficiency improvement benefit.

Concentrating collectors such as parabolic trough collector (PTC) is more suitable where the DNI ratio is more important. When DNI to global radiation ratio is less than 60% the benefit of concentrating collector become less evident [22]. The main advantage of this technology is the possible high concentration ratio up to 70, allowing output temperature up to 500°C [23]. As mentioned for the non-concentrating collectors,

the efficiency of concentrating collectors also correlates positively with the flow rate. In fact, in addition, to lower the heat loss, higher flow rate also enhances the heat transfer coefficient through more turbulent flow. To promote turbulent flow, some researchers went further to introduce fins in the receiver tube [24]. Also, nanofluids with tailored characteristics have been used experimentally to enhance heat transfer in the receiver. The technique achieved a collector efficiency boost up to 12.5% [25,26]. The heat loss for concentrating collectors is much less than that of the non-concentrating collectors as the receiver area is drastically reduced to a circular spot or to a partial area of a small diameter tube. Among the concentrating collectors, PTC is the most common one. Its peak optical efficiency can reach up to 63% while the theoretical limit is 75% [27].

2.2. Solar Thermal Absorption Cooling Systems

Solar thermal cooling has been used since the 18th century. However, modern study of direct conversion of heat into cold started in 1950. Swedish student-built diffusion absorption refrigerator that was powered by burning natural gas. Later on, solar heat has been used to supplement the heat requirement of the device. In the industrial scale, space cooling using ACH boomed in the USA, after the oil crisis in 1970. The will to become energy independent pushed for the development of lithium bromide chiller, improving its performance up of 50%. This was an important efficiency boost by considering that absorption diffusion refrigerator had a COP of 0.20-0.40. Today, commercial chiller has a COP typically in the range of 0.5-0.7. Experimental studies using a well-engineered fluids mixture, however, claimed a COP up to 0.8. The COP of the machine is governed by the three fluid streams temperature (Generator, evaporator, absorber condenser).

A chiller model for solar application has been validated experimentally by Marc et al. [28] revealed that as the generator temperature is varied between 70°C and 90°C, the COP changed from 0.58 to 0.74. Also, the cooling capacity increased from 10kw to 30 kW. A similar conclusion was confirmed by several studies of ACH [29–32].

In an effort to improve the economic feasibility of ACH, a new approach consisting of combining multiple ACH units, by using the heat rejected by the first unit to power the second unit, then use the second unit rejected heat to power the third unit and so on has emerged. Each unit is termed as an effect. In practice, up to three effects chillers are

available commercially. Double effect chiller COP is often in the range of 1.2 to 1.4 [33,34]. Amari et al. [35] showed that direct fired double-effect chiller was much more economical compared to single effect hot water driven chiller. The payback of double effect chiller was found to be as short as 3.5 years.

Roland et al. [36] studied a compound parabolic collector with a 23 kW double-effect chiller driven at 160°C-200°C to found the overall COP of the system. It was 0.99 while the efficiency of the solar unit was 36.7%. By considering the chiller and the collector efficiencies, it can be deduced conservatively that the COP of the chiller was 2.4.

A solar-powered double effect ACH for subzero cooling temperature was studied by Catalina et al. [37]. They found a COP ranging from 0.58 up to 0.95 as sun power was changing. This low value was due to the subzero cooling which was too low compared to the conventional 6°C-12°C chilled water temperature used for building cooling application.

To cope with sun intermittency, dual power gas-solar chiller has been studied in Indonesia by Lubis et al. [38]. By varying cooling water temperature(28°C-34°C) and hot water temperature (70°C-90°C), a COP variation from 1.4 up to 3.3 was observed. A similar study was done in China for a hotel cooling/heating [39]. The system was working on single effect mode on the sun and in double effect mode on gas.

2.3. Ground Source Cooling/Heating

Geothermal energy is a solar energy stored in the earth because of the daily radiation the earth receives. There are two types of geothermal systems: low grade geothermal that uses the earth at a temperature typically below 50°C and high grade geothermal that uses hot water or steam out of the earth at 100°C up to few hundred Celsius. For each point on the earth, the annual average temperature is nearly constant. As the point goes deeper from the surface, temperature approaches a constant value throughout the year. In the 17^{th} century, this was proven by French Physicist Lavoisier who measured a constant soil temperature at 85feet depth at Paris observatory center [40]. In 1799, Alexander Von Humboldt noted that the changes in the measurement taken since 1680 were no more than 1 degree. In 1838 temperature measurement at the

Royal Edinburg observatory showed that the temperature variation at 25feet depth was 1/20 of the surface variation while at 50 feet the variation reduces to 1/400. The constant earth temperature motivated researchers to use the earth as a heat source/sink in building cooling/heating systems.

In Japan, a ground source heat pump using a horizontal ground heat exchanger loop buried at 0.5m depth and an electrical AC unit showed that the annual COP of the system was 3.26 [41]. To maximize the capacity factor of the system, it was sized at 60-70% of the heating load. In a similar study in Turkey, it was found that the COP of the heat pump was between 4.03 and 4.18 [42]. An economic analysis showed the system was more cost effective compared to others heating systems powered by natural gas, LPG or fuel oil. In a combined borehole thermal energy storage and solar collector study in Shanghai for building cooling/heating application, it was found that the COP of the system was 4.5 if the collector was used, and 4.2 if the collector was not used [43]. Solar energy utilization reduced electricity usage by 26.1%

A seasonal thermal energy storage study using borehole at 500m to 1500m deep and solar collector at 110°C was carried in Germany in 2015 [44]. The efficiency of the system was quite low at 15% for the first 3 years, then went up to 25% within 30 years. In a 5 years simulation of BTES coupled to a solar collector in Finland, Rehman et al.[45] reported a heat storage efficiency improvement from 23% to 31% by using a control strategy to optimize the operation of the system. In a review of solar BTES by Gao et al.[46], the heat storage efficiency appeared to be between 9% to 41% over 5 years. The low efficiency of the system is due to the massive thermal mass of the earth which can dissipate heat easily and “swallow” any artificially introduced heat to the ground.

2.4. Similar Studies

Solar Borehole Thermal Energy Storage: In a simulation of solar thermal district heating coupled to a BTES, Flynn et al. [47] showed that the BETS efficiency can reach up to 46% depending on the location. Regions with higher heating demand had a higher efficiciencies due to the higher capacity factor of the boreholes. In a combination of solar collector-BTES-heat pump for building heating application, the system was able to save 32% of the electricity through an increased COP [48]. In this study waste heat rather than valuable heat will be the BTES heat source.

Night Cooling: Night cooling has already been investigated by numerous researchers. Miguel et al. [49] showed in their study of office building night cooling, that a good slab design for night ventilation is an efficient solution to lower indoor daytime temperature. In a similar study, Lin et al. [50] found that night roof ventilation can reduce 10-24% of the AC energy consumption while reducing the indoor peak temperature by 3-5°C. Ali et al. [51] in an experimental study of tank water night cooling by natural convection and sky radiation found that water temperature can be lowered by 6.6°C during the night. However, this result is obtained by keeping the deep of the water at 0.5m, meaning a large area may be necessary to achieve commercial or utility scale cooling. Also, water consumption was as high as 4.5%. To avoid the use of scarce water for cooling, Ana et al. [52] studied night sky radiative cooling for a CSP plant and found that 80-90% of the cooling load can be satisfied with this technique. In these studies cooling is shifted from day to night without exploring the opportunities to cool water 24h/day at a continuous low flow rate which can increase cooling performance.

Chilled Water Storage: The performance of solar assisted absorption chiller with chilled water storage has been studied by Rosiek et al.[53,54]. A portion of the load was sent to the low cooling demand period, in order to have a less frequent ON/OFF of the chiller. The element of interest was the electric energy consumption which was reduced by 20% thanks to the new design. Similar study focusing on saving on peak power tariff has been done by Lin et al. [55] in 2014. A 40% power cost saving was achieved. However, a reduction of the required chiller cooling capacity has not been explored by the previous study.

CHAPTER 3

SOLAR THERMAL ENERGY

In this chapter, the fundamentals of solar energy technology is explained. It starts with the generalities of solar energy, explaining how solar power is generated, how it reaches the earth and which portion of the energy can be used for concentrated solar technologies. The existing types of solar thermal collectors are presented in more details as well.

3.1. Solar Energy Fundamentals

It is commonly accepted that the sun is the source of all forms of energy on earth. In fact, in fossil fuel generation process, solar energy is first converted to carbon by plants through photosynthesis. Plants then constitute the green biomass or oil which is biomass deposited deep in the ground millions of years ago. For wind energy, the sun is at the center of wind flow by heating unevenly the earth, creating pressure differences which induce wind. The rain cycle necessary for hydropower is also powered by the sun through the evaporation process. In modern days, solar energy use as a renewable energy source is made in two ways:

(1) Solar photovoltaic which convert sunlight directly into electricity.

(2) Solar thermal which convert sunlight to heat; heat is then used for various applications including electricity generation, industrial heat process, space heating/cooling. Solar thermal cooling will be the focus of the thesis since air condition accounts for more than 50% of building energy consumption as mentioned in the introduction.

3.1.1. Generality of Solar System

The solar system is a structure born from the explosion of a supernova or star 4.5 billion years ago. It is formed by eight planets and one star, the sun, bound through gravity forces. Bodies such as moons, asteroids, and comets are found in the inter-

planets spaces. The system spans an estimated radius of 90 Astronomical Unit (1AU = 150Million kilometers, or sun-earth distance) centered at the sun. However, the farthest planet lies within 30AU away from the sun, the remaining space being covered by less known bodies. From the Sun in the outward direction, the planets are Mercury Venus, Earth, Mars, Jupiter, Saturn, Uranus, and Neptune as shown in figure 3.1. The first four planets are silicate planets. They have rocky surfaces, are composed of various solid materials including carbon, iron, calcium, potassium, and others silicate compounds. Each planet has an atmosphere made of gases such as oxygen, carbon dioxide, nitrogen, water vapor, krypton, xenon, but differs in components composition ratio and gas layer thickness. Jupiter and Saturn are gas-giant planets, meaning they are made of relatively hotter gases wrapped around a small solid core. Uranus and Neptune are ice-giant, implying they are formed by very low temperature frozen materials. Unlike the planets, the sun is made almost entirely of helium and hydrogen. The key difference between the sun and the planets is that the sun is burning its material in a nuclear fusion reaction at its core, radiating the generated energy outward while planets are mainly energy receiver masses. The closer to the sun a planet is the more energy it receives from the sun. However, the atmosphere of a planet and the magnetic field of its core may act as a radiation shield or a greenhouse, making the effectively trapped sun energy less proportional to the distance sun-planet.

3.1.2. Sun-Earth Energy Transfer

The sun is a star with a diameter of $1.39\ 10^{9}m$, a mass of $1.989\ 10^{30}kg$ that lies at 150 million km from earth as shown in figure 3.2 Energy is generated in the core of the sun by nuclear fusion. In the process, two hydrogen molecules combine to form a helium molecule ($H_2 + H_2 \longrightarrow He$). Since the mass of the reactant is less than the mass of the product, the missing mass is transformed into energy "E" following the Einstein formula:

$$E = mc^2 \tag{3.1}$$

where $m[kg]$ is the missing mass to be converted to energy, $c[ms^{-1}]$ the speed of the light $E[J]$ the energy released.

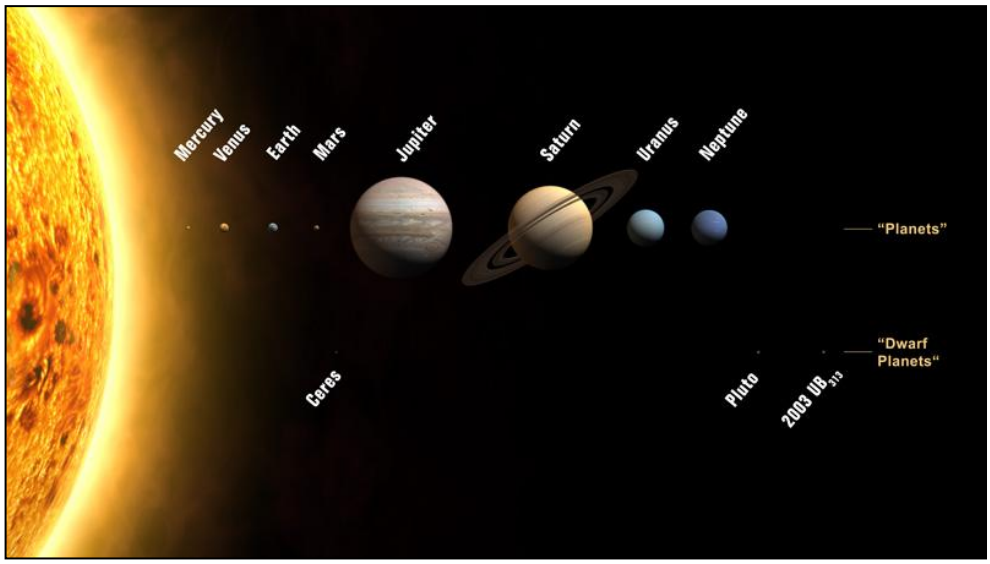

Figure 3.1. Solar System[56].

The full equation of the thermo-nuclear reaction is thus $H_2 + H_2 \longrightarrow He + E$). Proton in the hydrogen molecule having a mass of 1.00794u while helium has a mass of 4.03176u, the mass themass difference converted into kilogram is $4.84180\ 10^{-29} kg$ ($1u = 1.66054\ 10^{-27} kg$). Taking the speed of light as$299{,}792{,}458\ ms^{-1}$ the released energy per reaction obtained with equation 3.1 is $4.35159\ 10^{-12} Joules$.The frequency of the reaction is approximately $9.2\ 10^{37}\ Hertz$ so the corresponding energy generation rate P_{sun} is $4.00346\ 10^{26} Js^{-1}$. This power agrees with measured values and others analytical sun power calculations results. Ninety percent of this power is produced within 23% of the radius where the temperature reaches 8-40 million Kelvin. Heat is transfer from the core to the surface through the so-called convective zone by radiation and convection mainly. At the surface called photosphere, the temperature drops to 5000 Kelvin. From the photosphere outward, there are two layers the chromospheres and the corona with a temperature gradient of 5000 Kelvin to 10^6 Kelvin. However, the density of these regions is very low ($10^{-5} kgm^{-3}$). The reason for the high temperature of the corona is still unknown but its low density makes its contribution to solar radiation negligible. Sun power is radiated in all direction of the solar system. On the earth atmosphere upper layer, the radiation intensity or insolation is termed as the solar constant "G_{sc}". By considering the surface enclosed by a radius equal to sun-earth distance and the sun power calculated previously, solar constant is approximated through the following formula to be $1415 Js^{-1}m^{-2}$ or $1415 Wm^{-2}$

$$G_{sc} = \frac{P_{sun}}{4\pi r^2} \tag{3.2}$$

where $G_{SC}\left[\frac{W}{m^2}\right]$ the solar constant, $P_{sun}[W]$ the sun radiated power, $r[m]$ the sun radius.

The standard solar constant value has been subject to many debates from 1954 to 1983. A value of $1367 W/m^2$is recognized by the world radiation center as the solar constant.

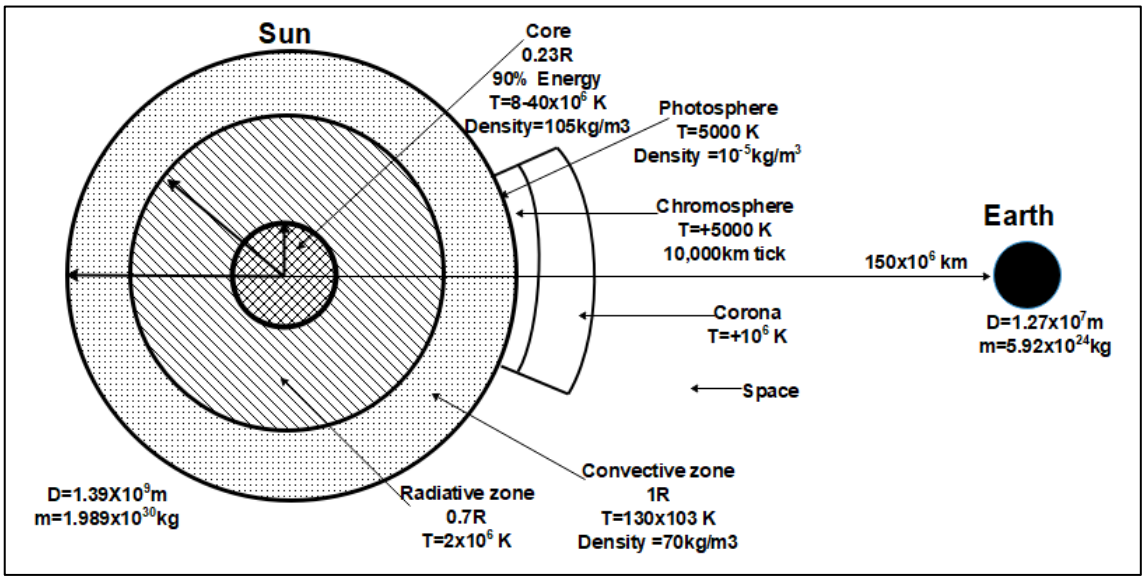

Figure 3.2. Sun-Earth Energy Transfer

3.1.3. Earth Surface Radiation

The extraterrestrial solar radiation spans over a width range of the electromagnetic spectrum. Particles having energy higher than the ultraviolet particles are almost entirely filtered out by the earth electromagnetic field. The solar constant spectral distribution is shown in table 1.1 It is an important information for solar application since each solar technology may only harvest energy contained in a specific wavelength bandwidth. In the design of solar thermal devices (mirror, absorber), the selected coating is frequently used to maximize/minimize the absorption/reflectance of light for a specific wavelength. Silicon solar photovoltaic cell under glass, for example, absorbs only wavelength between 0.4um to 1um limiting its theoretical efficiency to 30%. To increase performance, multiple layers cells are used, each cell absorbing a certain range of wavelength. From table 3.1, most of the energy lies in the visible light range and in the IR range.

Table 3.1.Solar Constant Spectral Distribution [57]

Wavelength [μm]	Power content [W/m^2]	Solar constant [%]
0 - 0.38 (UV)	87.48	6.4
0.38 - 0.78 (Visible)	656.16	48
0.78 - ∞ (IR)	623.35	45.6
Total	1366.99	100

The ozone layer absorbs most of the ultraviolet radiation while carbon dioxide absorbs part of the infrared radiation. From the upper atmosphere down to the earth surface, the solar ration is divided into 4 components as illustrated in figure 3.3:

- Direct Normal Irradiation (DNI): It is the sunlight that reaches the earth surface without any change of direction.
- Diffuse Irradiation (DIF): It is the sunlight that reaches the earth surface after a change of direction or scattering caused by cloud, air or others atmospheric particles.
- Reflected Irradiation (REF): It is the sunlight that hits any surface on earth such as grasses, trees, ground, water, and bounce back to the earth.
- Absorbed Irradiation (ABS): It is the sunlight that is absorbed by the atmosphere without reaching the ground.

From a solar constant of $1367W/m^2$, around 51% annually reached the earth directly without any path deviation. It is only this portion or the DNI that is convertible to useful energy by concentrating solar technology such as concentrating photovoltaic (CPV), concentrating solar power (CSP) or concentrating solar thermal (CST). For non-concentrating solar technology, DNI and DIF are the main useful source of energy. However, in recent years, with the development of bifacial solar PV, REF radiation is being harvested as well on the back side of the module.

3.1.4. Sun Light Concentration

DNI is arriving from space with a relatively low heat flux that cannot rise significantly the temperature of the receiver surface. To raise the temperature to a level suitable for performing a useful work, the concentration of sunlight on a smaller receiver area is necessary. The concentration ratio is defined as the ratio of the aperture area over the area of the receiver [58].

$$C_r = \frac{A_a}{A_r} \tag{3.3}$$

where $C_r[-]$ the sun light concentration ratio, $A_a[m^2]$ the soolar collector aperture area, $A_r[m^2]$ the solar collector receiver area.

However, it should be noted that this ratio cannot be infinite because of the sun-earth geometry which allows energy to be received through a finite acceptance angle $2\theta_s$ =0.53° as shown in figure 3.4. The calculation of C_r is based on ideal radiation energy balance between the sun and the receiver, both masses being assumed to be blackbodies. For a circular receiver the energy seen by the receiver from the sun Q_{sr} and the energy seen by the sun from the earth Q_{rs} are:

$$Q_{sr} = \frac{r^2}{R^2} A_a \sigma T_s^4 \tag{3.4}$$

$$Q_{rs} = A_r \sigma T_r^4 \tag{3.5}$$

where $Q_{sr}[W]$ the solar to receiver power transfer, $Q_{rs}[W]$ the receiver to solar power transfer, $A_a/A_r[m^2]$ the aperture/receiver area, $\sigma[\,m^2\,kg\,s^{-2}\,K^{-1}]$ the Boltzman constant, $T_s/T_r[K]$ the sun /receiver temperature. Equalizing the two terms gives:

$$\frac{A_a}{A_r} = \frac{R^2}{r^2} = \frac{1}{\sin^2(\theta_s)} \tag{3.6}$$

where $A_a/A_r[m^2]$ the aperture/receiver area, $R[m]$ the sun-earth distance, $r[m]$ the sun radius, $\theta_s[°]$: the sun-earth view angle. For a linear concentrator, the concentration ratio is:

$$C_r = \frac{1}{\sin(\theta_s)} \tag{3.7}$$

Considering the acceptance angle value, the maximum concentration ratio is 216 for a linear concentrator. In practice, this number is around 60-80 allowing the temperature to reach 550°C. For circular concentrator, the maximum concentration ratio is 47,747. In practice concentration over 600 is done, reaching a temperature of 800°C. Laboratory solar furnace even reaches a higher concentration ratio over 10,000 with a temperature of 2000°C. If light path is glass rather than air, the numerator of C_r equation becomes the glass refraction index or 1.5, increasing the concentration limit to over 70,000. Gleckman et al.[59] reported a concentration ratio of 56,000 by changing air with glass. Theoretical concentration ratio is hard to reach because of tracking error and the non ideal nature of the medium in which light travel.

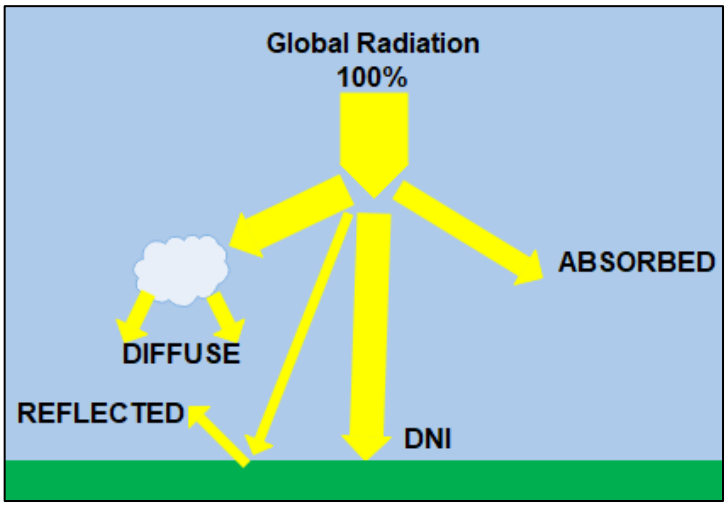

Figure 3.3. Modifications of Solar Constant by Atmosphere and Surfaces

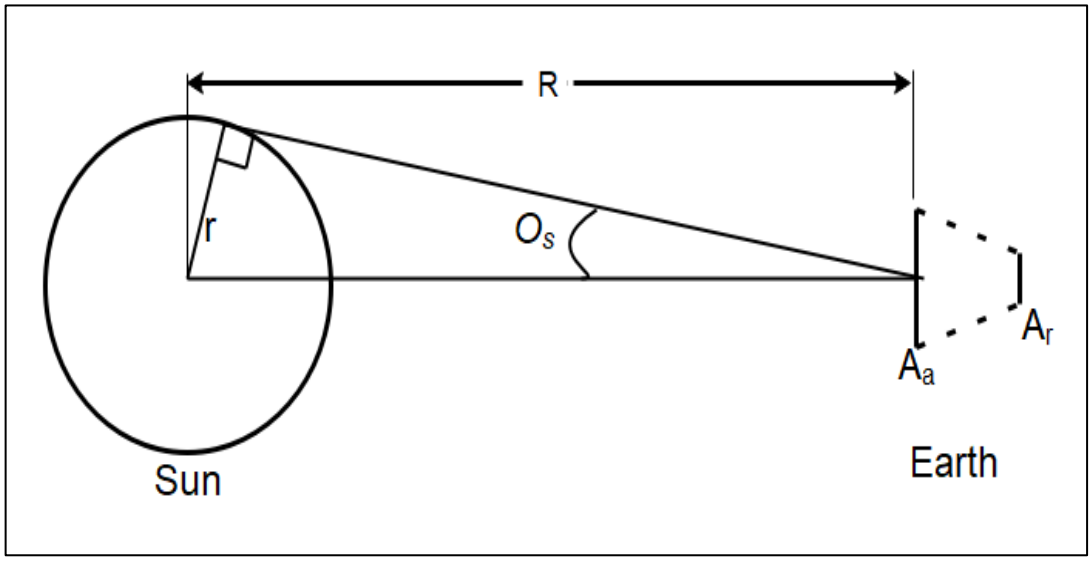

Figure 3.4. Sunlight Concentration Geometry [57]

3.2. Concentrating Solar Thermal Collectors

3.2.1. Overview of the Current Technologies

Concentrating collectors can be classified into two groups as shown in figure 3.5. **(1) Linear concentrator** concentrates sunlight on the linear receiver. Parabolic trough collector (PTC) and Linear Fresnel collector (LFC) are examples of linear concentrators. They are both commonly single-axis tracking, however an example of PTC with low concentration ratio that uses two axis tracking exists. The optical efficiency of PTC is

higher than that of LFC because the sunlight incidence angle on PTC mirror is less than that of LFC allowing PTC to receive light more directly. Due to higher efficiency, PTC is the preferred technology for electricity generation which requires high temperature greater than 400°C. For applications with a temperature less than 300°C, LFC may be a good choice despite its lower efficiency. In fact, the advantage of LFC is its lower cost compared to PTC. Linear mirrors are easy to manufactures, and to maintain compared to curved mirrors of PTC.

(2) Central concentrator concentrates sunlight onto a spot. Solar tower collector (STC) and parabolic dish collector (PDC) are examples of central concentrators. PDC is the most efficient of the collectors however it is limited by its scalability, a huge dish with high concentration ratio being too challenging to build. STC addresses the scalability issue of PDC by using multiple flat mirrors called heliostats to focus sunlight on the receiver. The incidence angle is increased; however, the high concentration ratio still makes this technology desirable for high-temperature applications such as electricity generation with a steam turbine.

3.2.2. Collector Energy Absorption Mechanism

The thermal energy output of solar collector is governed by the physical properties of materials, energy balance and mass transport. Sunlight tricking the collector mirror is broken into 3 parts as shown in figure 3.6: a transmitted energy that depends on the transmittance T, an absorbed energy that depends on the absorptance α and a reflected energy that depend on the reflectance ρ. The sum ρ+α+T=1 as indicated in figure 3.6. The reflectance of commercial mirrors can be as high as 0.96 by using an alloy of metals (Aluminum, zinc, Copper). Absorptance of the receiver can also be as high as 0.95 by using special coasting materials. Absorptance and reflectance of common materials are shown in table 3.3. Commercial collectors with their receiver are shown in figure 3.7.

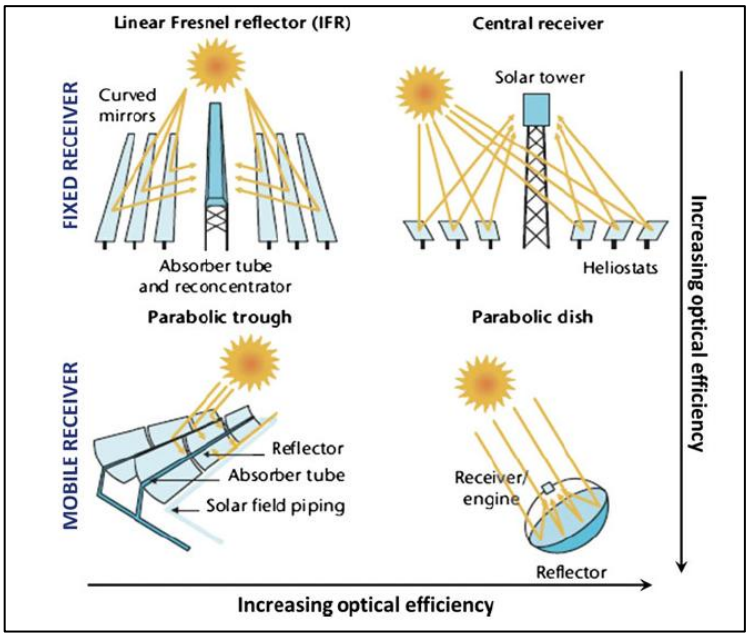

Figure 3.5. Concentrated Solar Thermal Technology[58]

Table 3.2. Type of Solar Thermal Collectors and Applications [57]

Type of Collector	**Concentration Ratio[-]**	**Typical Temperature Range [°C]**	**Application Example**
Flat-plate	1	60-120	Domestic hot water
Fixed concentrator	3-5	100-150	Fruit Drying
Parabolic Trough	10-50	150-350	Industrial heat process
Parabolic dish	200-500	250-700	Electricity generation
Central receiver	500 to >3000	500 to >1000	Solar furnace

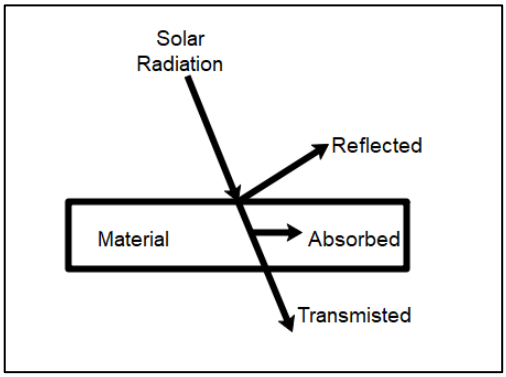

Figure 3.6. Solar Radiation-Material Contact Energy Breakdown

Table 3.3. Typical Absorptance /Reflectance of Common Materials [57]

Material	Absorptance	Material	Reflectance
Graphitic film	0.92	Silver	0.94
Black copper	0.97	Copper	0.75
Aluminum oxide	0.85	Anodized aluminum	0.82
Black chrome	0.97	Gold	0.76

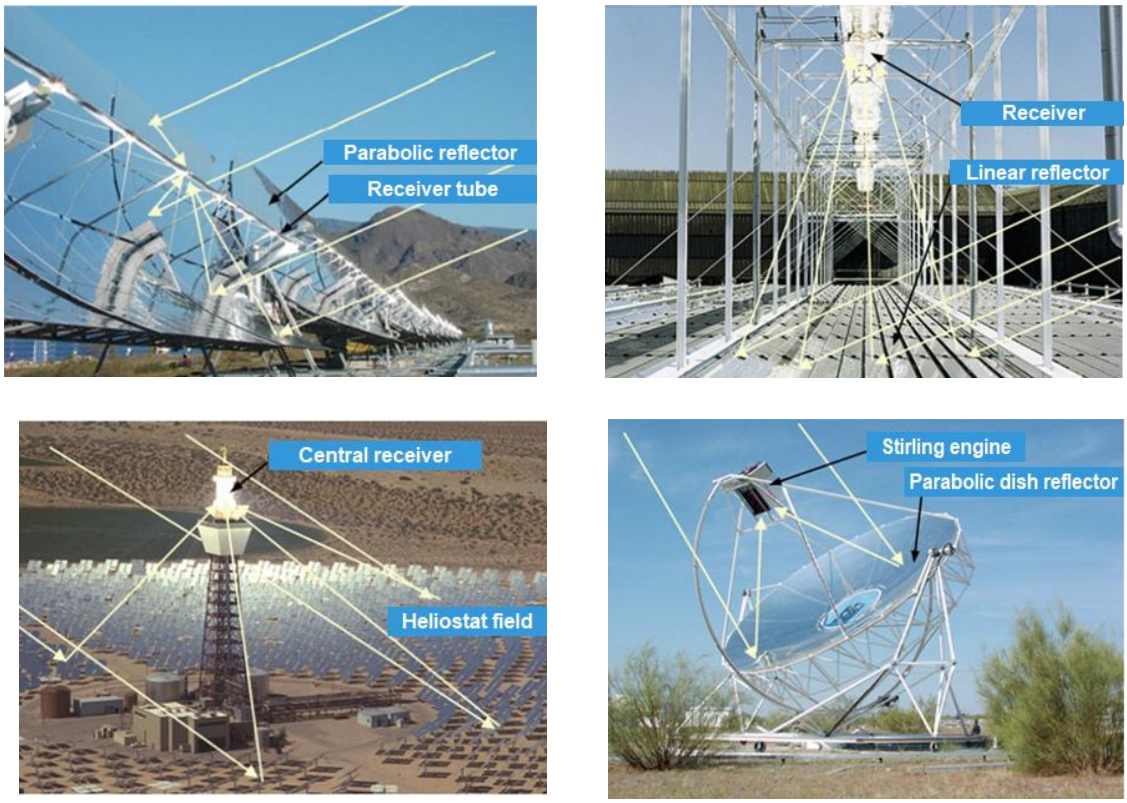

Figure 3.7. Commercial Solar Collectors [58]

3.3. PTC Calculations Methods

PTC Peak Efficiency [59]**:** A PTC diagram is shown in figure 3.8. It has a reflective mirror, a glass tube in which the receiver tube is located. As stated above, each material has its reflectance ρ, transmittance τ, and absorptance α. Starting from point 1 with a unit solar DNI, at point 2, the useful energy becomes $\rho_{mirror,}$ the absorbed and transmitted energy being lost. Likewise, at point 3, the energy is $\rho_{mirror}\,\tau_{glass}$, and at point 4 it is $\rho_{mirror}\tau_{glass}\alpha_{receiver.}$ From experience, the amount of energy at point 4 is always less than the ideal amount predicted the product $\rho_{mirror}\tau_{glass}\alpha_{receiver}$. This is due to the imperfection of the mirror shape and tracking error. The correcting term is called the intercept factor γ. It is defined as the fraction of light reflected by the mirror that effectively reaches the receiver. A typical value of γ is 0.90-0.94. The peak efficiency η_{0peak} of PTC is then:

$$\eta_{0peak} = \rho_{mirror}\tau_{glass}\alpha_{receiver}\gamma \tag{3.8}$$

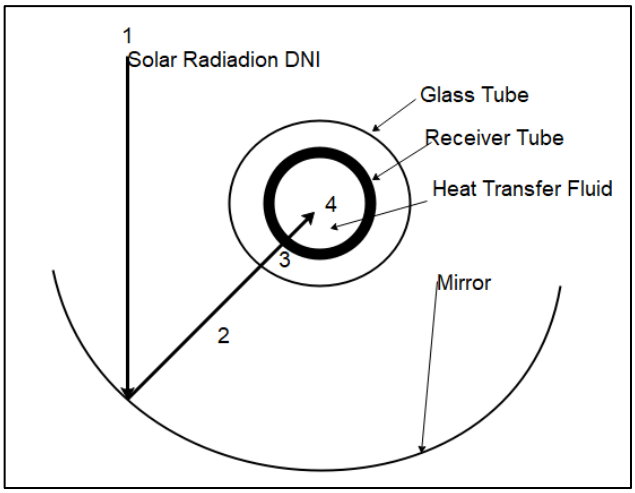

Figure 3.8. PTC Energy Absorption Illustration

PTC Real Peak Efficiency: In a real world, all sun rays are not likely to be normal to the aperture area for formula 3.8 to be valid. To account for non-zero incidence angle effect on the theoretical peak efficiency, an incidence angle modifier "IAM or K" which is a function of the light incidence angle i is introduced in the formula. In its simplified form, the IAM is:

$$K(i) = \frac{1}{\cos(i)} \tag{3.9}$$

When the incidence angle "i" is zero, K is 1, which doesn't change the peak theoretical efficiency. When K is non-zero, K<1 which reduces the peak efficiency. IAM formulas for commercial PTCs are given in table 3.4. In addition to losses due to non-unit IAM, there are ends losses factor F_{el} at the collector support poles where reflected light cannot reach the receiver. By reference to figure 3.9, the end loss factor F_{el} is given in equation 3.10 where Lc and z are in meter.

$$F_{el} = \frac{L_c - z}{L_c} \tag{3.10}$$

The last factor contributing to reducing the peak efficiency is the soiling factor of the mirror "F_s". It is the ratio of the actual mirror reflectance over the mirror reflectance when it is new. Considering all the terms mentioned above, the real peak efficiency expression becomes:

$$\eta_0 = \eta_{0peak} K(i) F_{el} F_s \tag{3.11}$$

Table 3.4. Incidence Angle Modifiers for Commercial PTCs [57]

Solar Collector	Incidence Angle modifier function k(i)
LS-2	$1 + 0.000884 * (i/\cos i) - 0.00005369(i^2/\cos i)$
IST	$1 + 0{,}0003178(i/\cos i) - 0.00003985(i^2/\cos i)$
Euro Trough	$1 - 5.25097 * 10^{-4} i/\cos i - 2.859621 * 10^{-5} i^2/\cos i$
Source: Principle of solar engineering D. Goswami [59]	

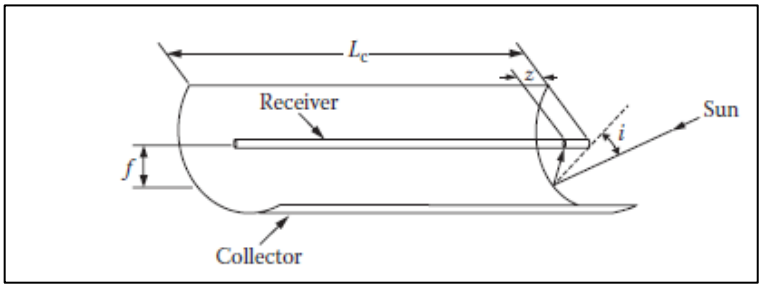

Figure 3.9. Collector Ends Loss Illustration[59]

PTC Thermal Losses: After energy absorption with an efficiency η0, the temperature of the receiver tube rise, creating also heat loss due to the temperature difference between the receiver and the ambient. Conduction, convection, and radiation forms of heat transfer mechanisms take place. Heat is first transferred from the fluid to the tube through convection, then goes from inside of the tube to the outside surface of the tube through conduction. Assuming a vacuum glass, heat is transferred from the receiver tube to the glass by radiation, then from inside the glass to outside of the glass by conduction. From the glass outer surface heat is lost by convection caused by surrounding air movement, and by radiation to the sky.

The simplified thermal resistance network is shown in figure 3.10. The receiver outer surface temperature is measured along with ambient temperature to calculate the heat loss as:

$$q_{loss} = A_k \frac{T_r - T_a}{R_k} + A_r \varepsilon_r \sigma (T_r^4 - T_a^4) \qquad (3.12)$$

where A_k, R_k are the effective area and equivalent thermal resistance due to conduction and convection. In the expression, the absorptance of glass is neglected so heat is radiated directly to space which is represented by the second term at the right side of the equation.

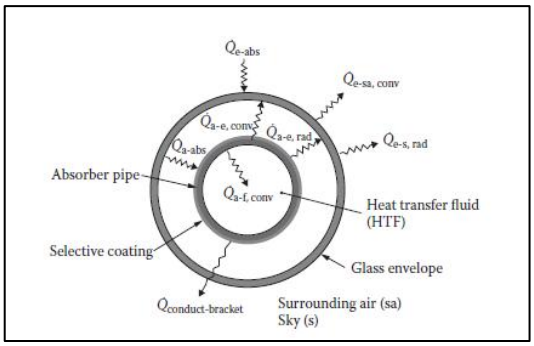

Figure 0.10. Receiver Tube Thermal Resistance Network [59]

An overall heat loss coefficient Uc is often used to simplify the heat loss equation as:

$$q_{loss} = U_c A_r (T_r - T_a) \tag{3.13}$$

$$U_c = a + b(T_r - T_a) + c(T_r - T_a)^2 \tag{3.14}$$

where $q_{loss}[W]$ the heat loss, $U_c[Wm^{-2}C]$ the overall heat transfer coefficient, $A_r[m^2]$ the receiver area, $T_r[°C]$ the receiver temperature, $T_a[°C]$ the ambient temperature, and a, b, c are constants determined experimentally.

PTC Efficiency: The efficiency of the collector η_c is the ratio of the useful harvested energy over the incoming solar radiation DNI. The useful energy is what is remaining when the heat loss is subtracted from the absorbed energy defined by the peak efficiency η_0.

$$\eta_c = \frac{Q_u}{DNI_a A_a} = \frac{\eta_0 DNI_a A_a - U_c A_r (T_r - T_a)}{DNI_a A_a} \tag{3.15}$$

$$\eta_c = \eta_0 - U_c \frac{T_r - T_a}{DNI_a} \frac{A_r}{A_a} \tag{3.16}$$

where $Q_u[W]$ is the useful harvested energy, $DNI_a[Wm^{-2}]$ is the aperture area solar DNI. The useful energy can also be expressed by considering the energy transported by the flowing heat transfer fluid as:

$$Q_u = m_{sc} C_p (T_{cin} - T_{cout}) \tag{3.17}$$

where $m_{sc}[kgs^{-1}]$ is the heat transfer fluid flow rate, $C_p[kJkg^{-1}°C^{-1}]$ the heat transfer fluid specific heat, $T_{cin}/\ T_{cout}[°C]$: the colletor inlet/outlet temperature.

When U_c in equation 3.16 is fully written, a third order term appears for the term (T_r-T_a). In the literature, this term is often referred as ΔT_m which is the difference between

the mean fluid temperature and the ambient temperature. From the collector testing and certification process, the second order efficiency function is determined as

$$\eta_c = \eta_0 - a_1 \frac{\Delta T}{DNI} - a_2 \frac{\Delta T^2}{DNI} \tag{3.18}$$

where $\eta_c[-]$ is the Instantaneous efficiency of the collector, $\eta_0[-]$ the zero loss effeciency of the collector, $\Delta T[C]$ the receiver tube mean temperature to ambient temperature difference, $DNI[W]$ the solar DNI, $a_1[WC^{-1}]$ the first order heat loss coefficient, $a_2[WC^{-2}]$ the second order heat loss coefficient, and a_1,a_2 are constants determined experimentally. Constants for different types of collectors are given in table 3.5. From the corresponding curves in figure 3.11, it can be seen that the suitability of the technology depends on the application temperature range. For temperature less than 100°C, flat plate collector is more suitable while for temperature over 150°C, PTC if more suitable.

Table 3.5. Solar Collector Efficiency Function Coefficient [60]

	η_0 [-]	a_1 [W/m^{2}C]	a_2 [W/m^{2}C]
Flat plate collector	0.78	3.80	0.03
Evacuated tube collector	0.61	0.85	0.005
Linear Fresnel collector	0.58	0.000	0.0004
Parabolic trough collector	0.75	0.1123	0.00128
Peak Sun Efficiency: DNI=1000W/m2 for FPC, ETC; DNI=850W/m2 for LFC, PTC			
Half Sun Efficiency: DNI=500W/m2 for FPC, ETC; DNI=450W/m2 for LFC, PTC			

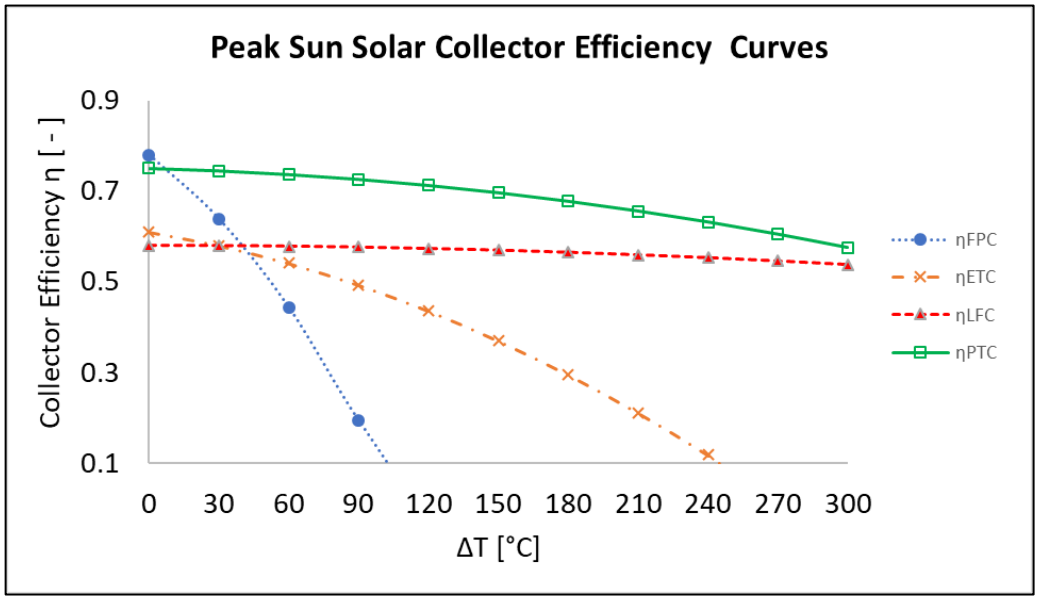

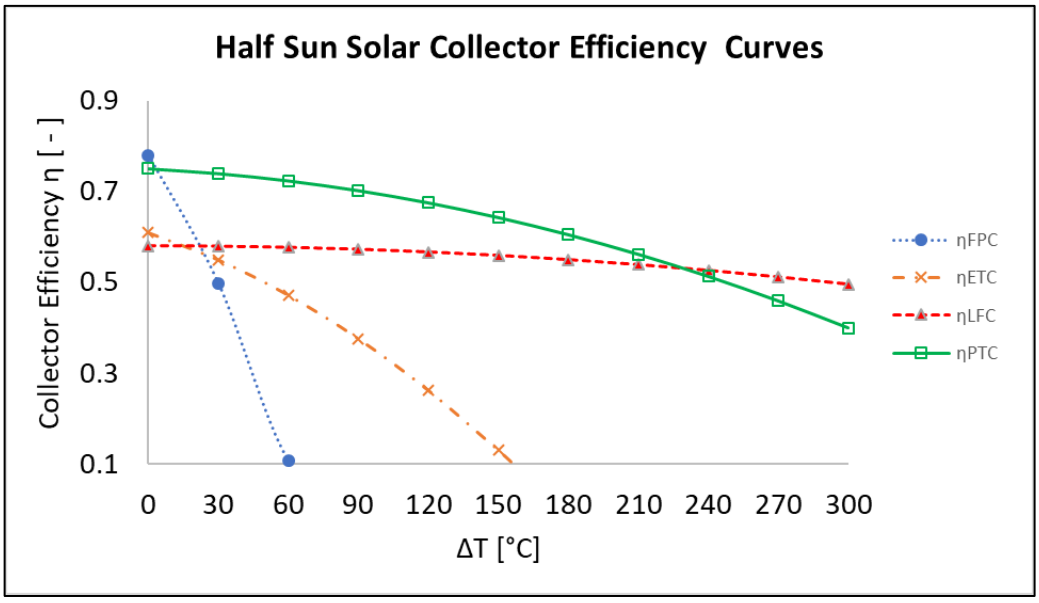

Figure 3.11. Solar Collectors Efficiency Curves

CHAPTER 4

HEAT DRIVEN CHILLER & STORAGE SYSTEMS

In this chapter, the absorption chiller (ACH) which is a central element of the cooling system is explained by showing how its internal components work, and how energy is flowing through the machine. Cooling tower and storage tanks heat transfer mechanism are briefly explained, then ground heat exchanger technology is presented. The chapter ends with a detailed description of the proposed studies systems.

From the law of nature, heat or any substance diffuses from high temperature or high concentration zone to low temperature or low concentration zone. However, Air conditions or heat pumps are machines that move heat from a lower temperature (T_L) medium such as inside a fridge(0°C-5°C) to a higher temperature (T_H) medium such as in a kitchen (20°C-30°C). Heat pumps can be used for either cooling or heating. For a building cooling for example, in summer heat is removed from the living space at T_L and rejected in the atmosphere at T_H. In winter, for building heating, heat is still removed from the atmosphere T_L and injected in the building at T_H. To defy the law of nature by transferring heat from T_L to T_H, a work input is necessary to operate the machines. In a refrigerator for example, an electromechanical compressor is used to power the heat transfer process. In less common machines such as absorption chillers or adsorption chillers, the power source is heat rather than a mechanical compressor.

In an adsorption chiller, the cooling is governed by the thermodynamic interaction between a solid absorbent (e.g. silica gel) and a liquid refrigerant (e.g. water). In an absorption chiller, the refrigerant is liquid (e.g. water, ammonia), and the absorbent is liquid as well (e.g.: Lithium Bromide, water). Table 4.1 presents the characteristics of the two technologies. Adsorption chiller works at lower heat source temperature compared to absorption chiller. In terms of efficiency, both machines are similar. However, adsorption chiller is available in lower cooling/heating capacity. In fact, for the same cooling/heating capacity adsorption chiller is more expensive and occupies a bigger volume compared to absorption chiller.

Table 4.1. Characteristics of Heat Driven Chillers [61]

Process	**Adsorption**		**Absorption**		
Refrigerant/ Sorbent	Water/ silica gel	Water/ zeolite	Water/LiBr single effect	Water/LiBr Double effect	Ammonia / water
Heat Source Temperature [°C]	60-90	45-95	75-110	135-200	65-180
Capacity [kW]	7.5-500	9-430	10.5-20000	174-6000	14-700
COP Heating [-]	1.4-1.6	1.3-1.5	1.4-1.6	1.8-2.2	1.4-1.6
COP Cooling [-]	0.5-0.7	0.5-0.6	0.6-0.7	0.9-1.3	0.5-0.7

4.1. Chiller Working Principle

Adsorption Chiller: The machine has 3 main parts, an evaporator, 2 adsorption chambers, and a condenser as shown in figure 4.1. The system works alternately, each chamber going through a cycle of adsorption/desorption. Adsorption is when the chamber absorbs water vapor, and desorption is when the saturated humid chamber is being dried. The system works as follows:

- **(A cycle)** At the start of the cycle, chamber 1 has a completely dry silica gel. A valve connecting it to the evaporator opens while the condenser connecting valve is closed. The dry silica gel absorbs water vapor from the evaporator at low pressure which creates the cooling effect. Cooling water is passed through the chamber to extend the adsorption period.
- At the same time, chamber 2 is closed to the evaporator and is open to the condenser. hot water is circulated in chamber 2, drying it by evaporating its water to the condenser. Cooling water out of chamber 1, condenses water vapor at the condenser, and send it back to the evaporator. When chamber 2 is completely dry and chamber 1 completely humid, their valves opening/closing are reversed.
- Chamber 2 is now opened to the evaporator, closed to the condenser, while chamber 1 is closed to the evaporator and opened to the condenser.
- **(B cycle).** Hot water is circulated in chamber 1 to dry it, while cooling water is circulated in chamber 2 to support water adsorption from the evaporator, thus enhancing the cooling effect. The drying/humidification cycle is repeated as explained above to provide cooling if the heat absorbed by the evaporator is the output of interest or to provide heating if heat rejected by the condenser is the needed output.

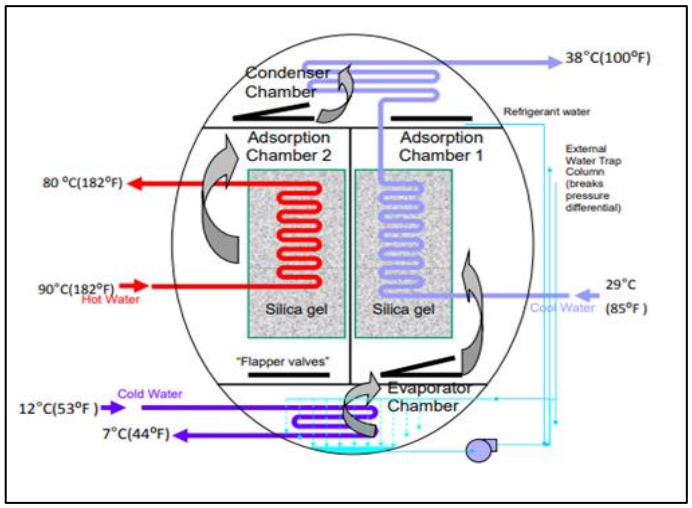

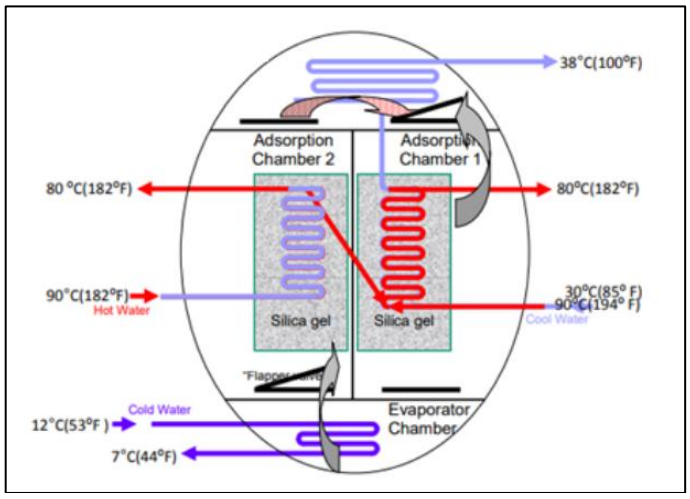

Figure 4.1. Adsorption Chiller Working Principle [61]

Figure 4.2. Commercial Adsorption Chiller [61]

Absorption Chiller: As stated, absorption chiller is driven by heat. To understand its working principle, it is useful to start with the most known chiller, the mechanical vapor

compression cooling system shown in figure 4.3. The system is composed of an evaporator, a compressor, a condenser, and an expansion valve. The working principle can be broken into four steps:

- From point (1), low pressure, low-temperature refrigerant gas is compressed by the compressor.
- At point (2), high pressure, high-temperature gas exits from the compressor and enters the condenser. As the condenser is cooled, the refrigerant gas condenses.
- At point (3), condensed liquid refrigerant exits the condenser, still at high pressure. The expansion valve or throttling valve is opened slightly, creating a pressure drop for the refrigerant accumulated at (3)
- At point (4), the refrigerant is cooled by the throttling effect that just occurred at the expansion valve. During the throttling process, the low pressure at (4) causes a small fraction of the refrigerant to evaporate by removing latent heat from the bulk fluid. Low-temperature low-pressure liquid refrigerant enters the evaporator where the evaporation process continues, removing heat and chilling the water. Refrigerant gas exits the evaporator at point (1). The gas is compressed and the cycle repeats.

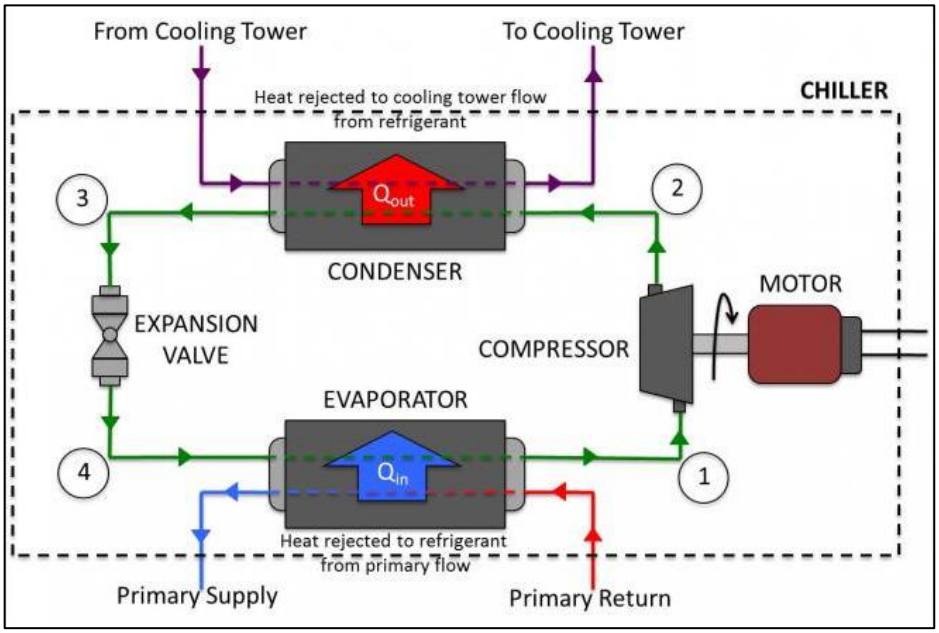

Figure 4.3. Vapor Compression Chiller [62]

In an absorption chiller, the section from the inlet of the condenser to the outlet of the evaporator works in the same way as in the vapor compression chiller. From the evaporator outlet to the condenser inlet, this section is specific to an absorption chiller.

In this section compression of the refrigerant is done thermally rather than mechanically, by using an absorber and a generator. Unlike in the vapor compression chiller system where a single fluid, the refrigerant, circulates through this section, in an absorption chiller, there is a mixture of two fluids in the compression section. A simplified diagram of absorption chiller is shown in figure 4.4. The working principle is as follows:

- In the absorber, there is a dilute solution of refrigerant and absorbent (water-Lithium bromide or Ammonia-water). The solution-pump pumps the mixture to the generator.
- At the generator pressure, the boiling temperature of the refrigerant is much less than that of the absorbent, making the refrigerant evaporates, leaving a concentrated absorbent solution.
- The refrigerant gets into the condenser, follows the refrigerant loop as explained for a vapor compression chiller until a gas refrigerant exit at the evaporator outlet.
- The concentrated absorbent solution from the generator flows to the absorber where it absorbs the gas refrigerant coming from the evaporator. The absorber is cooled by cooling water because the lower its temperature is, the higher the absorption capacity of the absorbent, thus the higher the cooling capacity at the evaporator. A diluted solution is recreated at the absorber, completing the cycle.

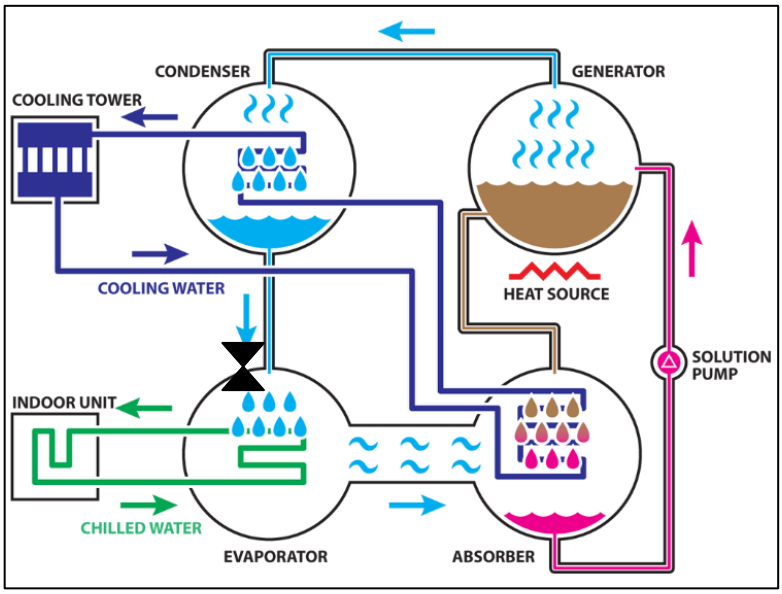

Figure 4.4. Simplified Absorption Chiller Diagram [63]

4.2. Working Fluid Pair

Many fluid pairs have been proposed for absorption chiller operation. However, the most common refrigerant-absorbent pairs are water-lithium bromide (H_2O-LiBr) and ammonia-water (NH_3-H_2O). In a vacuum, the evaporating temperature of water is 0°C while that of ammonia is -77°C.The main difference between the two pairs is that ammonia-water can be used for subzero cooling applications while water-lithium bromide is limited to cooling temperature above 0°C. In figure 4.5 is shown the evaporation temperature vs. pressure for the two refrigerants. For the given pressure range, ammonia provides a lower evaporating temperature than water. For building cooling/heating application, H_2O-LiBr is the most used. In fact, water as a refrigerant offers a unit mass cooling capacity as much as twice that of ammonia. At 1 atm for example, latent heat of vaporization of water is 2700kJ/kg versus 1000kJ/kg for ammonia. One of the worth mentioning issue with H_2O-LiBr is the crystallization of LiBr that occurs when the concentration is high, and temperature drops suddenly such as in the event of a power cut or too low-temperature cooling water circulating at the absorber. Electronic control solved the problem by implementing a smooth shutdown strategy and a smart control, preventing the chiller from operating in the crystallization zone.

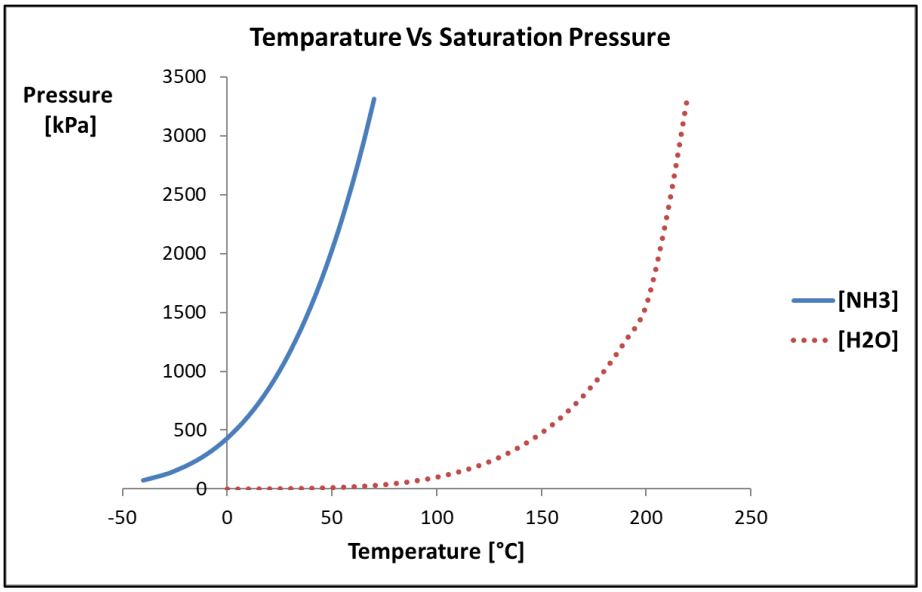

Figure 4.5. Ammonia and Water Vaporization Temperature-Pressure

4.3. Absorption Chiller Calculations

H_2O-LiBr absorption chiller (ACH) can be single effect, double effect or triple effect. Each effect working principle is as described above. In multi-effect chiller, the heat rejected by the condenser of a previous effect is used as a heat source to power the generator of the next effect. In this ways, the condenser heat is used to provide additional cooling, rather than being rejected in the atmosphere. The COP of the chiller is usually around 0.6, 1.2, 1.8 for a single effect, double effects and triple effects chiller respectively. In practice, for commercial chillers, there are up to three effects because, beyond this number, the economic advantage of the machine is declining. Also, for multi-effect chiller, the driving temperature is high compared to single effect chiller which may constitute a technical disadvantage if the heat source is already at a relatively low temperature.

Absorption chiller calculation is governed by energy and mass balance equations. A single effect chiller will be used to walk through the calculations process for convenience and clarity since multi-effect chiller calculations can be done by simple superimposition of many single effects calculations. In figure 19 is shown a diagram of single effect water-lithium bromide chiller. In term of components, it is as described in figure 4.6, except that a solution heat exchanger is added to recover heat from the concentrated solution flowing out of the generator.

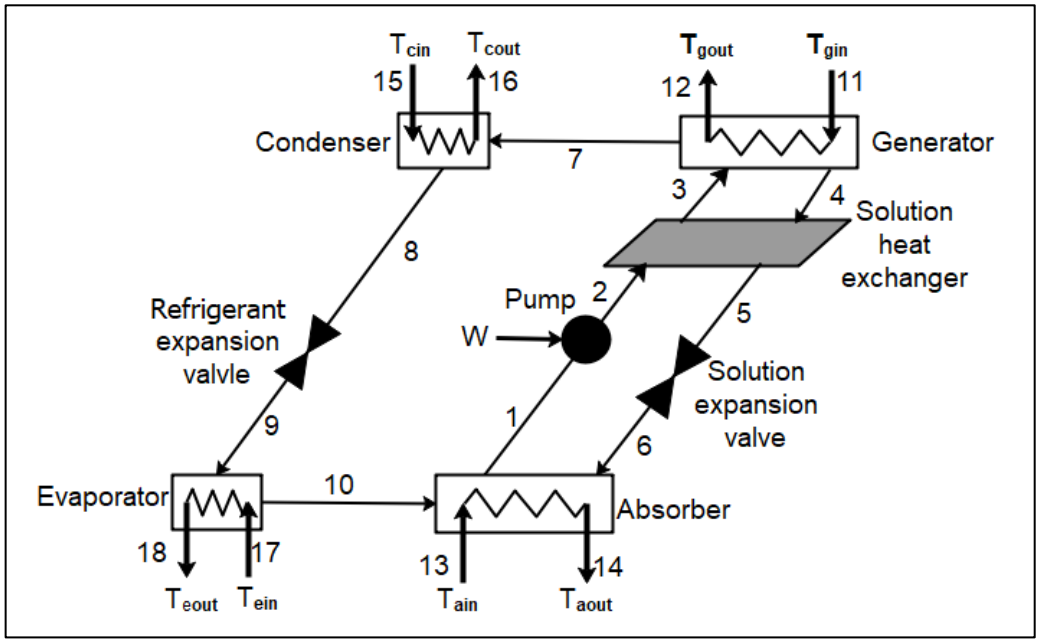

Figure 4.6. Single Effect LiBr Absorption Chiller Diagram

At each point of the diagram, the state of the fluid is defined by the temperature "T", the pressure "P", the concentration of lithium bromide "x", the enthalpy "h", the mass flow rate "m" and the quality "y" or vapor fraction of the fluid. If the fluid is a pure substance (water only for point 7-18) two parameters are enough to define the state of the fluid. However, if the fluid is a mixture, the concentration ratio "x" is needed in addition to the other two parameters to define the state of the fluid. The energy transfer in the system is often modeled using the UA model or the effectiveness model. They are explained with the example below. Consider the heat exchanger in figure 4.7 with inlet-outlet temperature for hot water and cold water noted T_H and T_C respectively.

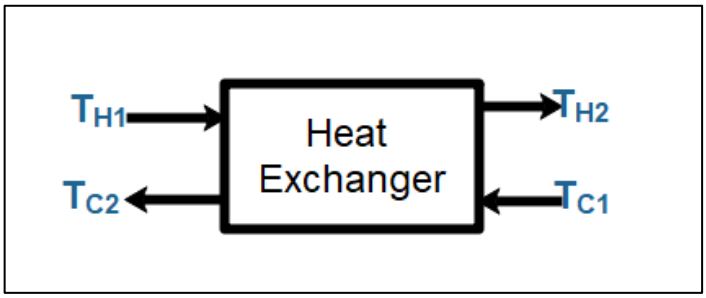

Figure 4.7. Counter Flow Heat Exchanger

Heat Exchanger UA model

In this model, the overall heat transfer coefficient U and the heat transfer area A of the heat exchanger are specified as a "UA" value. The heat transferred is given in equation 4.1 where ΔT_{LM} is the log mean temperature difference of the hot/cold fluids.

$$Q = UA\Delta T_{LM} \tag{4.1}$$

$$\Delta T_{LM} = \frac{(T_{h1}-T_{c1})-(T_{h2}-T_{c2})}{\ln\left(\frac{T_{h1}-T_{c1}}{T_{h2}-T_{c2}}\right)} \tag{4.2}$$

where $Q[W]$ is the heat exchanger heat transferred, $U[Wm^{-2}C^{-1}]$ the heat exchanger heat transfert coefficient, $A[m^2]$ the heat exchanger heat transfert area, $\Delta T_{LM}[°C]$ the heat exchanger logmean temperature difference, $T_h/T_c[°C]$ the heat exchanger hot/cold ends temperatures. The challenge with equation 4.1 is that the U value is function of other parameters such as the fluid state and the mass flow rate. It can lead to wrong results if those values deviate far from the heat exchanger rated values.

Heat Exchanger Effectiveness Model

In this model, the ratio of the actual heat transfer over the maximum possible heat transfer is specified as the effectiveness of the heat exchanger. The actual heat transfer can be taken on either cold or hot side ($mc_p\Delta T$). The maximum heat transfer occurs when the hot fluid exits at the cold fluid inlet temperature. However, in order to match the heat lost by the hot fluid to the heat gained by the cold fluid, the minimum heat capacity of the two fluids should be used to calculate the heat transfered. The equation is given by:

$$\varepsilon = \frac{(m_c c_{pc})(T_{c2} - T_{c1})}{(mc_p)_{min}(T_{h1} - T_{c2})} \tag{4.3}$$

where $\varepsilon[-]$ is the heat exchanger effectiveness, $mc_p[kJC^{-1}]$ the heat capacity of cold side fluid, $mc_p[kJC^{-1}]$ the heat capacity of either fluids, $T_h/T_c[°C]$ the heat exchange hot/cold ends temperatures. Strictly speaking, equation 4.3 is valid when there is no phase change in the heat transfer process. However in the case that phase change occurs, it is still used by assuming that the non-phase change side has the minimum heat capacity. In the particular case where both heat capacity rates are nearly the same (Case for solution heat exchanger), the equation resume to:

$$\varepsilon = \frac{(T_{c1} - T_{c2})}{(T_{h1} - T_{c2})} = \frac{(T_{h1} - T_{h2})}{(T_{h1} - T_{c2})} \tag{4.4}$$

By reference to the Single Effect LiBr Absorption Chiller Diagram in figure 19 above, the energy balance (EB) and mass balance (MB) are written for each component using the mass flow rate "m", the LiBr concentration "x", the fluid (H_2O/ LiBr) enthalpy "h", the node pressure "P", the pump work input W, and the heat transfer equations defined previously.

Generator

$MB_{mixture}$: $m_3 = m_7 + m_4$

MB_{libr}: $m_3 x_3 = m_7 x_7 + m_4 x_4$

MB_{H2O}: $m_3(1 - x_3) = m_7(1 - x_7) + m_4(1 - x_4)$

$MB_{hot\ fluid}$: $m_{11} = m_{12}$

EB: $m_3 h_3 + m_{11} h_{11} = m_4 h_4 + m_7 h_7 + m_{12} h_{12}$

$Q_g = UA_g \Delta T_{LM_g} = m_{11}(h_{11} - h_{12})$

$\Delta T_{LM_g} = \frac{(T_{11} - T_4) - (T_{12} - T_7)}{\ln(\frac{T_{11} - T_4}{T_{12} - T_7})}$

Condenser

$MB_{refrigerant}$: $m_7 = m_8$

$MB_{cooling\ water}$: $m_{15} = m_{16}$

EB: $m_7 h_7 + m_{15} h_{15} = m_8 h_8 + m_{16} h_{16}$

$Q_c = UA_c \Delta T_{LM_c} = m_{15}(h_{16} - h_{15})$

$\Delta T_{LM_c} = \frac{(T_{15} - T_8) - (T_{16} - T_8)}{\ln(\frac{T_{15} - T_8}{T_{16} - T_8})}$

Throttling valve

MB: $m_8 = m_9$

EB: $h_8 = h_9$

Evaporator

$MB_{refrigerant}$: $m_9 = m_{10}$

$MB_{chilled\ water}$: $m_{17} = m_{18}$

EB: $m_9 h_9 + m_{17} h_{17} = m_{10} h_{10} + m_{18} h_{18}$

$Q_e = UA_e \Delta T_{LM_e} = m_{17}(h_{17} - h_{18})$

$\Delta T_{LM_e} = \frac{(T_{17} - T_{10}) - (T_{18} - T_9)}{\ln(\frac{T_{17} - T_{10}}{T_{18} - T_9})}$

Absorber

$MB_{mixture}$: $m_6 + m_{10} = m_1$

MB_{libr}: $m_6 x_6 + m_{10} x_{10} = m_1 x_1$

MB_{H2O}: $m_6(1 - x_6) + m_{10}(1 - x_{10}) = m_1(1 - x_1)$

$MB_{hot\ fluid}$: $m_{13} = m_{14}$

EB: $m_6 h_6 + m_{10} h_{10} + m_{13} h_{13} = m_1 h_1 + m_{14} h_{14}$

$Q_a = UA_a \Delta T_{LM_a} = m_{13}(h_{14} - h_{13})$

$\Delta T_{LM_a} = \frac{(T_6 - T_{14}) - (T_1 - T_{13})}{\ln(\frac{T_6 - T_{14}}{T_1 - T_{13}})}$

Pump

MB: $m_1 = m_2$

EB: $W + m_1 h_1 = m_2 h_2$

$W = \frac{(P_2 - P_1) v m_1}{\eta_{Pump}}$

Solution expansion valve

MB: $m_5 = m_6$

EB: $m_5 h_5 = m_6 h_6$

Solution heat exchanger

MB: $m_2 = m_3$

$m_4 = m_5$

EB: $m_2 h_2 + m_4 h_4 = m_3 h_3 + m_4 h_4$

$Q_{SHX} = \varepsilon_{shx} m_4 c_{p4}(T_4 - T_5)$

$Q_{SHX} = m_4(h_4 - h_5)$

$\varepsilon_{SHX} = \frac{T_4 - T_5}{T_4 - T_2}$

Using Engineering Equation Solver (EES), the equations can be solved on a click as long as the number of unknows match with the number of equations. To this end some assumptions about the state of the fluids at some points are made below:

- At node 1, there is no vapor in the mixture; quality=0
- At node 4, the fluid is completely in a liquid state; quality=0
- At node 7, the refrigerant is in a vapor state; quality=1
- At node 7, there is only pure refrigerant x=0
- At node 8 refrigerant has completely condensed quality =0

More details of ACH calculations and EES codes for different types of chiller can be found in "absorption chillers and heat pumps" book [64]. Figures 4.8-4.10 show the effects of the chiller three fluids stream temperatures on the COP and the cooling capacity.

- From figure 21, it can be seen that after the generator temperature surpasses the minimum required inlet temperature, the COP variation becomes negligible. However, for the cooling capacity, it is linearly proportional to generator temperate.
- From figure 22, increasing the evaporator inlet temperature doesn't increase significantly the COP. However, the cooling capacity is showing a tendency to slightly increase with increasing evaporator temperature.
- From figure 23, increasing the cooling water temperature doesn't affect much the COP but the cooling capacity decreases linearly proportional.

From these 3 observations, it can be concluded that absorption chillers are constant COP machines when operated within the design specifications and the effect of fluid streams temperature variation is to modulate the cooling capacity.

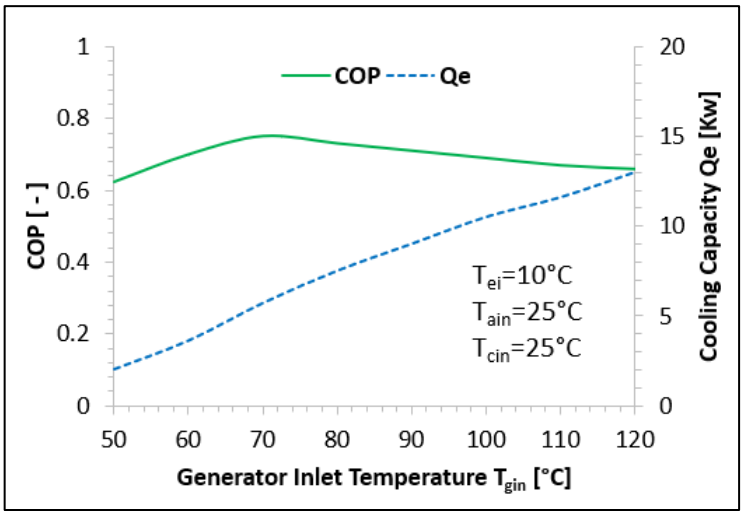

Figure 4.8.Generator Temperature Effect on COP and Cooling Capacity

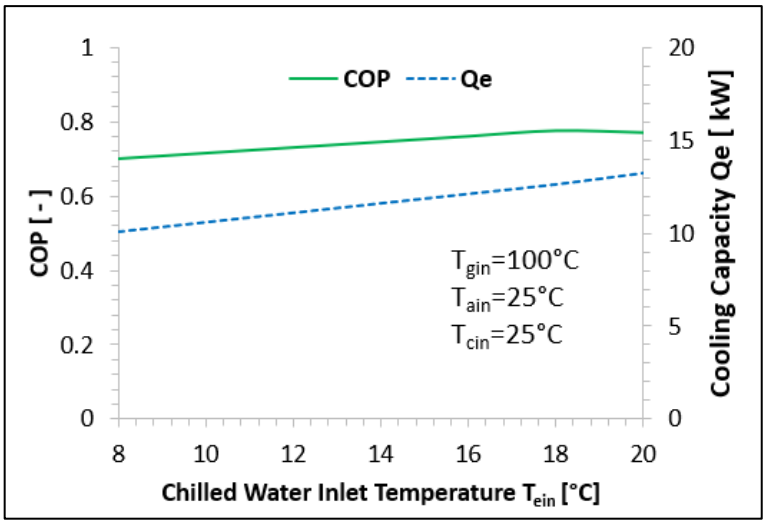

Figure 4.9. Chilled Water Temperature Effect on COP and Cooling Capacity

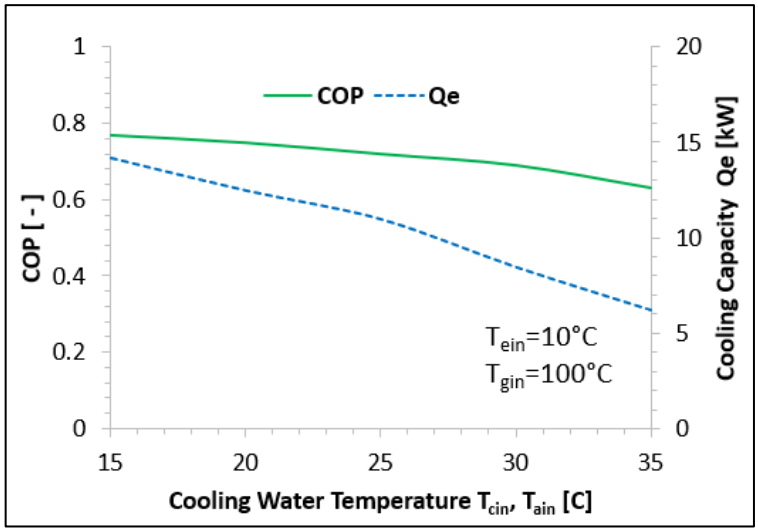

Figure 4.10. Cooling Water Temperature Effect on COP and Cooling Capacity

The chiller mass/energy balance equations mentioned above are useful in the design phase for system optimization. They are more suitable for steady-state analysis, or parametric analysis by changing a variable at a time. However, for system integration it is tedious to solve these equations simultaneously when all fluid inlet temperatures are changing, cooling load is changing and the efficiencies of heat exchangers are changing. The most used model for system integration is the characteristic temperature "ΔΔT" function model that determines the performance of the chiller using external fluid streams data. It uses the average temperatures of the 3 fluid streams (Generator, Evaporator, and Absorber-Condenser) to express their corresponding heat flow as well as the COP of the machine. ΔΔT is given by:

$$\Delta\Delta T = T_G + aT_{AC} + eT_E \tag{4.5}$$

where $\Delta\Delta T[°C]$ is the characteristic temperature function,$T_G/T_{AC}/T_E[°C]$ the generator, absorber-condenser, and the evaporator mean temperatures, and $a, e[-]$ are coefficients charateristics of the chiller.

The cooling power Q_E, the generator power Q_G, the heat rejection rate of the absorber and condenser Q_{AC} and the COP are then given by the following equations where the constants again depend on the chiller.

$$Q_E = s_E\Delta\Delta T + r_E \tag{4.6}$$

$$Q_G = s_G\Delta\Delta T + r_G \tag{4.7}$$

$$Q_{AC} = Q_E + Q_G \tag{4.8}$$

$$COP = \frac{Q_E}{Q_G} \tag{4.9}$$

where $Q_E/Q_G/Q_{AC}[kW]$ are the evaporator, generator, absorber-condenser powers, $s_E, r_E, s_G, r_G[-]$ constants characteristics of the chiller, and $COP[-]$ the coefficient of performance of the chiller. The COP is calculated without the work input of the solution-pump because it is negligible (<0.01% of heat) compared to heat power. The constants "a, e, s, r," in equations 4.5-4.9 are obtained through a regression analysis by using the manufacturer provided test dataset. The drawback of this model is that it is limited to a narrow range of fluid temperature inputs. Once the operating conditions are far from the predetermined operation range, the validity of the equation becomes questionable.

4.4. Cooling Tower

The cooling of the condenser of the thermal engine is an importing parameter that determines the efficiency of the system. There are generally three types of cooling techniques employed to remove heat from a condenser: dry cooling, liquid cooling, and evaporative cooling. The first method uses ambient air as a heat sink. Since air is free and doesn't have any availability issues, this method is often the first one to be considered. In hot day however, the high temperature of air makes it less ideal as a heat sink. Liquid cooling uses a large body of water (river, sea, lac) as a cooling medium. At the same flow rate, water has a convective heat transfer coefficient much higher than that of air, which provides a higher heat removal rate. When a natural water reservoir is not available, evaporative cooling tower is an effective way to cool a condenser. It takes advantage of the high latent heat of vaporization of water to cool a large volume of water by evaporating a fraction of the water. Water consumption is the major drawback of this technique so it is not ideal for desert regions where water is scarce.

Figure 4.11. Commercial Cooling Tower [65]

An induced draft counterflow cooling tower (CT) with a fill is used [66]. Hot water enters the tower from the top and flows down through the fill. A fan on the top is sucking air from the bottom of the tower, blowing through the wet fill, evaporating a small fraction of water. For evaporation to occur, a fraction of water absorbs latent heat

from the bulk water thus creating the cooling effect. Water vapor is discharged from the top of the tower. The cooling efficiency of CT is given by [67]:

$$\varepsilon = \frac{T_{inh} - T_{outc}}{T_{inh} - T_{wb}} \tag{4.10}$$

where $\varepsilon[-]$ is the cooling efficiency, $T_{inh}[°C]$ the cooling tower hot water inlet temperature, $T_{outc}[°C]$ the cooling tower cool water outlet temperature, and $T_{wb}[°C]$ the wet bulb temperature. The efficiency and the outlet temperature are unknown, so another expression is needed to solve equation 4.10. A correlation detailed by Mansour et al. [68] is used to calculate the CT efficiency as following.

$$\varepsilon = \frac{\varepsilon^*}{\varepsilon^* + 1} \tag{4.11}$$

$$\varepsilon^* = \frac{CroNTU}{1 - 0.5NTU\left(Cro - \frac{L}{G}\right)} \tag{4.12}$$

$$NTU = c\left(\frac{L}{G}\right)^{n+1} \tag{4.13}$$

$$Cro = \frac{b}{C_p} \tag{4.14}$$

$$h_s = a + bT_{wb} \tag{4.15}$$

In the "NTU" term in equation 4.13, "L/G" represents the liquid-gas (water-air) flow ratio. Nailing et al. [67] in their study of the effect of air-water flow ratio on counterflow cooling tower found that a ratio of 0.83 was the optimum value so this number is used in this thesis. However, the optimum value has been reported to varies depending on ambient conditions and the fill type, so care must be taken when using it. One should ensure that cooling tower material is the same as that used in the study to expect more accurate results from the formula. The constants "c" and "n" are characteristics of the tower, obtained experimentally. They depend on the geometry of the tower and the roughness of the fill material. Typical values of "c" range from 1.5 to 4, while that of "n" range from -0.4 to -0.8. CT used by Nailing et al. [67] with c=2.3 and n=-0.72 is selected for the study. These values are close to the default values of CT parameters used in TRNSYS. In the "Cro" term, b is the slope coefficient in equation 4.15 which express the saturation enthalpy h_s of water vapor as a function of wet bulb temperature T_{wb}. C_p is the specific heat capacity of water. With Equations 4.11-4.15, the outlet temperature of the CT can be calculated.

4.5. Ground Source Heat Exchanger

Ground source heat exchanger is a technology that uses the earth massif heat capacity as a heat source or as a heat sink. The specific heat capacity of the earth is typically 2 times less than that of water depending on the soil; meaning for the same volume, water can store heat 2 times more than the earth. Table 4.2 shows the properties of different soils. It should be noted that these values are affected by the earth moisture content, so they can change from time to time depending on weather conditions such as rain, snow, groundwater level and so on.

On a large space-time scale, the earth-sun thermal interaction is close to a steady state system behavior. The energy received by the earth from the sun on daytime warm up the atmosphere, buildings and trees, then at night this energy is lost back to space through radiation at low sky temperature. This energy balance keeps the earth at a nearly constant temperature. However, due to the massif release of greenhouse gases in the atmosphere, the gases reflect earth emitted radiation back to earth rather than letting it back to space. Therefore, the earth is gradually warming up, destroying the natural equilibrium set millions of years ago.

Due to the earth-sun quasi-thermal balance, the average annual surface temperature is the same as the deep ground temperature. The closer to the surface a point is, the more temperature fluctuation it will experience. This being a direct consequence of the daily and seasonal air temperature variations. The soil temperature as a function of the depth and day number is given in equation 4.16.

$$T(z,t) = T_a + A_0 e^{-\frac{z}{d}} \sin\left(\frac{2\pi(t-t_0)}{365} - \frac{z}{d} - \frac{\pi}{2}\right) \tag{4.16}$$

$$d = \left(\frac{2D_h}{\omega}\right)^{0.5} \tag{4.17}$$

where $T_a[°C]$ is the average ambient air temperature, $A_0[°C]$ the ambient temperature amplitude, $z[m]$ Depth in the soil, $D_h[m^2/s]$ the soil thermal diffusivity, $\omega[-]$ the constant equal to 2π/365, $t[day]$ the day number of the year, $t_0[day]$ a time lag from abritrary date.

Figure 4.12 shows the earth annual temperature for different depth in Izmir. Average ambient temperature and its amplitude are set to 15°C, while the thermal diffusivity is taken for granite soil. At 20m depth, the annual temperature variation is less than 5% of the average temperature. Also, there is a lag between temperature peak at different depths. This is due to the finite time heat needs to move from an earth layer to the next one. The earth temperature gradient has lead engineers to design two type of ground source heat exchanger: Horizontal ground heat exchangers that are installed at a depth typically less than 5m and vertical borehole heat exchangers that are installed at a depth typically between 20m and 200m.

Table 4.2. Soils Properties [69]

Soil Type	**Density [kg/m^3]**	**Thermal conductivity [W/m°C]**	**Heat capacity [kJ/kg.°C]**	**Thermal diffusivity [m^2/s]**
Clay	1500	1.4	880	1.06×10^{-6}
Limestone	2500	1.3	900	5.77×10^{-7}
Granite	2640	3	820	1.38×10^{-6}

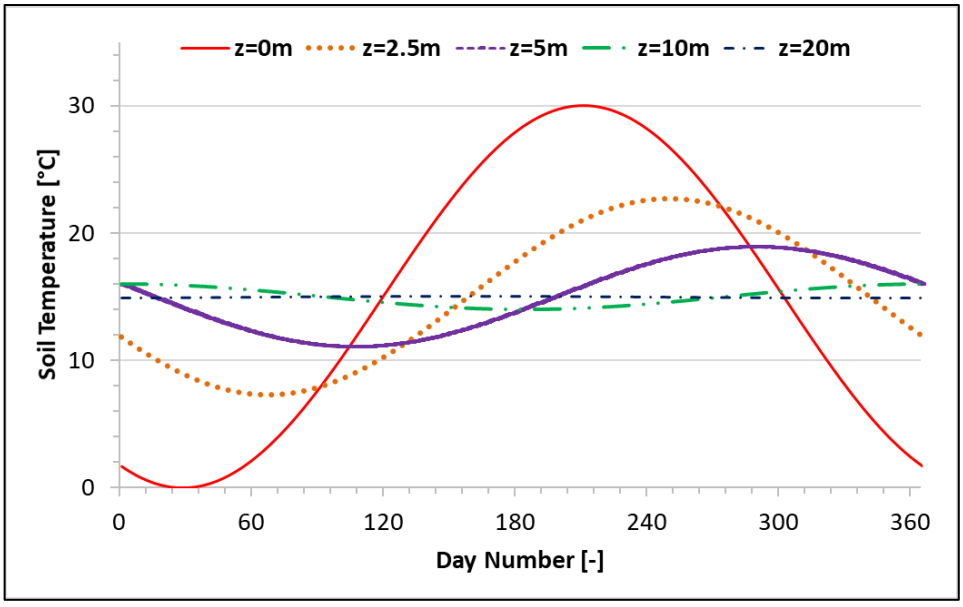

Figure 4.12. Earth Annual Temperature at Different Depth

The horizontal ground heat exchanger show in figure 4.13 is installed by laying at a moderate depth (1-3m) horizontal pipes in which a heat transfer fluid (HTF) is circulated to extract or reject heat from/to the ground. Water is commonly used as a

HTF. In the area where the surface temperature is negative part of the year, glycol is added to water to prevent freezing. The specific heat extraction/rejection possible with these systems is typically between 10 W - 30 W per m^2 heat transfer area. Horizontal ground heat exchangers suffer from the requirement of large land to provide sufficient heat transfer. This is a drawback especially for a commercial building or densely populated cities. Also, due to the proximity to earth, the system is much more affected by the ground surface temperature variations, which doesn't guaranty a long term stable performance.

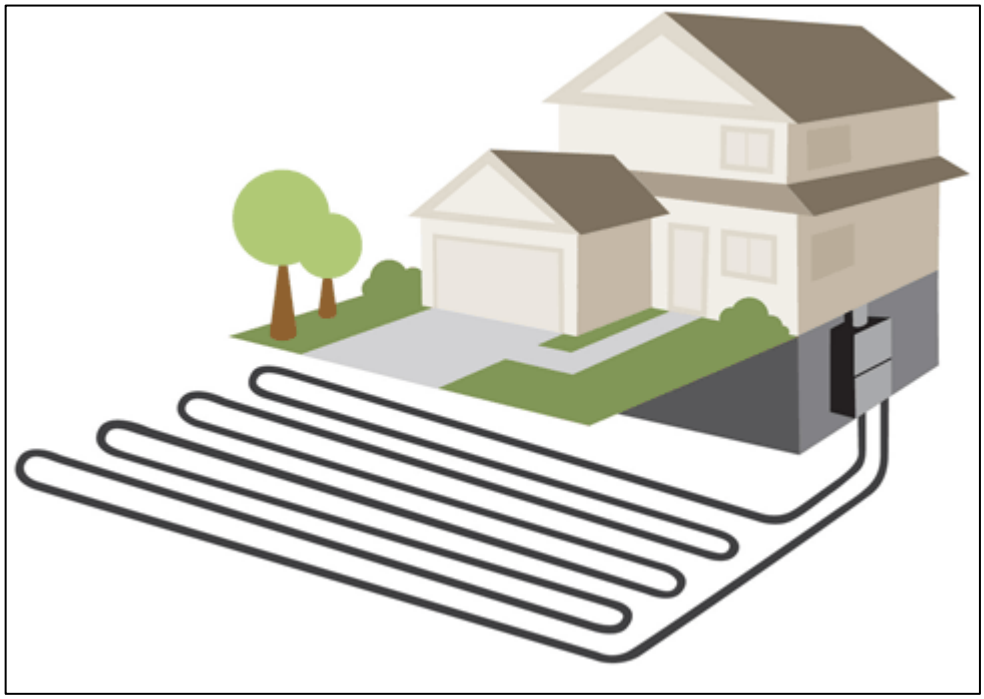

Figure 4.13. Horizontal Ground Source Heat Exchanger

Vertical ground heat exchanger is installed by drilling a hole deep tens of meters and inserting in a U tubes in which the HTF circulates to extract/reject heat from the ground. A schematic of the system is shown in figure 4.14. Below 20m-30m the undisturbed soil temperature is almost constant all year round, allowing a more stable performance to be expected compared to the horizontal system. In an attempt to improve the system efficiency, different configurations of the heat exchanger tubes have been proposed. Three of them are shown in figure 4.15. In the double U pipe, two U pipes are placed in a borehole. It saves drilling cost, however thermal interaction between legs of the tubes reduces the effective heat transfer rate. In coaxial tube configuration, hot fluid enters the tube through the outer flow space to allow for maximum heat transfer with the earth

since this surface has the largest area. The return fluid is collected through the central tube. Vertical borehole occupies less land compared to the horizontal heat exchanger. The specific heat transfer can reach 50 W per meter of tube. In an application where a single borehole has impractical length to satisfy the heat transfer area requirement, multiple boreholes field is done. The shape of the field whether it is a square, a rectangle, circular or more irregular will affect the thermal interaction between boreholes, complicating the thermal analysis of the system.

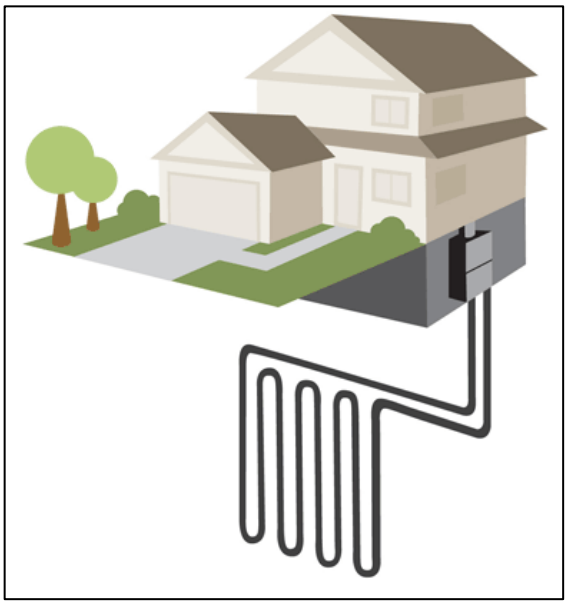

Figure 4.14. Vertical Ground Source Heat Exchanger

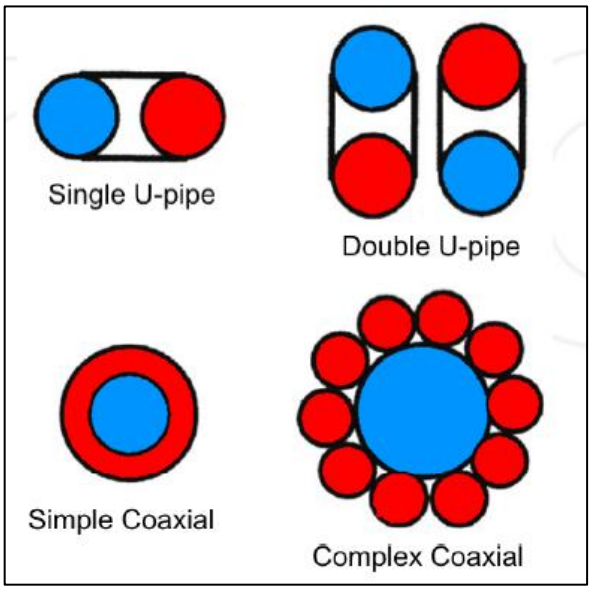

Figure 4.15. Single Vertical Borehole& Tubes Design

4.6. Borehole Thermal Energy Storage Calculations

There are different models in the literature for borehole thermal energy analysis. There are Ingersoll model, IGSHPA approach, Hellstrom model, Kavanaugh approach and Eskilson model. The latest one is the most used for engineering application because it has a compact mathematical model for multiple boreholes analysis. The borehole heat transfer calculations are governed by basics convection, conduction heat transfer equations. To understand the concept, a single borehole with the equivalent thermal resistance network is shown in figure 4.16.

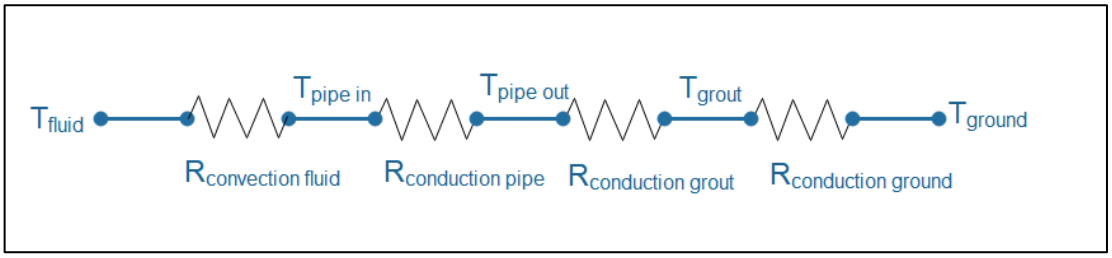

Figure 4.16. Borehole Thermal Resistance Network

From inside the pipe at a temperature T_{fluid}, heat flows through the wall of the pipe, the grout, then diffuse gradually into the ground, leaving the far field ground temperature T_{ground} undisturbed. Water flowing inside the pipe has a corresponding convective heat transfer coefficient which depends on the mass flow rate, the properties of the fluid and the roughness of the pipe inner surface. If either laminar flow or turbulent flow occurs, the convection resistance $R_{convection\text{-}fluid}$ is usually negligible compared to the most significant resistance, $R_{conduction\text{-}ground}$. The smallest resistance in the network is that of the pipe resistance $R_{conduction\text{-}pipe}$, because of the thickness being in the order of 2-5mm. PVC tube is the most common material for borehole U tube as it is relatively cheap compared to metal tube, and it also has less long-term performance degradation issues. The grout resistance $R_{conductive\ grout}$ can be modulated by selecting the most appropriate filling material. The total borehole resistance is then:

$$R_{total} = R_{fluid} + R_{pipe} + R_{grout} + R_{ground} \tag{4.18}$$

When a unit heat q[W/m] is flowing from the borehole to the ground or vis-versa, the grout-ground temperature difference ΔT_r is given by

$$\Delta T_r = T_{grout} - T_{ground} = qR_{ground} \tag{4.19}$$

If determining the borehole thermal resistance R_{bh} (R_{fluid}, R_{pipe} and R_{grout}) are straightforward, the ground resistance calculations is a very challenging task capable of spoiling a student's whole weekend. In fact, the ground resistance is complex to evaluate as it depends on many factors such as the ground properties (Conductivity, heat capacity, density), the U tubes configuration (diameter, material, legs spacing) and the boreholes configurations if multiple boreholes are used. To solve these difficulties, Eskilson combined the total ground resistance using a single non-dimensional number referred as the g function. The ground unit resistance R_{ground} is then defined as:

$$R_{ground} = \frac{g}{2k_{ground}\pi} \tag{4.20}$$

$$\Delta T_r = \frac{q}{2k_{ground}\pi} g \tag{4.21}$$

Where q[W/m] is the heat injection/extraction per meter. For a single borehole or when the boreholes spacing is greater than $r_\infty = 4\sqrt{\alpha t}$, the g function is only function of time, the borehole geometry and the ground thermal diffusivity as show in equation 4.22.

$$g\left(\frac{t}{t_s}, \frac{r}{H}\right) = \begin{cases} \ln\left(\frac{H}{2r}\right) + \frac{1}{2}\ln\left(\frac{t}{t_s}\right) & , \frac{5r^2}{\alpha} < t < t_s \\ \ln\left(\frac{H}{2r}\right) & , t > t_s \end{cases} \tag{4.22}$$

where $g[-]$ is the g-function, $t[s]$ the time, $r[m]$ the borehole radius, $H[m]$ the borehole depth, $\alpha[\,m^2 s^{-1}]$ the soil thermal diffusivity, $t_s[s] = H^2/9\alpha$ the characteristic time scale, or steady state time. t_s of often over 3 decades, which means heat transfer in the ground is by essence a transient process. The borehole equations given above assumes a constant heat flow which is seldom the case for daily engineering applications such as building cooling/heating. To accommodate with the load variation, a superimposition technique know as load aggregation is used. The first heat pulse is assumed constant over the entire analysis time, then for the next heat pulse, an imaginary heat pulse is set such that the sum of the previous heat pulse and the imaginary heat pulse is equal to the real heat pulse. The process is repeated until the last heat pulse occurs. As the number of time steps grows, the computation efforts become more and more demanding, but this is the current well know way of dealing with varying load. Load aggregation is used to calculate borehole temperature as:

$$\Delta T_r = \sum_{i=1}^{n} \frac{q_i - q_{i-1}}{2\pi k} g\left(\frac{t_n - t_{i-1}}{t_s}, \frac{r_b}{H}\right) \tag{4.22}$$

$$T_{fluid} = T_{grd} + \sum_{i=1}^{n} \frac{q_i - q_{i-1}}{2\pi k} g\left(\frac{t_n - t_{i-1}}{t_s}, \frac{r_b}{H}\right) + q_i R_{bh} \quad (4.23)$$

where $q_i[Wm^{-1}]$ is the power extracted or rejected per meter, $T_{bh}[°C]$ the average borehole temperature, T_{grd} $[°C]$ the undisturbed ground temperature, k $[W/m°C]$ the ground thermal conductivity, $g[-]$ the g-function, r_b $[m]$ the borehole radius,$i[h]$: the time step index, $H[m]$ the borehole depth, $t_s = \frac{H^2}{9\alpha}[s]$ the time scale. Once the heat rejected/extracted from the ground and the fluid mean temperature are known, the outlet temperature is calculated using a simple energy balance $Q = mC_p\Delta T$.

CHAPTER 5

METHODOLOGY

5.1. Simulation Software

5.1.1. EES

Engineering Equation Solver (EES) is a very powerful tool for the design and optimization of engineering devices. Its power relies on its ability to solve a system of linear and nonlinear equations simultaneously. The writing order of the equations doesn't matter for the program. For absorption chiller analysis, the energy balance and mass balance equations for all nodes of the machine are entered into the program and the solution is obtained in a simple click. Fluids such as water, ammonia, lithium bromide already have their state properties built in, thus avoiding the hassle of evaluating non-linear parameters such as enthalpy, specific volume, quality, temperature, pressure, and others. Despite its simplicity, EES is limited to steady-state analysis which is only a part of the engineering system analysis requirement. However, the software still allows parametric study which is the summation of multiple steady-state simulations. In the design of the chiller, it has been a useful tool in understanding the internal operation of the machine.

5.1.2. TRNSYS

TRNSYS (Pronounced trans-sys) is a software suitable for the simulation of energy systems. It is labeled as a transient system simulator however steady-state solution can be obtained by setting the simulation time long enough to reach the steady period of the system. Solar photovoltaic plants analysis, building energy consumption study, fuel cell system integration, the library of TRNSYS has the components used in these energy systems so the analysis can be made faster by using these built-in models. Also, non-existing components can be modeled in others software such as EES, Matlab or Excel and connected to TRNSYS for a dynamic simulation. The software has typical

meteorological year data (TMY) for hundreds of cities in all continents. This is a handful resource for the analysis of weather-dependent systems such as solar thermal plant, wind farm, and air conditioning. Data used in this thesis (solar insolation, dry bulb temperature, wet bulb temperature) has been extracted from TRNSYS. Equivalent data given by SODA-PRO, a weather data company are compared with that of TRNSYS in table 8. It shows that the average error is 10.4%, -2.5%, 8.9% for solar radiation, dry bulb temperature, and relative humidity respectively. In addition to weather data, TRNSYS provided the cooling tower for one of the system under study. The cooling tower code for other systems has been calibrated based on the predicted performance indicated by TRNSYS.

5.1.3. MATLAB

MATLAB is a well know software in the academic field. It is a robust simulation tool especially for systems having data in vectors of matrix forms. For simulation of the thermal system, the usage of the software is not straightforward like TRNSYS because of the lack of built-in components library. For C language-like programmers it is relatively easy to use MATLAB for simple algebraic iterative operations. Like TRNSYS, MATLAB can also work with excel data to improve simulation flexibility. All systems workflow in the thesis is coded using MATLAB far case A and Case C.

5.2. Typical Meteorological Year Data

Weather data is very important for renewable energy system analysis. For solar energy and wind energy, the instantaneous harvested power is directly proportional to solar radiation, ambient temperature, and wind speed. For hydropower, the effect of weather on power is in the long term. To assess the feasibility of renewable energy project, a weather forecast data of up to 25-30 years is often required by investors as a mean to reduce the uncertainty of their investment. Weather forecast for such a long time is nearly impossible. Historical weather data of the project is used to provide a realistic average condition likely to occur during the life cycle of the project. This representative year data is known as the Typical Meteorological Year (TMY). To generate TMY data, the average weather value of the last 25-30 years is recorder. The

value of a particular year that has the less deviation from the 25-30 years average is kept as the value of the TMY. Despite this cautious approach, TMY data from different sources may differ significantly. This is due to the difference is ground measurement devices, and also the difference in data interpolation methods used to predict weather condition in locations not covered by the meteorological survey. In table 5.1 are shown İzmir TMY data from TRNSYS and from SODA-Pro (Professional solar data software). As it can be seen, the error between the two sources can be as little as 2.3% or as big as 43.7% depending on the parameters. Since TRNSYS is well known in the academic field, its weather database has been used for the simulation.

Table 5.1. TRNSYS Vs SODAPRO TMY Data

Solar Radiation		TRNSYS	SODA-PRO	ERROR% Ref-TRNSYS	ERROR% Ref-SODAPRO
Annual Radiation [kWh/m^2/year]	DNI	1443.9	1919.0	32.9	-24.8
	Diffuse	808.6	562.6	-30.4	43.7
	Reflected	54.6	65.4	19.7	-16.4
	Global	2307.1	2547.0	10.4	-9.4
24h-DNI [W/m^2]	Minimum	0.0	0.0	0.0	0.0
	Maximum	855.7	1042.0	21.8	-17.9
	Average	164.8	219.1	32.9	-24.8
24h-Diffuse [W/m^2]	Minimum	0.0	0.0	0.0	0.0
	Maximum	491.1	356.0	-27.5	37.9
	Average	92.3	64.2	-30.4	43.7
24h-Reflected [W/m^2]	Minimum	0.0	0.0	0.0	0.0
	Maximum	25.3	33.0	30.3	-23.3
	Average	6.2	7.5	19.7	-16.4
24h-Global [W/m^2]	Minimum	0.0	0.0	0.0	0.0
	Maximum	1045.5	1136.0	8.7	-8.0
	Average	263.4	290.8	10.4	-9.4
Ambient Temperature [°C]	Minimum	-3.1	-2.7	-12.3	14.1
	Maximum	38.0	39.7	4.5	-4.3
	Average	17.1	16.6	-2.5	2.6
Relative Humidity [RH%]	Minimum	26.5	14.8	-44.2	79.3
	Maximum	99.0	111.2	12.3	-10.9
	Average	60.8	66.2	8.9	-8.1

5.3. Building Load Information

5.3.1. Building Information

A building located in Izmir city has been chosen as the load of the systems under study. The building named OZDILEK has a shopping center as well as a five stars hotel. Our analysis is focused on the shopping mall only. It is next to a touristic area, so it is a well-crowded mall. From data collected in 2003 by Canbay et al. [70], the mall welcome 11000 people on weekdays from 9:00 to 22:00 and 20000 people on the weekend from 9:00 to 23:00. The mall is divided into five air conditioning zones in two floors which total an area of 16000 m^2. The cooling is done by 3 electric driven central chillers with a total cooling capacity of 1020 kW while the heating is done by 2 LPG gas fired boilers with a total capacity of 840 kW. The chiller has been reported to operate 28 weeks per year or 2674 hours from April to November while no information was given for the boiler. The heat load of a building depends on two factors: the heat gain/loss through the wall and the internal heat generation. The first parameter depends on the wall material (bricks, glass, insulation) on the inside-outside temperature difference, and the inside-outside convective heat transfer coefficient. The second parameter depends on the building occupancy and the heat generated by electric equipment. The hourly occupancy ratio is given in figure 5.1.

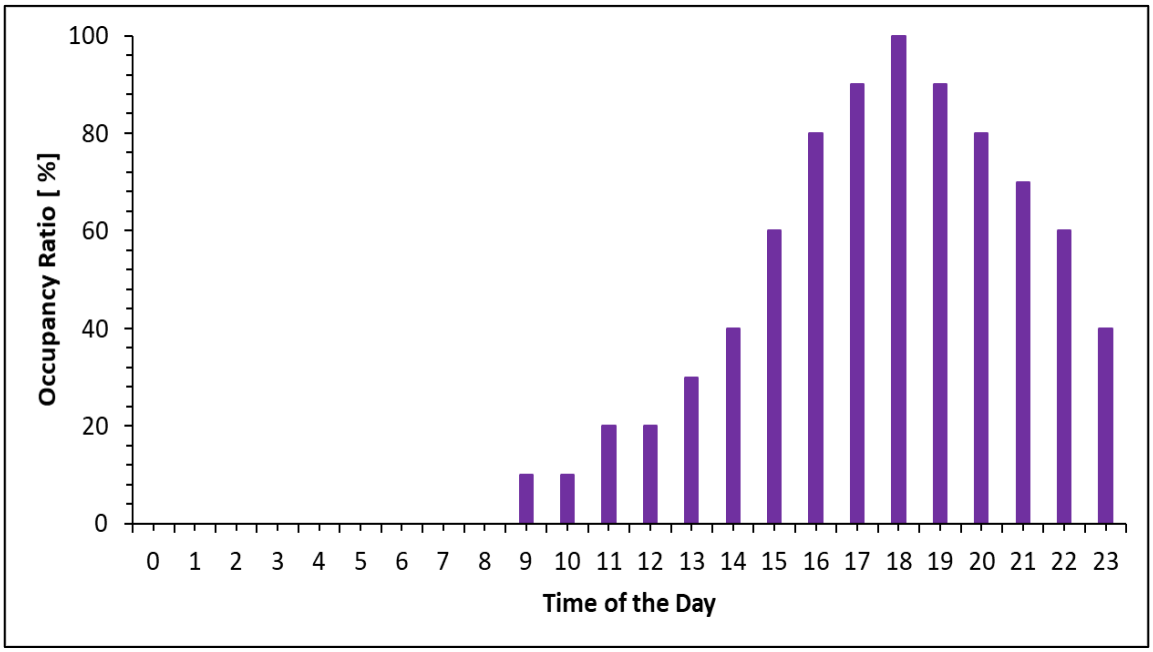

Figure 5.1. Building Daily Occupancy Ratio [70]

5.3.2. Load Profile Data Generation

To model the cooling/heating system, an hourly heat load profile is necessary (the smaller the time step the more accurate the result is, but more computational effort is required). Since no hourly information was given, the hourly heat load profile has been made by considering the maximum cooling capacity and by making the following assumptions:

- Heat load is only a function of internal heat generation. Since the building has a high occupancy reaching up to 20 000 people, daily internal heat generation is far the most important contributor to shaping the heat profile. Also, there are industrial cooling devices, electrical equipment, restaurant cooking pots and so on generating heat in the building which makes this assumption stronger.

- Environmental temperature variation has a negligible effect of heat profile. The daytime temperature fluctuation being typically less than 10°C and the building being well insulated, outside temperature variation doesn't impact well the heat load profile. Also, the Radiation heat gain/loss is negligible.

Determination of cooling load:

1- Maximum cooling capacity is 1020 kW
2- Heat load is proportional to the occupancy ratio
3- Minimum chiller heat load is 10%
4- The chiller operates 14 hours a day (9:00-23:00) from May 1 to October 30

The generated cooling load is shown in figure 5.2.

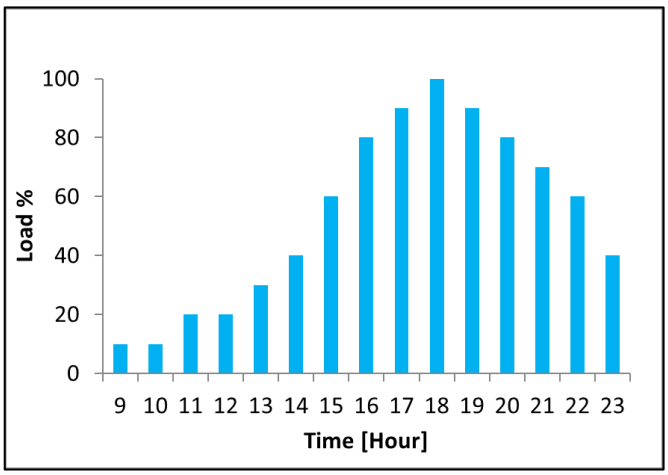

Figure 5.2. Building Cooling Load

Determination of heating load:

1- Maximum heating capacity is 840 kW
2- Heat load is proportional to the complement of the occupancy ratio
3- Minimum heat load is 10%
4- From heat load calculation result using LPG bill, the maximum heat load is 756 kW. Using the assumptions above, 84 kW is added to the hourly load to bring the maximum to 840 kW.
5- The boiler operates 14 hours a day (9:00-23:00) from November 1 to April 30

The generated heating load is shown in figure 5.3.

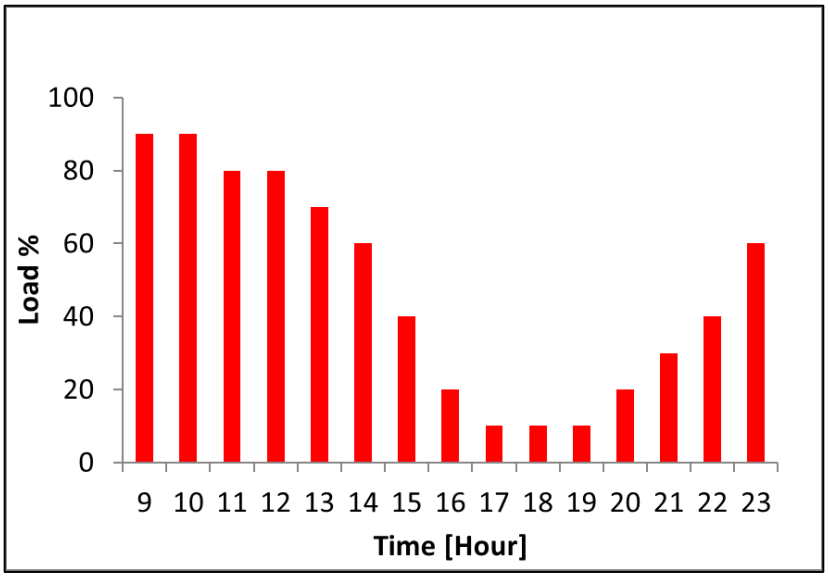

Figure 5.3. Building Heating Load

5.4. Case A Systems (Chiller & Boreholes)

5.4.1. Systems Description

In this case study, a reference system consisting of a solar collector, a single hot storage tank, a backup boiler, an absorption chiller, a cooling tower, and the building is considered. Two models are then proposed, the first model adding a second hot storage tank to the reference system and the last model adding a borehole thermal energy storage to the first model. The simulation is done for a whole year using the load profiles given figures 5.4-5.6.

- **Reference Model 1**

The reference model is shown in figure 5.4 for both cooling and heating seasons. The collector harvests solar energy and stores it in the storage tank. Heat in the tank is used to power the absorption chiller that produces chilled water. In cloudy hours or when solar heat is not enough to meet the chiller requirement, a fossil fuel fired backup boiler is used to supplement the missing heat. The cooling tower provides cool water to cool down the absorber and the condenser of the chiller. In summer, the chiller provides cold water directly to the building. In winter, the chiller is disconnected and hot water from the boiler outlet flows directly to the building to provide heating.

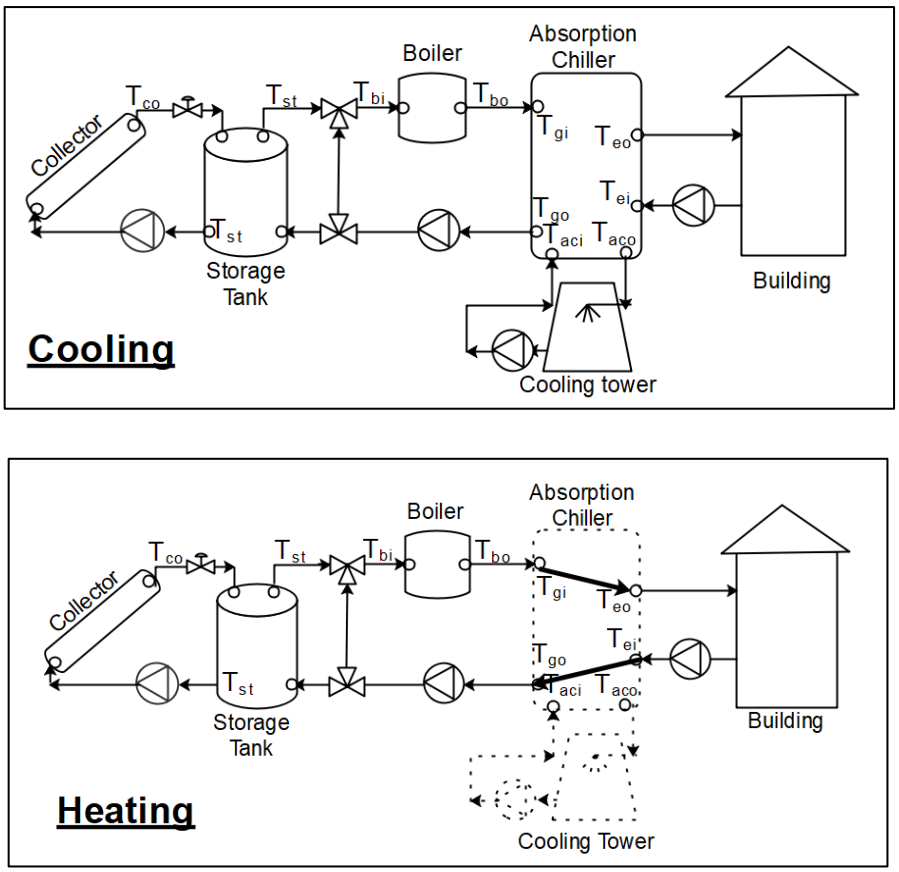

Figure 5.4. Case A Reference Model 1 (Cooling/Heating)

- **Proposed Model 2**

The first proposed model is shown in figure 5.5. The only modification of the system in figure 5.4 is the addition of a second hot tank. It is expected that separating the chiller return water from the collector hot water will improve the efficiency of the system. By not allowing the generator inlet/outlet water to mix, the exergy of solar heat in model 2 is better conserved compared to the reference model 1.

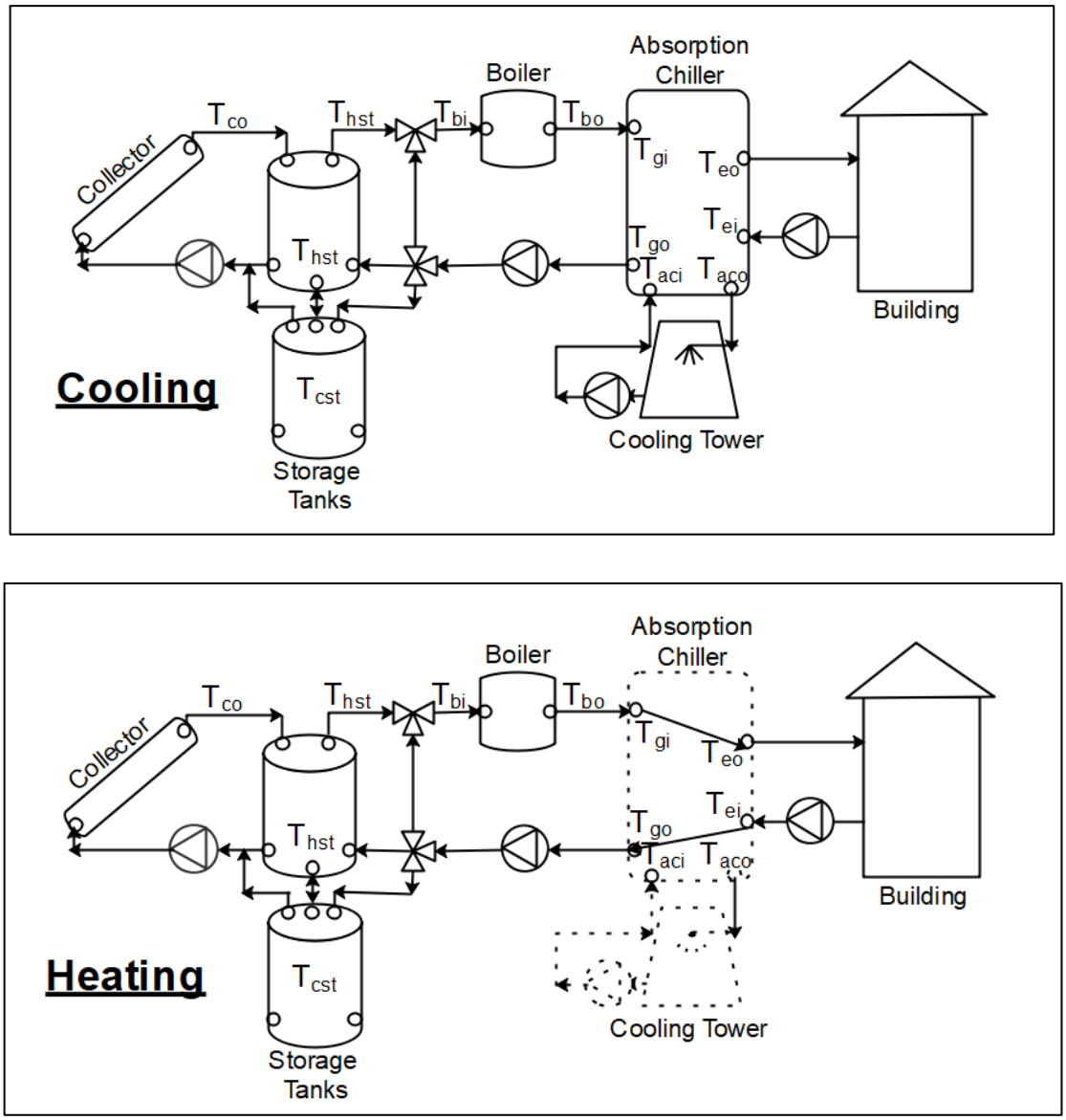

Figure 5.5. case A, Model 2 (Cooling/ Heating)

- **Proposed Model 3**

The proposed model 3 is shown in figure 35. In summer, rather than rejecting the cooling tower heat to the atmosphere, a borehole is used to store this energy. In winter, the absorption chiller is run as a heat pump, extracting heat from the borehole to assist to the heating of the building. If the chiller evaporator was left at ambient temperature, extracting heat from the air would have been impossible whenever the ambient temperature is over 15°C.

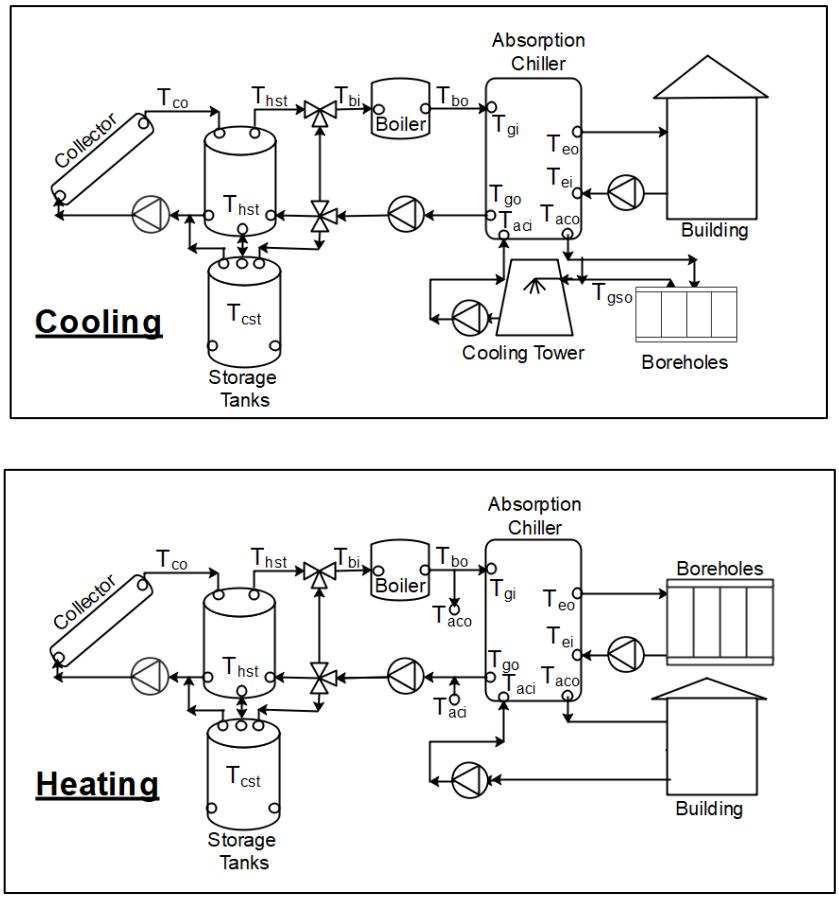

Figure 5.6. Case A, Model 3 (Cooling/Heating)

5.4.2. Systems Modelling

- **Solar Collector**

A single axis tracking parabolic trough solar collector from IEA SHC - TASK 33 database is used [71]. Single axis tracker is less efficient than dual axis tracker. However, due to its simplicity and lower cost, it is still the most used in solar thermal applications. The model of the collector is based on the second order efficiency function defined in equation 3.18

$$\text{“ } \eta = \eta_0 - a_1 \frac{\Delta T}{DNI} - a_2 \frac{\Delta T^2}{DNI} \quad ; \quad \eta_0 = 0.75 \; ; \quad a_1 = 0.1123 \; ; a_2 = 0.00128 \text{ ”}$$

Using equation 3.17, the collector efficiency is also given by:

$$\text{“ } \eta' = \frac{Q_{useful}}{A_c DNI} \; ; \quad Q_{useful} = m_{sc} C_p (T_{cout} - T_{cin}) \text{ ”}$$

From the manufacturer test data, the collector mass flow rate can be obtained. With DNI data which is taken from TRNSYS Typical Meteorological Year (TMY) database for

Izmir city, the only unknown of the efficiency equations is the collector outlet temperature. To solve for it, the two efficiencies equations are iterated. Alternatively, since there are only second order equations involved, they can be expanded in the form

$$“\ AT_{cout}^2 + BT_{cout} + C = 0.”$$

When the determinant $\Delta = B^2 - 4AC > 0$, a real solution for T_{cout} exists. However, T_{cout} must be greater than T_{cin} by 3°C in order to have harvested energy. When the temperature difference $T_{cout} - T_{cin}$ is less than 3°C it is considered not worthy to run the collector pump to harvest heat.

The solar fraction which is the ratio of solar energy to the total energy needed to power the system is an important performance indicator for this study. It is defined as:

$$“Solar\ Fraction\ (sf)[-] = \frac{Solar\ heat\ (Qs)\ [kW]}{Solar\ heat\ (Qs)[kW] + Boiler\ heat\ (Qb)[kW]}\ ” \quad (5.1)$$

- **Storage Tank**

The storage tanks are modeled using the “U” value of the insulation material. For the collector hot water tank, 10cm tick Rockwool [72] with a U value of 0.44W/m$^{2^\circ}$C is assumed. From TMY data, it has been observed that the average wind speed is always less than 4m/s so the thermal resistance associated with outside convective heat transfer coefficient has been neglected. The heat loss or heat gain is given by

$$“\ Q_{loss} = UA(T_{tank} - T_{ambient})” \quad (5.2)$$

For a double tanks system, the water route into/out of the tanks is decided to maximize the exergy of hot water. For example, if the chiller hot return water is hotter than both tanks temperatures, tanks are simply bypassed to conserve the exergy of heat.

- **Boiler**

The boiler is assumed to be a fossil fuel powered machine, with an efficiency of 90%. Also, it is assumed that any heating requirement not satisfied by the solar heat is supplied by the boiler.

- **Absorption Chiller**

Absorption chiller (ACH) is modeled according to its characteristic temperature function ΔΔT which determines the performance of the chiller using external fluid streams data as explained in equations 4.5-4.9.

“ΔΔT is given by: $\Delta\Delta T = T_G + aT_{AC} + eT_E$ ”

Where the constants “a” and “e” are dependents on the specific chiller characteristics.

The cooling power Q_E, the generator power Q_G, the heat rejection rate of the absorber and condenser Q_{AC} and the COP are then given by the chiller equations repeated below where the constants again depend on the chiller.

$$“Q_E = s_E \Delta\Delta T + r_E \; ; \;\; Q_G = s_G \Delta\Delta T + r_G \;\; ; \; Q_{AC} = Q_E + Q_G \; ; \; COP = \frac{Q_E}{Q_G}”$$

The design conditions and characteristic coefficients of the case study ACH is given in table 5.2. It is a double effect ACH working with hot water as the heat source. For a cooling load of this size, economically a double effect ACH with a COP of 1.3 is preferred to a single effect ACH with a COP of 0.7 [33].

Table 5.2. Absorption Chiller Nominal Operating Conditions [51]

Parameter	**unit**	**Value**	**Characteristics coefficients**	
Chilled water T_E in/out	°C	14/7	a	-2.46
Cooling water T_{AC} in/out	°C	30/37	e	4.38
Hot water T_G	°C	180/165	s_E	18.1
Chilled water flow rate	m^3/h	143	r_E	-1350.5
Cooling water flow rate	m^3/h	244	s_G	12.54
Hot water flow rate	m^3/h	51	r_G	-917.3
Cooling capacity	kW	1163		
COP	-	1.33		

A system performance ratio “spr” has been defined in equation 5.3 to track the overall system performance. It displays how much total heat is used per unit cooling power.

$$System\ Performance\ Ratio\ spr[-] = \frac{Cooling\ load\ QL[kW]}{Solar\ heat\ Qs[kW] + boiler\ heat\ Qb[kW]} \qquad (5.3)$$

- ## Cooling Tower

The cooling tower is modeled using the efficiency equations 4.10-4.15. Through an experimental study the constant of the equations are determined for a specific temperature, flow rates, operation range. Extrapolation should be avoided when using these equations.

$$“\varepsilon = \frac{T_{inh} - T_{outc}}{T_{inh} - T_{wb}} \;\; ; \;\; \varepsilon = \frac{\varepsilon^*}{\varepsilon^* + 1} \; ; \quad \varepsilon^* = \frac{CroNTU}{1 - 0.5NTU\left(Cro - \frac{L}{G}\right)} ; \; NTU = c\left(\frac{L}{G}\right)^{n+1} \; ; Cro = \frac{b}{C_p} \;\; ”$$

- **Borehole Thermal Energy Storage**

The borehole field is a 5x5 U tubes spaced by 5m. Each U tube is 100m deep in127mm grout diameter. The total U tube length is L. The closer the tubes, the more the thermal

interactions will take place, saturating the field earlier. The average borehole fluid temperature T_{fav} is repeated below

$$“\ T_{fav} = T_{grd} + q_i R_{bh} + \sum_{i=1}^{n} \frac{q_i - q_{i-1}}{2pik}\, g\left(\frac{t_n - t_{i-1}}{t_s}, \frac{r_b}{H}\right)\ ”$$

where R_{bh} is the borehole thermal resistance. It is a function of the fluid flow regime and the tubes/grout material. From the toolbox accompanying the “Geothermal heat pump and heat engine systems” book, it has been observed that the change of R_{bh} with flow rate is negligible. A constant R_{bh} value of $0.11 mKW^{-1}$ which covers the entire flow range is thus assumed. The g function of a single borehole is used for the calculation because it gives the same result for multi boreholes field for 1-year time (figure 5.7) and it is much simpler to calculate. If the simulation time was longer, the g functions will deviate from each other as the time progress. The heat extracted/injected in the borehole is given by

$$“q_i L = m_{bh} C_p (T_{inbh} - T_{outbh})\ ”$$

where m_{bh} is the borehole fluid mass flow rate and L the total borehole length. To prevent long term ground thermal imbalance, the fluid inlet/outlet temperature are set (7°C/14°C in winter, 36°C/28°C in summer) and if the ground cannot receive/provide the corresponding heat, the borehole is just bypassed at the time step. q_i from heat extraction/injection and q_i from the average fluid temperature given above are equalized to calculate the fluid mass flow rate. If the mass flow rate is greater than the available flow out of the evaporator(winter) or the condenser(summer), the borehole is bypassed otherwise the flow is totally or partially passed through the borehole and the eventual remaining flow bypass the borehole.

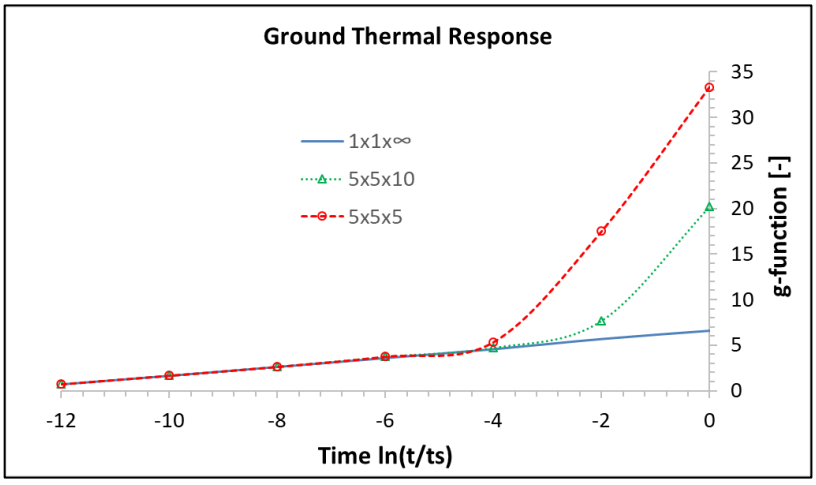

Figure 5.7. g-Function for Different Boreholes Configurations

5.5. Case B Systems (Cooling Water & Night Cooling)

5.5.1. System Description

In this case study, an attempt to improve the overall performance of a cooling system by using low night temperature and low fan power is done. This is achieved by setting a Low Continuous Flow (LCF) rates through the CT. TRNSYS is used to simulate a condenser-cooling tower system operating between 8am-4pm such as those used in office buildings or schools. In two simulation Models, storage tanks are added to the system to extend the water cooling process beyond the regular operation time. An analysis of system performance obtained by LCF versus that given by intermittent high fluids flow rates is done. Also, the effects of storing water in a different number of tanks on system performance are investigated. Finally, water cooling results will be applied to an absorption chiller cooling to investigate the change of performance of the system. In this section, the regular cooling system and the proposed two systems are modeled using TRNSYS. Each system is illustrated in a simple figure for clarity. However, system components connections logic in TRNSYS remains the same as indicated in the figure.

- **Model 1 (Reference system, Intermittent Cooling)**

A regular cooling system formed by a condenser, a CT, a pump and connecting pipes is showed in figure 5.8. Condenser used in refrigeration industry or in power plant can be a tube and shell type heat exchanger. Depending on the flow rate, single pass or multiple-pass tube bundle are used to achieve the required heat transfer. Since the goal in this study is to lower cooling water temperature, the internal configuration of the condenser is not taken into account. It is assumed that the heat transfer area of the condenser, as well as its material, is designed to allow 'Q_{cond}' heat exchange. CT used in the small and medium-size industrial application (where flow rate <45000m^3/h) is a mechanical draft type. Warm water entering the CT is spread over a fill to increase the contact area between water and the air being forced through the fill by the fan. The CT and the condenser are switched ON/OFF simultaneously during operation. This is a single loop intermittent flow system. Between 8am-4pm, the condenser is under heat load (Q_{cond}). The pump maintains a mass flow rate through the system while the CT fan

is kept at its rated speed. From 4pm-8am the condenser heat load is zero, so the system is turned OFF. This simultaneous start-stop is the typical operation mode of commercial or industrial cooling system

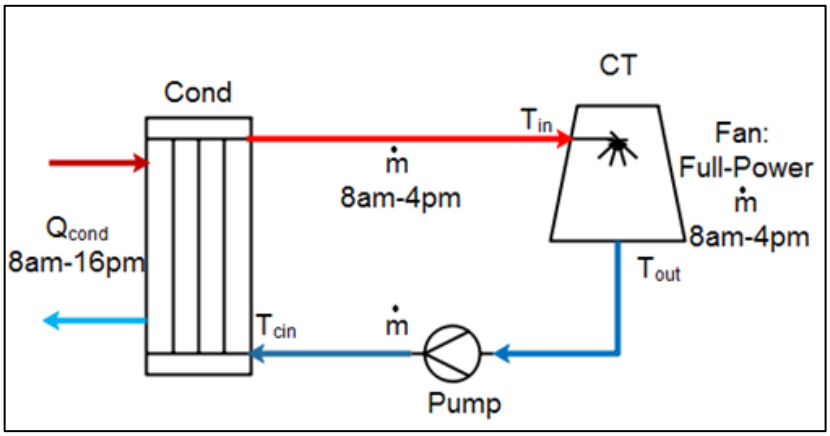

Figure 5.8. Case B, Reference Model M1

- **Model 2 (2 Storage Tanks, Continuous Cooling 24h/24)**

To improve the performance of the system in figure 37, the system has been modified by adding 2 tanks as illustrated in figure 38. In the new system, between 8am-4pm, hot water out of the condenser ($\dot{m} = 2000$ kg/h) is partially ($2\dot{m}/3$) stored in tank T2 and the remaining ($\dot{m}/3$) is cooled in the CT then discharged in tank T1. Between 4pm-8am, hot water in tank T2 is cooled at a rate of ($\dot{m}/3$) and stored in tank T1 for the next cycle. In this configuration, LCF water cooling is achieved by reducing the mass flow rate through the CT to 1/3 of the flow rate in the regular system. Also, the air mass flow rate is reduced by setting the fan power to 1/3 of its rated value. Initially, tank T1 contains cool water of mass M_i or volume V_i representing a supply autonomy of 6 hours at a flow rate $\dot{m}$. Cool water produced during the ON time (8am-4pm) is $\dot{m}\Delta t_{ON}/3$. The total required cooling water $\dot{m}\Delta t_{ON}$ can be expressed as:

$$\dot{m}\Delta t_{ON} = M_i + \frac{\dot{m}}{3}\Delta t_{ON} \qquad (5.4)$$

To minimize storage volume, initial cool water M_i must be produced only during OFF time (4pm-8am) as given below.

$$M_i = \frac{\dot{m}}{3}\Delta t_{OFF} \qquad (5.5)$$

Equivalently stated, the volume of cool water at the end of the condenser operation must be as low as possible, zero ideally. M_i value from equation 5.4 or equation 5.5 must match to provide a cyclic cooling process. With the 8h/24h operation, from either

equation, the storage capacity of each tank $M_i = 2\dot{m}\Delta t_{ON} / 3$. For $\dot{m}$ = 2000 kg/h, this corresponds to M_i= 10,670 kg or V_i = 10.67m^3 of water.

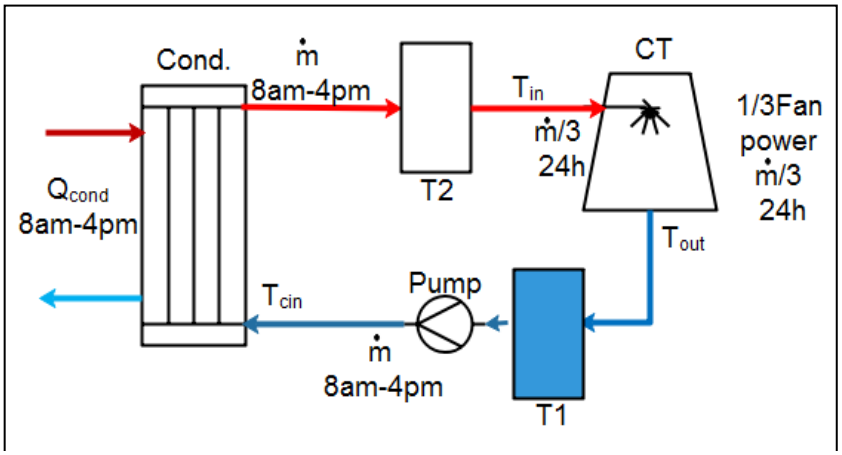

Figure 5.9. Case B, Model 2

- **Model 3 (5 Storage Tank, Continuous Cooling 24h/24)**

A set up made to further reduce the total storage mass of the system of figure 5.9 is displayed in figure 5.10. In terms of flow rates, model 3 works as model 2 described previously. It can be noted that in figure 5.9, at anytime only 50% of storage capacity is being occupied by the fluid (either by cool water or by hot water). The idea is to reduce as much as possible this unused storage capacity by using smaller tanks to contain the the required water mass M_i and two smaller extra tanks to receive hot/cool water while the current cool water supplying tank is discharging to make space for future hot/cool water. Five tanks have been used for convenient scheduling because preliminary results showed that tanks number affect only storage volume but not water average temperature.

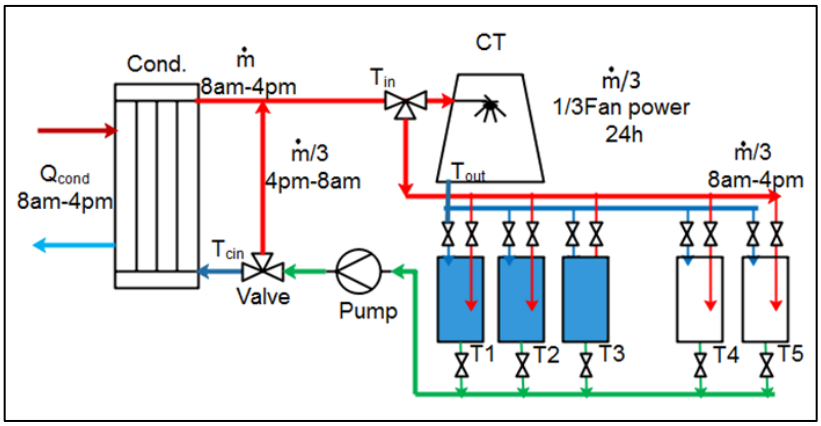

Figure 5.10. Case B, Model 3

The schematic in figure 5.11 shows the flow scheduling process. Each column represents the state of a tank at different time of the day. Each tank has 2 hours supply capacity at $\dot{m}$ =2000kg/h and 6 hours supply capacity when the flow rate is reduced to $\dot{m}/3$. Starting from the set of tanks displayed for "6am-8am", from 8am to 10am, T1 is supplying the condenser with cool water at a mass flow rate $\dot{m}$. Hot water out of the condenser is partially (1/3) cooled in the CT and discharged in T4 while the remaining (2/3) hot water flows directly to T5. At 10am T1 becomes an empty tank. The process continues as illustrated in figure 4 until 4pm when the condenser stops operating. From 4pm to 8am, hot water stored in T1, T2 and T5 bypass the condenser to get cooled in the CT at a rate of $\dot{m}/3$. Equation 5.6 and equation 5.7 provide the relationship between the number of tanks, their size and the total storage capacity.

$$M_{1tank} = \frac{M_i}{n} \tag{5.6}$$

$$Total\ tanks\ capacity = (n+2)M_{1tank} \tag{5.7}$$

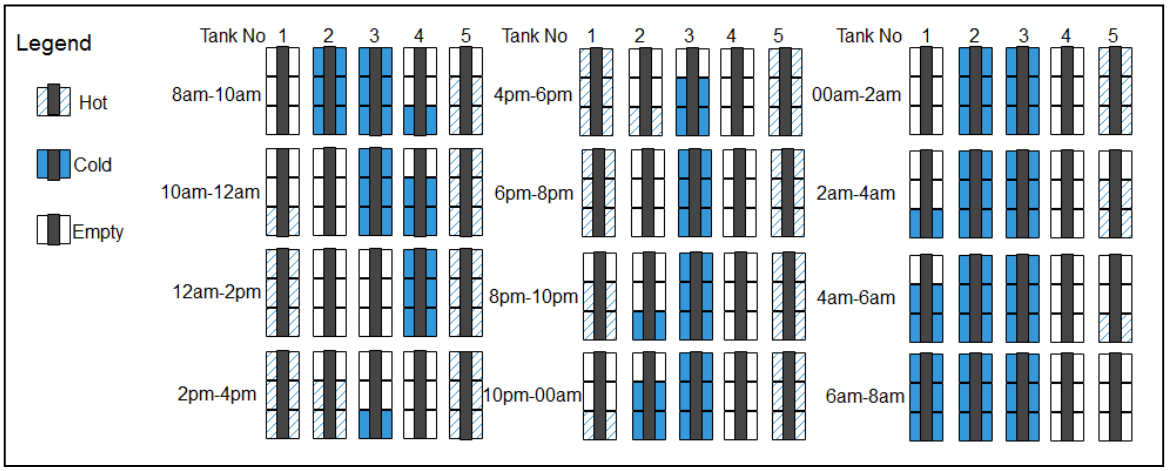

Figure 5.11. Flow Scheduling Schematic

5.5.2. CT Simulation Tool and Parameters

TRNSYS software is used to model the investigated cooling systems. The software is well suited for thermal system simulation as it has common thermal components in its library. Major components used in this study are the cooling tower and weather data generator. Weather data for the first week of July in Izmir city has been used because it is within the hottest period of the year. By using typical specifications (range, approach) of commercial CTs, the CT has been calibrated to cool

water from 40°C to 30°C at 25°C wet bulb temperature. Heat load is taken as the sum of two components; a base load of 22.5 kW and 0.5 kW per degree above 25°C as given in equation 5.8.

$$Q_{cond} = Q_{base} + 0.5(T_{amb} - 25)\ for\ T_{amb} > 25°C$$

$$Q_{cond} = Q_{base}\ \ for\ T_{amb} \leq 25°C \tag{5.8}$$

This represents a typical heat rejection of 10 kW cooling capacity of an absorption chiller. In figure 5.12 and figure 5.13 are plotted the weather data (ambient temperature, wet bulb temperature, and relative humidity) obtained from TRNSYS and the corresponding generated heat load profile of the condenser.

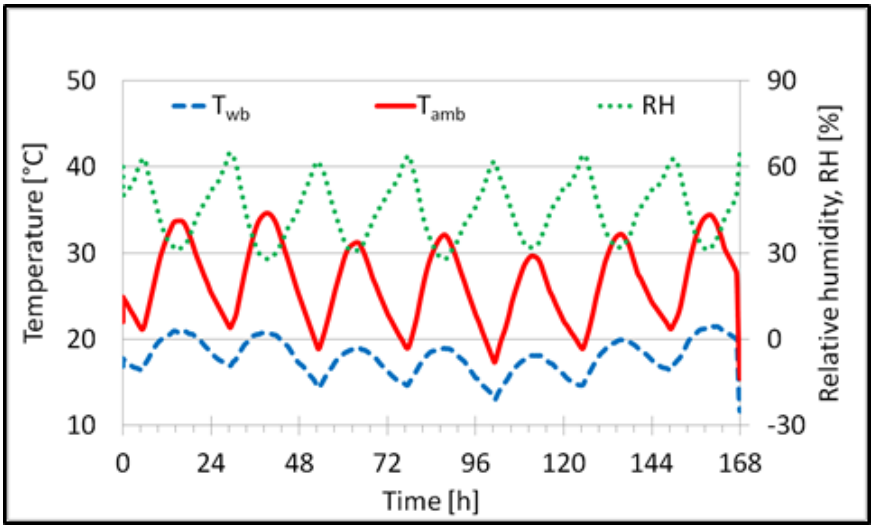

Figure 5.12. Meteorological Input Data [73]

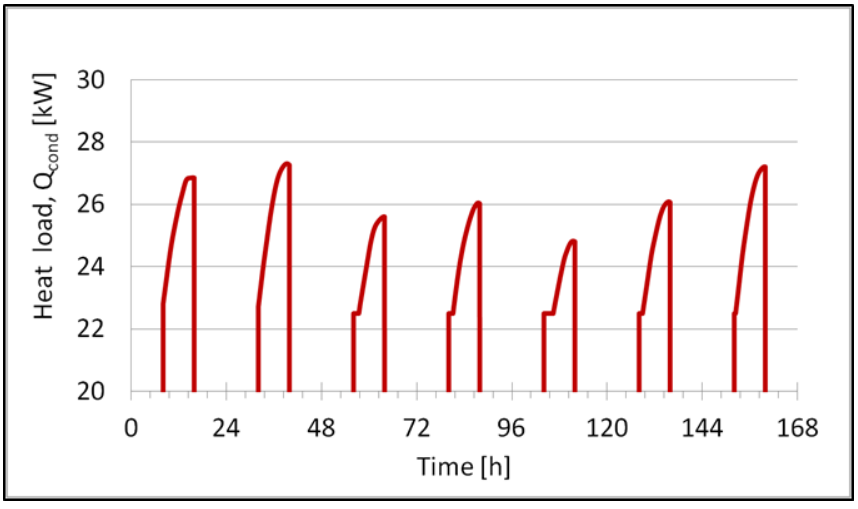

Figure 5.13. TMY Data & Condenser Daily Heat Load

The condenser is a tube and shell heat exchanger as mentioned previously. Strictly speaking, a condenser changes the phase of the fluid from a gas to a liquid through latent heat transfer. However, the condenser in this paper can also work as a single-phase liquid-liquid heat exchanger as it is the case for the cooling of the absorber of an absorption chiller. Analysis of two-phase flow is a tedious task which requires knowledge of the fluids temperature –pressure dependent properties, the condenser tube material properties, the surface tension at the two-phase interface (vapor-water droplet) and so on [74]. However, there are simplified condenser models in the literature which use design working conditions to reduce the number of unknown and solve heat transfer problem more conveniently [75]. An energy balance and predefined parameters are the basis of this type of analysis [76]. These parameters are:

-Qcond, the heat exchanged by the two fluid streams

-ε effectiveness of heat exchanger set to 0.8

-Two stream inlet temperature T vapor in(T_{vi}), T water in (T_{wi})

The maximum heat transfer is given by

$$Q_{max} = m_w C_{pw}(T_{vi} - T_{wi}) \tag{5.9}$$

The heat transfer Qcond is related to Qmax through the equation'

$$Q_{cond} = \varepsilon Q_{max} \tag{5.10}$$

While the latent heat rejection is given by,

$$Q_{cond} = m_v h_{fg} \tag{5.11}$$

where h_{fg} is the specific latent heat of condensation of the vapor.

Finally, the outlet cooling water temperature is given by

$$T_{wo} = T_{wi} + \frac{Q_{cond}}{m_w C_{pw}} \tag{5.12}$$

After defining the analysis method of the condenser, the next component of interest in the system is the cooling tower. Following SPX company CT sizing procedure, the CT fan is sized at 0.85hp/ton of cooling capacity of a vapor compression cooling system [77]. Taking into account the COP of these devices (COP=4), this is equivalent to

0.85hp/1.25ton of heat rejected. Following this sizing scheme, a 3kW fan is used for the CT under study. In the results, the fan power of the proposed models is expressed as a fraction of the regular system fan power by using the fan law given in Fantech datasheet (equation 5.13) [78].

$$P_2 = P_1 \left(\frac{V_2}{V_1}\right)^3 \tag{5.13}$$

This makes the sizing accuracy a noncritical value to visualize the exact effect of fan speed reduction on system performance. In table 5.3 is summarized the parameters of the CT. The following assumptions have been made to simplify the study of the systems:

-Water temperature in the tanks is uniform

-Tanks heat loss/gain is negligible

-Cooling tower parameters change negligibly within the operation range

-Makeup water temperature is equal to the ambient temperature

Table 5.3. Cooling Tower Parameters

Parameters	**Regular Model 1**	**Model 2 & Model 3**
Flow geometry	Counterflow	Counterflow
Water flow rate	2000kg/h	666.67 kg/h
Cell rated air flow	1280m^3/h	1280 m^3/h
Mass transfer coefficient [5]	1.96	1.96
Mass transfer exponent	-0.69	-0.69
Air velocity ratio	1	0.69
Power	3 kW	3 kW

The performance of CT is commonly measured through its cooling efficiency. The cooling efficiency defined in equation 12 is a measurement of how much the outlet temperature is close to the theoretical possible temperature which is the wet bulb temperature. In the literature the CT inlet-outlet temperature difference is known as its range and the temperature difference between the outlet and the wet bulb temperature is known as the approach. With these definitions, efficiency is the ratio of the range over the sum of the range and the approach.

$$\eta = \frac{T_{in} - T_{out}}{T_{in} - T_{wb}} \tag{5.14}$$

To investigate the real benefits of the models, additional indicators of the cooling system performance will be taken into account. The main function of the CT is to

supply low-temperature fluid to the condenser so the average water temperature at the condenser inlet $\bar{T}_{cin}$ will be a comparison element (equation5.15). In refrigeration applications or in power plant, the condenser temperature determines its operating pressure. The lower the temperature, the lower the pressure and the higher the efficiency of the system.

$$\bar{T}_{cin} = \frac{1}{i+1}\sum T_{cin} \tag{5.15}$$

Also, on the fan side, the heat rejection per unit work input in equation 5.16 gives information about the electric energy performance of the cooling system. Monitoring this parameter is important to ensure that the blades of fan are clean, or the tension of the driving belt is good enough to achieve the rated air volume flow rate. Lastly, water loss rate "*wl* [kg/s]"is considered as a performance indicator as well. For applications that cannot rely on abundant sea water, this parameter is important as it is directly proportional to water expenditure.

$$\Phi = \frac{Q_{reject}[kW]}{W_{fan}[kW]} \tag{5.16}$$

5.6. Case C Systems (Chiller & Chilled Water Storage)

In the literature, storage tank function has been limited to peak load shifting and power saving without tackling the system size/cost reduction potential. Sabina et al. [79] studied solar assisted ACH with chilled water storage tank and reported an electrical energy saving of 20% due to the ability of the system to operate more smoothly with less frequent ON/OFF. In a Similar study by Zhu et al. [80], a system operation cost reduction of 20.5% was found. Shifting peak load in a large scale may lead to the same issue of huge power demand at night. For an electric chiller which has a relatively low specific cost, simple load shifting may be satisfying, but for absorption chiller which is quite expensive, reducing the size of the chiller is critical for the feasibility of the project.

In this case study, in addition to peak load shifting, the base load itself is further shifted in an attempt to have the most possible uniform low power demand. Also, it is expected that this action will reduce the size of the chiller as well. In the study, storage tanks are

added to the solar absorption cooling system, in order to analyze their effects on the overall system thermal performance. First, tanks are used to store chilled water to support the building load. Secondly, tanks are further attached to the cooling tower to partially store hot water on daytime and cool it at night. The aim of this study is to increase the **utilization ratio** or **capacity factor** of solar absorption cooling system by trading off the expensive rated cooling capacity of the chiller with a much cheaper storage tank. Reducing the peak power of the system, in turn, will reduce its CAPEX, provided that the eventual drawbacks of the modifications do not outweigh their benefits.

5.6.1. System Description

In this study, 3 cooling systems cases are investigated. The reference system consists of a solar collector, a hot storage tank, a backup boiler, an absorption chiller, and a cooling tower. The first proposed system adds 2 chilled water storage (CHWS) tanks to the reference system, while the second proposed system further adds 2 cooling water storage (CWS) tanks to the first system.

- **Reference System (Model S_1)**

In the reference system in figure 5.14, the absorption chiller cools directly the building, which means that it should be sized to satisfy the maximum cooling load. This may be an inefficient investment in equipment resources as the full power of the machine may be used only a few hours a day, remaining idle most of the time. In this system, the cooling tower is switched ON/OFF simultaneously with the chiller. However, it should be noted that in commercial buildings, cooling is often done less than 12h/day during daytime. In the thermal power side of the system, the solar collector harvested energy is first used to power the system. In the case that hot water temperature is not high enough to meet the chiller requirement, a fossil fuel-fired boiler is used to upgrade the temperature. When thermal hot storage tank is too hot or too cold for the chiller, the tank is bypassed, or the tank water is mixed with the chiller return hot water to get the desired temperature.

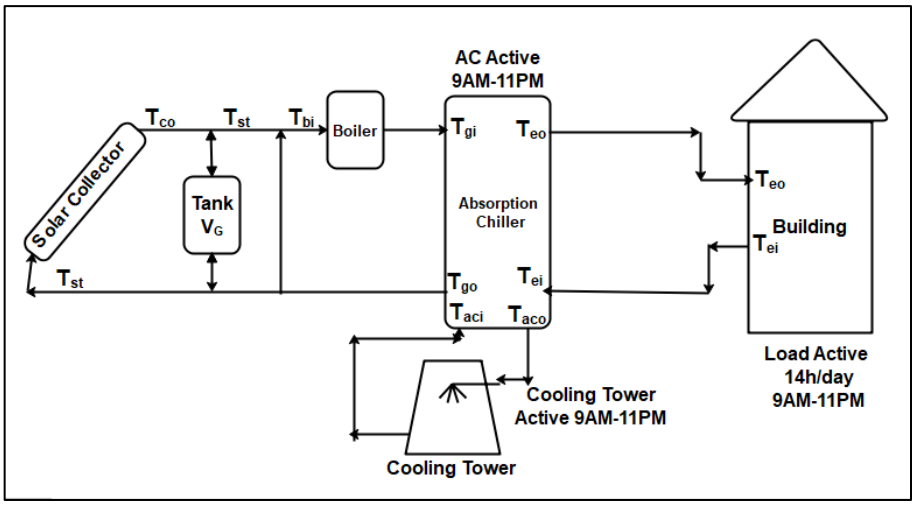

Figure 5.14. Case C, Reference Model 1

- **Proposed System (Model S_2, Chilled Water Tank)**

In the first proposed system in figure 5.15, CHWS tanks V_E are added to the reference system for two reasons: (1) when the harvested solar energy is more than the heat required to satisfy the cooling load, the extra energy is used to chill water for later use. The temperature difference between the CHWS tank V_E and the ambient is certainly less than that between the hot tank V_G and the ambient. Therefore, producing and storing chilled water incurs much less heat loss compared to storing hot water for later chilled water production. (2) By storing chilled water in low cooling load time, during peak hours, the chiller power requirement can be reduced by using both the chiller and the stored chilled water to satisfy the cooling load. Reducing the required chiller cooling capacity is an important point as it saves capital investment in the cooling system as well as operation and maintenance cost.

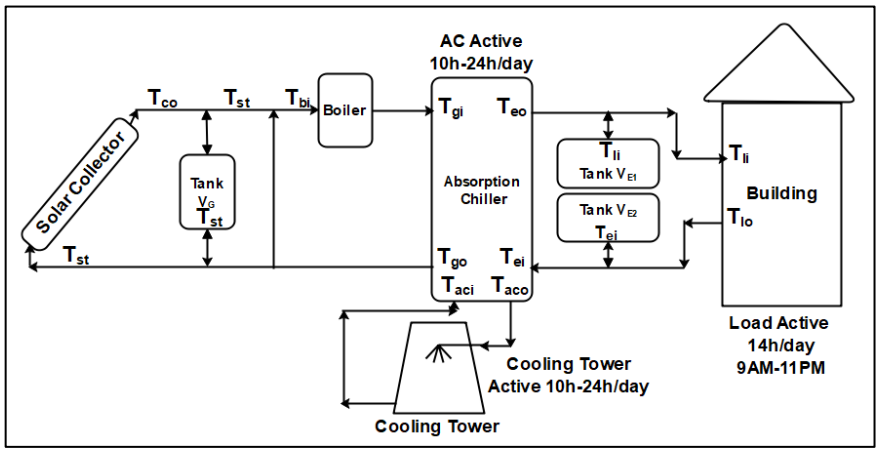

Figure 5.15. Case C, Proposed Cooling System, S_2

- **Proposed System (Model S_3, Chilled/Cooling Water Tanks)**

In the second proposed system in figure 5.16, CWS tank V_{CT} are added to assist the cooling tower in providing low-temperature cooling water to the chiller. At startup, the cooling water cool tank "Tank V_{CT1}" is full. As the system operates, water is drawn from the cool tank at a mass flow rate "m" to cool down the condenser and absorber of the chiller. However, from the outlet of these components, only a fraction "$1/n_{CT}$" of water(where $n_{CT}>1$) is passed through the cooling tower and back to the cool tank, while the remaining fraction "$(1-1/n_{CT})$" is stored in the warm tank "Tank V_{CT2}". The number "n_{CT}", the flow rate "m" and CWS tank volume V_{CT} are calibrated such that at the end of chiller operation, tank V_{CT1} is empty and tank V_{CT2} is full. When the chiller is off at night, warm water in V_{CT2} is cooled at a low flow rate "m/ n_{CT}" to fill back the cool tank V_{CT1} by the morning. In this configuration, cooling tower always operates at a lower flow rate "m/ n_{CT}" rather than intermittently at a unit flow rate "m" or "0" as in the reference system. It is expected that cooling water slowly at night will take advantage of low night temperature/power tariff to improve the performance of the system.

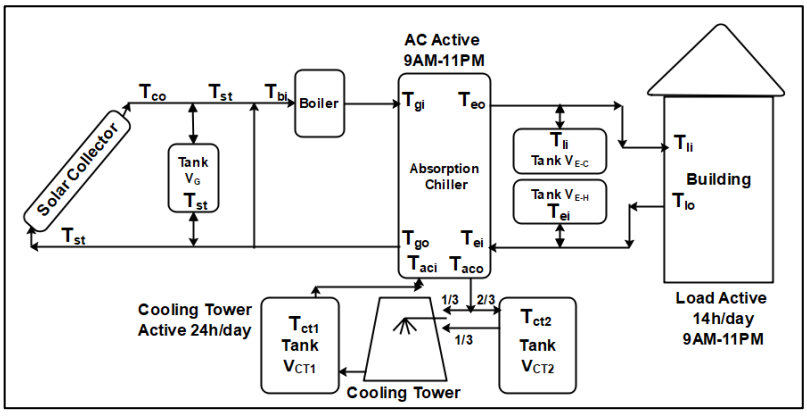

Figure 5.16. Proposed Cooling System, S3

5.6.2. System Components Models

In this section, the mathematical models for each component are described. To simplify the analysis, electrical energy consumption by pumps, fan, and monitoring devices have not been covered. This is due to the fact that in solar heat driven applications such as absorption chiller system, electrical energy consumption magnitude is negligible compared to that of thermal energy.

- **Load and Weather Data**

The cooling load profile of a shopping center located in Izmir is used for the case study. The hourly load profile is given again in figure 5.17. The mall has a high occupancy rate reaching up to ten thousand people during the weekend. It has been reported that due to the massive internal load and the good insulation of the building, the load profile does not depend much on weather conditions [70]. From Excel, a curve fitting function in equation 5.17 is generated for calculations convenience as the used time step is 15 minutes rather than 1 hour as shown in figure 5.17. With the load, function interpolation is made easy for any time step simulation.

$$Q(t) = 0.0471t^5 - 1.7452t^4 + 20.861t^3 - 89.021t^2 + 175.87t - 24196 \quad (5.17)$$

where $Q[kW]$ is the cooling load, and $t[h]$ the time of the day.

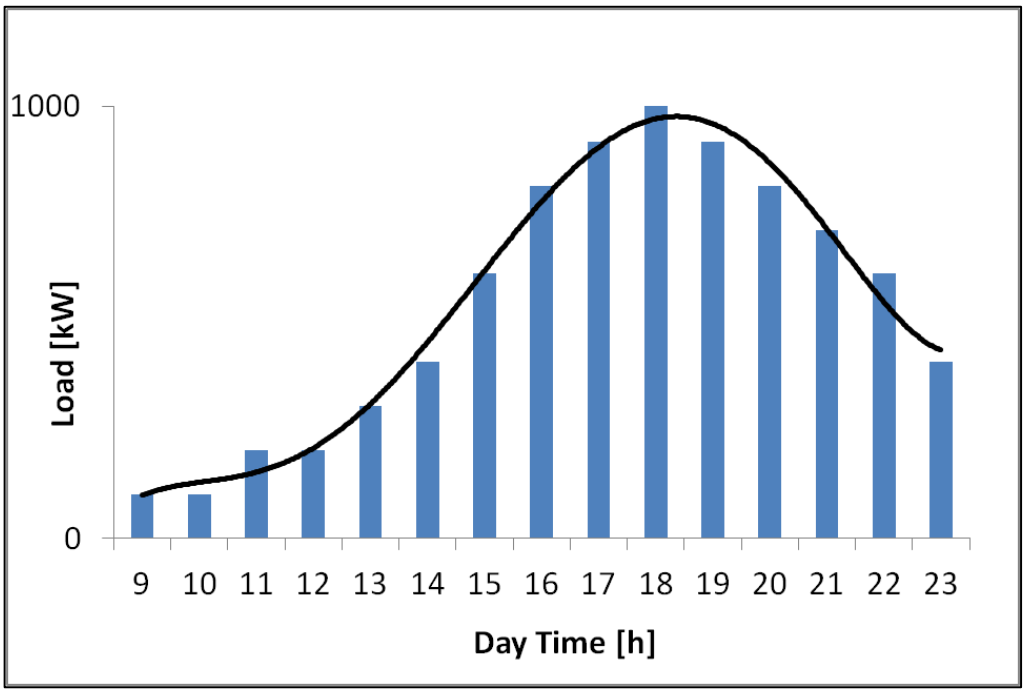

Figure 5.17. Cooling Load Profile

The typical meteorological year (TMY) data of the city is obtained from **TRNSYS** database [73]. A brief summary of data is shown in table 5.4. Direct Normal Irradiation (DNI) ratio of the city reached the critical value of 60% from which multi-effect absorption chiller usage is cost effective compared to single effect chiller [22]. It can be observed that night time dry/wet bulb temperature is less than daytime temperatures which make night cooling an attractive initiative.

Table 5.4. İzmir TMY Summary [73]

Parameters		**İzmir Data**		**Unit**	
Annual Solar Radiation	Global Radiation G	2382.18		kWh/m2/yr	
	Direct Normal Radiation DNI / DNI%	**1448.46**	**60.80**	**kWh/m2/yr**	**%**
	Diffuse Radiation DIF / DIF%	879.23	36.91	kWh/m2/yr	%
	Reflected Radiation REF / REF%	879.23	2.29	kWh/m2/yr	%
Annual Ambient Temperature	Minimum /Maximum	-3.41	37.97	°C	°C
	Average	**17.06**		**°C**	
Annual Relative Humidity	Minimum /Maximum	26.13	99.75	RH%	RH%
	Average	60.83		RH%	
Cooling Season Ambient Temperature	Average Day / Night	25.25	21.06	°C	°C
Cooling Season Wet Bulb Temperature	**Average Day / Night**	**17.38**	**15.67**	**°C**	**°C**

- **Solar Collector**

The solar collector model explained for Case A is used in this case study. The model is based on the second order efficiency function and an energy balance from solar heat and the heat transfer fluid.

- **Storage Tank**

The storage tanks are modeled using the "U" value of the insulation material. For the collector hot water tank, V_G and the CHWS tanks V_E, 10cm tick Rockwool[72] with a U value of 0.44W/m$^{2^\circ}$C is assumed while for the cooling tower 10cm concrete[81] block with a U value of 33 W/m$^{2^\circ}$C is used. From TMY data, it has been observed that the average wind speed is always less than 4m/s so the thermal resistance associated with

outside convective heat transfer coefficient has been neglected. The heat loss or heat gain is given by

$$“Q_{loss} = UA(T_{tank} - T_{ambient}) \text{ ”}$$

In order to quantify the heat loss of both tanks V_G and V_E a heat loss term has been defined as

$$“ Total\ heat\ loss\ Qloss = Qloss(hot\ tank) + \frac{Qloss(cold\ tanks)}{COP_{chiller}} \text{ ”} \quad (5.18)$$

The heat loss in the cold tank V_E has been converted to the equivalent heat input necessary at the generator to provide the lost cooling power.

- **Absorption Chiller**

The absorption chiller model in case A is reused for this case study. In addition, the capacity factor or utilization ratio of the chiller which is an important economic parameter is used to measure the improvement of the proposed system in terms of CAPEX and OPEX reduction potential. It is defined as:

$$“ Capacity\ Factor\ CF[-] = \frac{\sum Cooling\ Load\ [kW] * Load\ time\ [h]}{Chiller\ Rated\ Power[kW] * Cooling\ Season\ Duration[h]} \text{ ”} \quad (5.19)$$

- **Cooling Tower**

Cooling tower model from Case A is reused for this case study.

5.6.3. Flow Scheduling

To ensure cooling water will always be available for the chiller to operate, storage tank volume and cooling tower flow rate must be calibrated along with the chiller mass flow rate and the operating time. Considering that cooling tower will work continuously at a reduced mass flow rate m_{ac}/ n_{CT}, starting from the end of the cooling time where cold side tank V_{CT1} is empty and hot side tank V_{CT2} is full, the mass of hot water is given by equation 5.20. During off time ΔT_{OFF}, cooling tower works at m_{ac}/ n_{CT} flow rate, transferring hot water M_{acOFF} from the hot tank to the cold tank. During the ON time ΔT_{ON}, the cumulative water mass required to cool the chiller ($m_{ac}\Delta T_{ON}$) is equal to cold water mass available at the start time M_{acON} plus water that is circulated back to the cold tank during the same period ($m_{ac}\Delta T_{ON}/ n_{CT}$) as given in equation 5.21. Since cold water mass at start time is equal to hot water mass at the end time, equation 5.20 and 5.21 are solved to find the flow splitting term n_{CT}. The constraint of the

solution is that ΔT_{ON} plus ΔT_{OFF} must be equal to the cooling cycle which is 24h in our study. The solution is given in equation 5.24.

$$M_{ac_{OFF}} = \frac{1}{n_{CT}} m_{ac} \Delta t_{OFF} \quad (5.20)$$

$$m_{ac} \Delta t_{ON} = M_{ac_{ON}} + \frac{1}{n_{CT}} m_{ac} \Delta t_{ON} \quad (5.21)$$

$$M_{ac_{ON}} = M_{ac_{OFF}} \quad (5.22)$$

$$\Delta t_{ON} + \Delta t_{OFF} = constant = 24 \quad (5.23)$$

$$n_{CT} = \frac{\Delta t_{OFF}}{\Delta t_{ON}} + 1 \quad (5.24)$$

5.6.4. Simulation Data Flow Diagram

A Matlab code is created to simulate the cooling systems. The simulation can be separated into two sections as showed in figure 5.18: (a) The heating power supply section where the solar collector, the boiler and the hot tank supply heat to the chiller. (b) the cooling process section where the absorption chiller, the cooling tower and eventually the cold tank handle the building load.

In the (b) side, building cooling load power data is sent to the cold tank if it is existing (1) or directly to the chiller if it is not existing (1.1). Cold tank water is used first, and then if it is not enough, the chiller completes the remaining load. From that point, the evaporator fluid stream temperature and flow rate are known by using the chiller characteristics equations. The cooling water inlet temperature is read from the cooling tower sump (2). From the outlet of the absorber-condenser, the wet bulb temperature is used to update cooling water temperature (2). In the case hot cooling water is stored; the cooling process is just spread over an entire 24h. From point (2) cooling water fluid stream data are known by using chiller equations. With absorption chiller equations , the generator hot fluid stream data are calculated (3).

Now heat source (8) has to satisfy the heat requested at point (3). In the (a) side, DNI and ambient temperature together (4) with the collector second order efficiency curve are used to calculate the useful heat harvested from the sun (5). Heat is stored totally in the hot tank or sent to the boiler if the chiller is in operation (6). The boiler checks if the received heat (6) match with the chiller requested heat (3). If yes, heat at (8) is output, otherwise, fossil fuel heat (7) is used to supplement the missing heat before the heat

power is output at (8). Now all data at different points of the system are known. The parameters of interest are processed to output the simulation results.

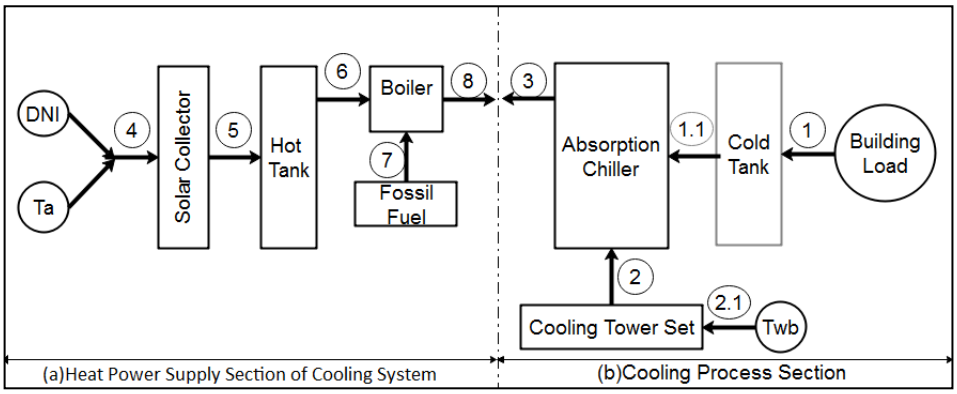

Figure 5.18. Simulation Data Flow Diagram

CHAPTER 6

RESULTS AND DISCUSSION

6.1. Case A (Chiller & Boreholes)

6.1.1. Temperatures

In figure 6.1, the generator temperature profile T_g for model 1 and model 2 are similar. For model 3, T_{g3} is greater than T_{g1} and T_{g2} by approximately 10°C in summer. In winter, the temperature difference between T_{g3} and T_{g1}/T_{g2} reach 70°C. For the storage tanks temperatures T_{st}, there is a noticeable difference for both systems in summer, while in winter, only T_{st3} is completely different from T_{st1} and T_{st2}. The generator temperature being a function of the cooling load of the chiller, the addition of a second hot storage tank for model 2 doesn't affect the heat source side, which in result didn't change T_{g2} compare to T_{g1}. For model 1 and model 2 cooling water temperature is around 25°C. When boreholes are added in model 3, the cooling water outlet is set to 36°C in order to enhance heat storage in the ground. This however increases the generator temperature as observed in figure 6.1 by increasing the characteristic temperature function ΔΔT of the chiller. In winter the net high generator temperature T_{g3} is due to the operation of the chiller as a heat pump for the building.

In winter, for model 1 and model 2 the heat source is operated at low temperature by providing a direct heating to the building. In this case, the second tank doesn't give any temperature lift for the hot tank. However, in summer T_{st2} is on average 8°C greater than T_{st1}. From these observations, it can be deduced that double hot storage tanks effectively increase hot water temperature if the heat source is operating at a higher temperature (134°C-142°C in our case). For domestic hot water application for example, double tanks is not necessary as the system temperature is typically below 100°C. In summer, T_{s3} is on average 23°C greater than T_{s1}. This means that higher cooling water temperature with double hot storage tanks togheter contributed to rise the storage tank temperature.

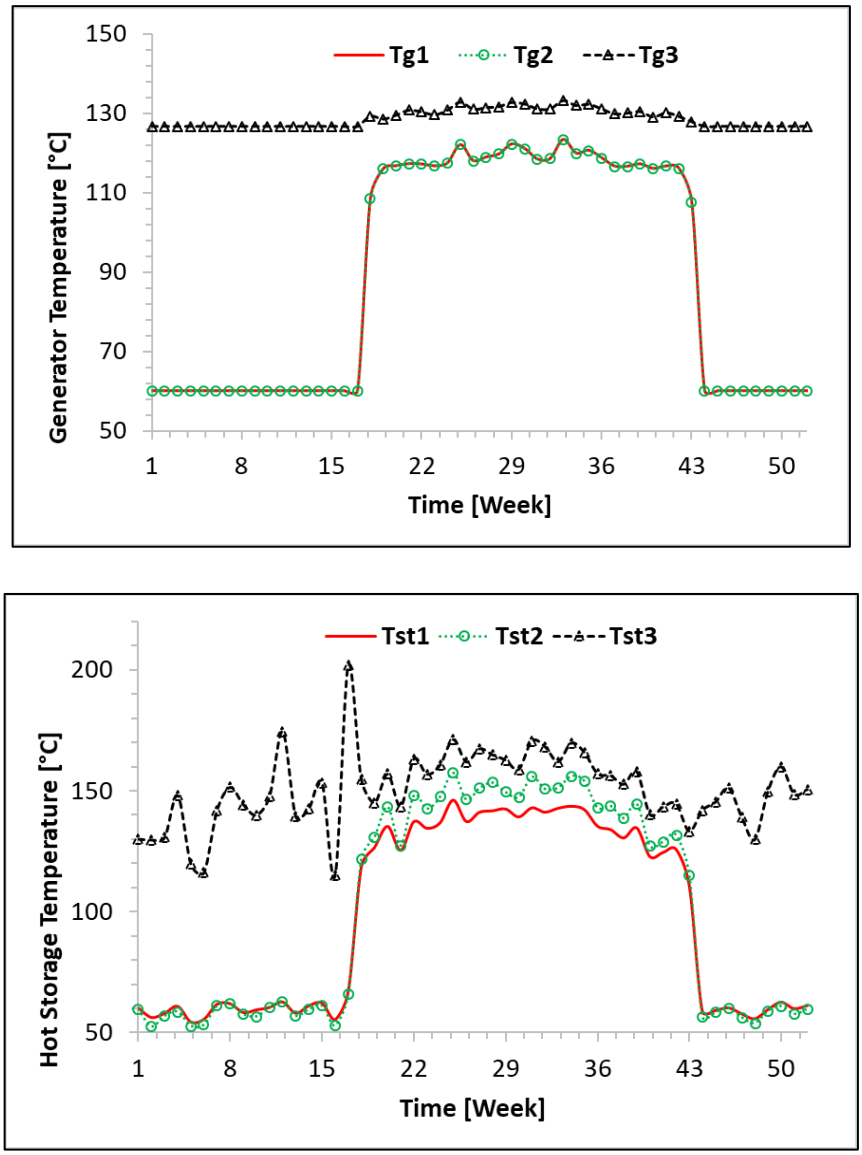

Figure 6.1. Generator & Hot Storage Tank Temperatures

6.1.2. Heat Power

The solar heat Q_s effectively used to provide cooling/heating, the boiler heat Q_b, and tanks heat loss Q_{loss} are shown in figure 6.2. Solar heat profiles Q_{s1}, Q_{s2} are similar with an average magnitude of 212 kW in summer and 137 kW in winter. For the summer, Q_{s3} is nearly equal to Q_{s1} and Q_{s2}. However, in winter Q_{s3} drops to an average of 90 kW. The chiller operation in winter is the main reason for the reduction of the amount of solar heat harvested. In fact, in winter the collector is operating at around 50°C for model 1 and model 2 and at around 134°C for model 3. A collector efficiency reduction for model 3 is thus expected in winter.

The boiler heat is the complement of the solar heat. When one is getting high, the other is decreasing and vice versa. For model 1 and model 2, the boiler average heat power is 249 kW and 159 kW for winter and summer respectively. This result was expected since solar radiation is less in winter compared to summer, what increases the demand from the boiler. However, for model 3, the boiler heat is remarkably low at an average of 79 kW in winter versus 249 kW for model 1 and model 2. The chiller operation as a heat pump reduces significantly the heat power needed. It should be noted that boreholes made possible the usage of the chiller as a heat pump in winter. Since ambient temperature is mostly less than 15°C in winter and the evaporator temperature being in the range of 7°C-14°C, an air source heat pump will work poorly or even malfunction in such weather condition.

The heat loss profiles show that model 2 has a greater loss compared to model 1. Since heat loss is proportional to the tanks temperature and surface area, it can be deduced that the addition of the second tank to model 2 is the driver of the heat loss. Model 3 heat loss is greater than that of model 2 which implies that the storage tank is not the only responsible of the heat loss. In fact, the borehole operation increases the generator temperature which in turn increases the tank temperature that favors the heat loss.

6.1.3. Borehole Thermal Energy Storage

The borehole specific heat injected/extracted is shown in figure 6.3. For heat extraction in winter, it starts at approximately 10 W/m then slightly reduces as the time progress. For heat injection, it starts from 22W/m and it is also slightly decreasing over time. The nearly constant ground heat load has been fixed in the code by switching off the borehole fluid flow when an abrupt heat injection/extraction would have occurred through an uncontrolled fluid flow. With this operation scheme, a long-term thermal imbalance of the ground is avoided. For the first year, the borehole efficiency is 37% which mean that 63% of the injected heat has been dissipated in the ground. However, this heat may still contribute as a heat source in the future if multi years simulation was done. In the literature, borehole thermal energy storage efficiency varies from 20% up to 80% as mentioned previously.

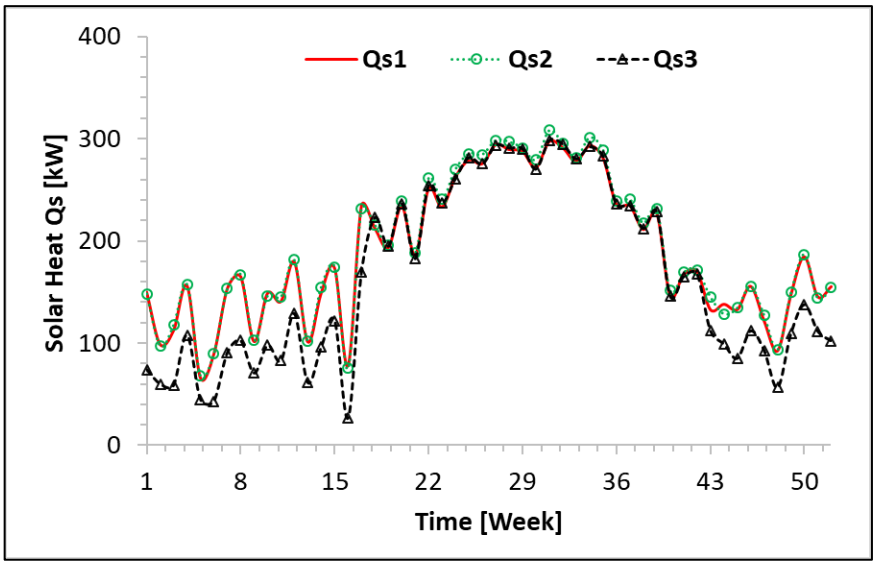

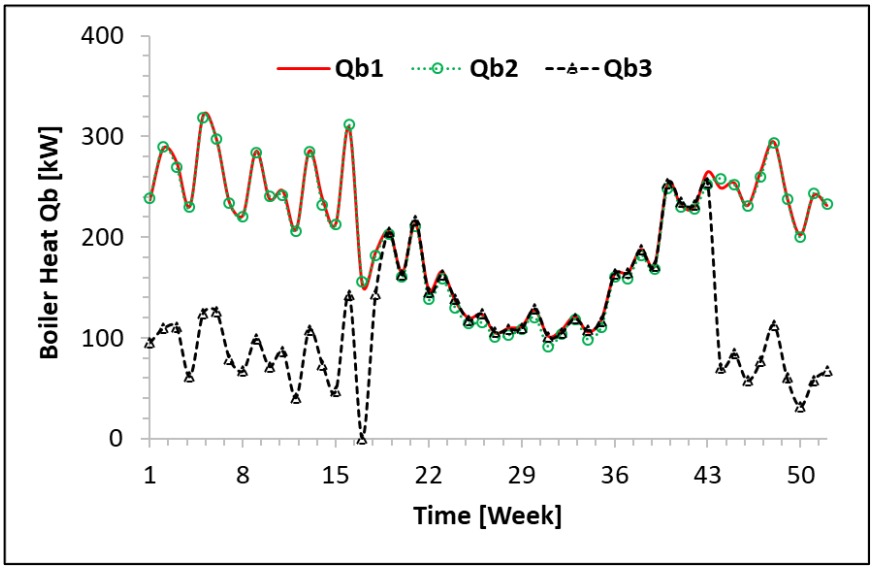

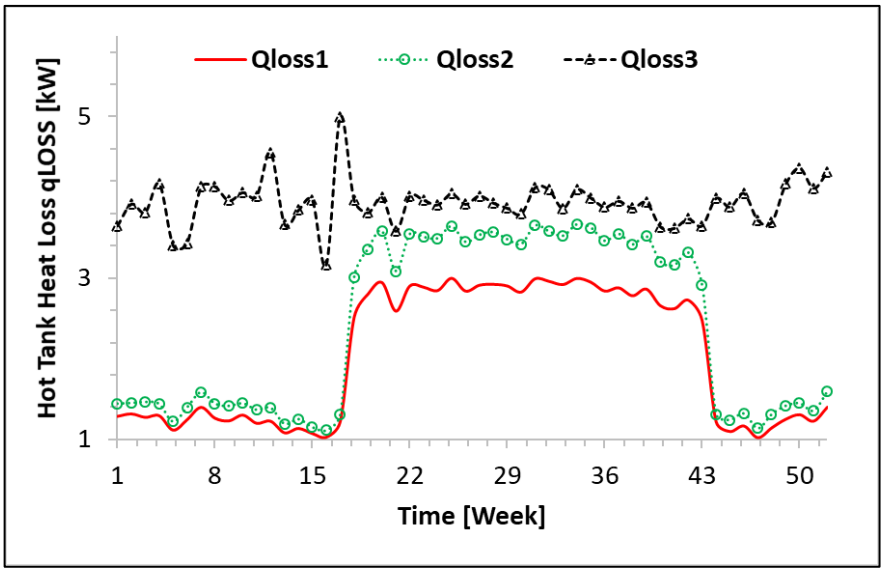

Figure 6.2. Heat Power Profiles (Solar, Boiler, Heat Loss)

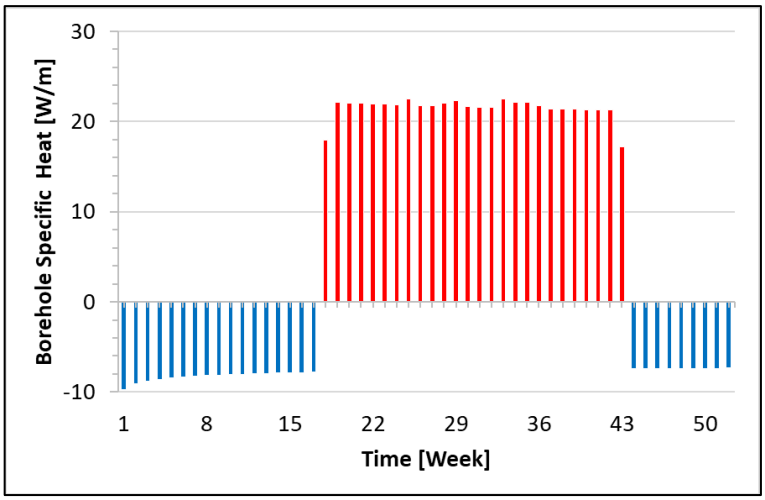

Figure 6.3. Borehole Specific Heat Load

6.1.4. Performance Indicators

The collector efficiency Efc, the solar fraction sf and the system performance ratio spr profiles are shown in figure 6.4. A summary of the seasonal performance is shown in figure 6.5. The collector efficiency is nearly the same for all models in summer. In winter, model 3 collector efficiency drops by 15% compared to the other two models. As stated previously, the chiller operation in winter is the cause of the efficiency drops since higher heat source temperature is needed to power the heat pump.
The solar fraction of both models is nearly the same for the summer. However, in winter, model 3 solar fraction increases by at least 40% compared to the other two models. In fact, the heat stored in summer in the boreholes is used in winter as a hidden solar heat, boosting the solar fraction significantly.
The system performance ratios show an exceptionally high value of 1.75 in winter for model 3 versus 0.83, 0.84 for model 1 and model 2. As with the solar fraction, the borehole is the reason of this good performance. In summer all three models have the same spr. The tank addition thus affects the temperature profiles and not the overall system performance.

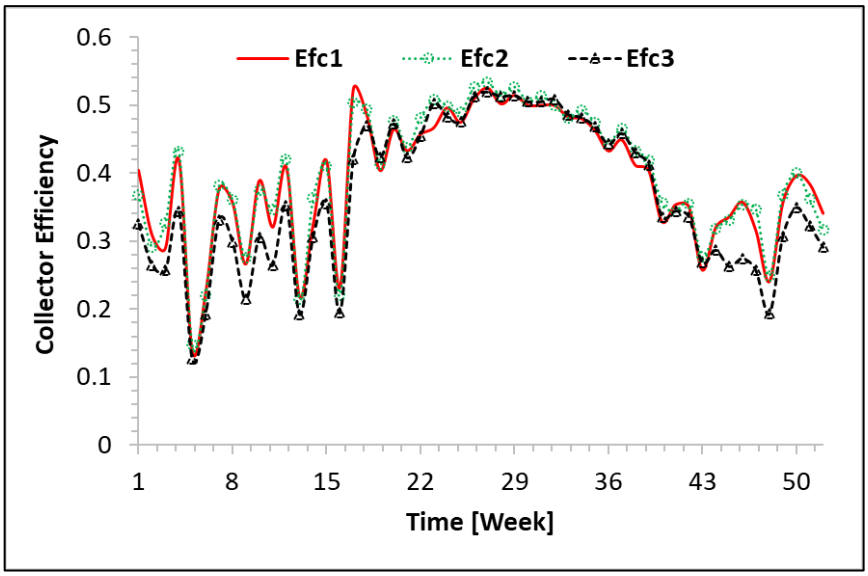

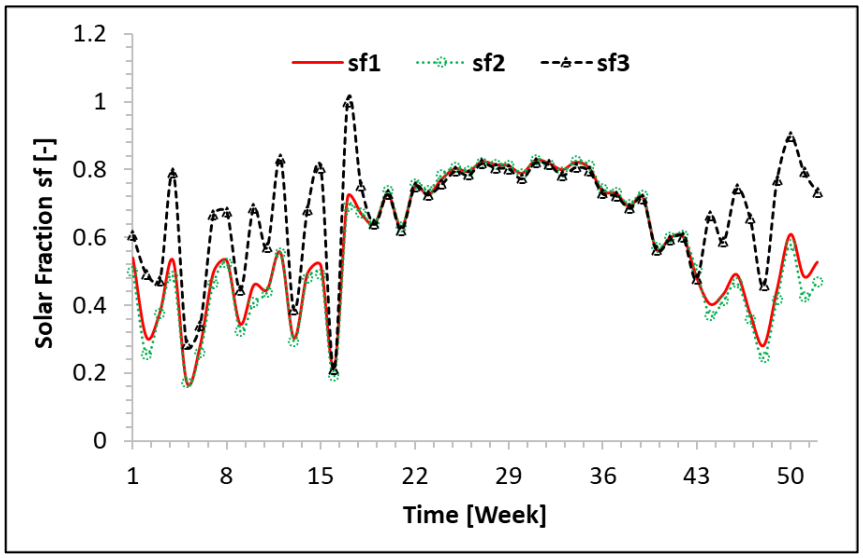

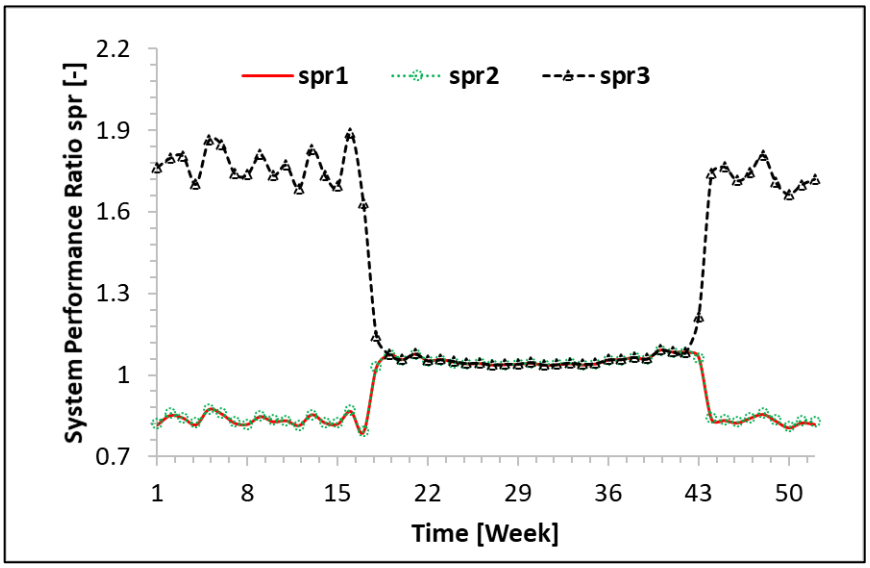

Figure 6.4. Performance Indicators (PTC efficiency, Solar Fraction, System Performance Ratio)

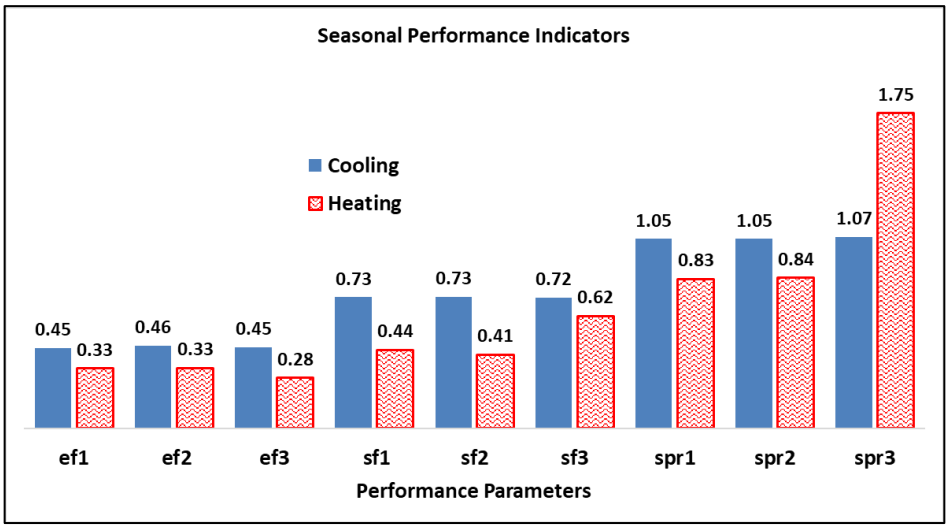

Figure 6.5. Seasonal Performance Indicators

6.2. Case B (Night Cooling of Water)

6.2.1. Storage Volume Minimization

In figure 6.6 is plotted the variation of the total storage capacity along with the size of the single tank when the volume reduction strategy described for model 3 is applied. When only two tanks of the volume V_i are used as in model 2, the total required storage capacity resumes to $2V_i$. The control scheme suggested to reduce the storage capacity increases it to $3V_i$ when only 3 tanks are used. This happens because of the change in an operation mode; two empty tanks being added. Effective volume reduction is obtained by using at least 5 tanks. With 5 tanks, the capacity becomes $1.67V_i$ against $2V_i$ in model 2. As the number of tanks increases further, storage capacity is getting reduced toward V_i which is the theoretical minimum capacity. However, splitting water into more tanks reduces drastically the size of the single tank which may become impractical to use. At 12 tanks the single tank size is only 10% of V_i. Given the mass flow rate in this study, this represents 12 tanks of 1.067m^3 each.

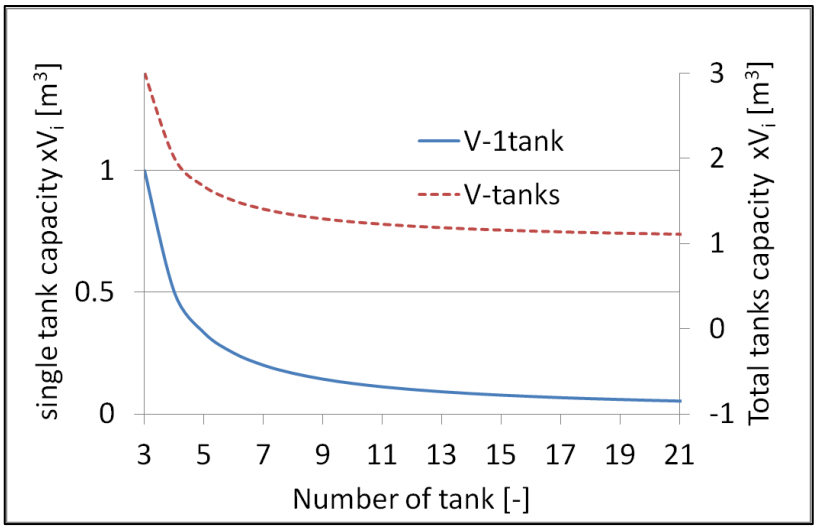

Figure 6.6.Tanks Number vs. Total Storage Capacity

6.2.2. Thermal Response

Figure 6.7 shows the cooling efficiencies of the three systems under study. The cooling efficiencies of model 2 and model 3 are approximately 36% higher than that of the regular system. In both model 2 and model 3, the water mass flow rate is reduced to 1/3 and air mass flow rate is reduced to 0.69. That is, the ratio $\dot{m}_{water}/\dot{m}_{air}$ is reduced to 0.47 of its reference value. Reducing $\dot{m}_{water}/\dot{m}_{air}$ ratio in turn increases the NTU of the CT which increases the cooling efficiency as observed in figure 6.7. Physically, the higher relative air velocity in model 2 and model 3 removes faster the humid air at the water-air interface, creating a higher potential for mass transfer by evaporation.

Figure 6.8 shows the heat rejection per unit fan power of the systems. The heat rejected per unit fan input power for model 2 and model 3 is greater than that of the regular Model. During the off time more heat is rejected per unit fan power. In fact, the wet bulb temperature is lower during the off time as shown in the weather data, which allows more heat rejection.

The cooling efficiencies curves for model 2 and model 3 being flat in the off time while wet bulb temperature is lower means that the CTs outlets temperatures must be lower as well. In table 6.1 below, it can be seen that in fact, both models 2,3 have a condenser inlet water temperature around 20% lower than that of the regular system. Still, from the weather data, the low night ambient temperature contributes to the lower CT outlet

temperature since water temperature is lowered by the action of both latent heat loss and sensible heat loss.

Model 2 and Model 3 give nearly the same average results which means that using multiple tanks only reduce the total storage volume. Using more tanks gives less uniform curves since each tank has a distinct discrete temperature profile.

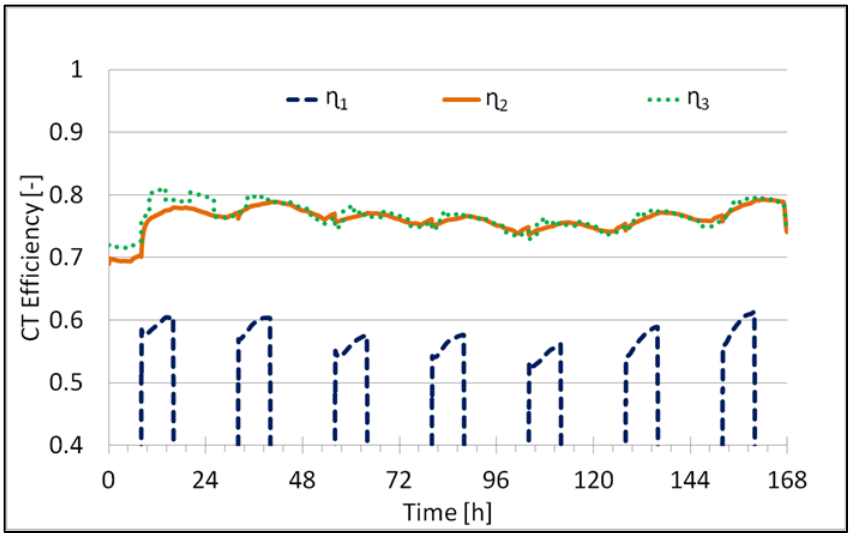

Figure 6.7. Cooling Tower Cooling Efficiency

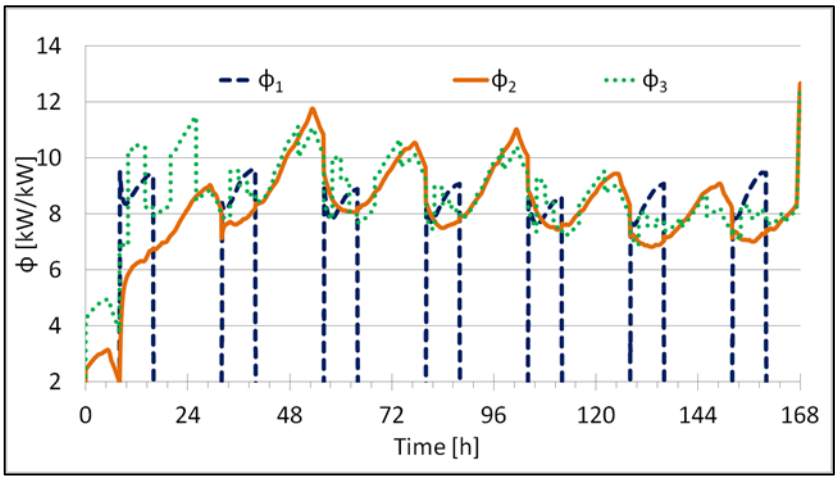

Figure 6.8. Ratio of Heat Rejection to Fan Power

Table 6.1. Condenser Inlet Temperature and Fan Power

	Regular	Model 2	Model 3
Condenser inlet Twi. [°C]	26.9	21.03	21.6
T decrease [%]	-	21.82	19.70
Fan power [kW]	3	1	1
Fan power decrease [%]	-	67.16	67.16

6.2.3. Water Loss and Fan Power

Figure 6.9 shows there is no significant difference in water loss for all 3 models. The average water losses are 1.64%, 1.66% and 1.74% for the regular system, model 1 and model 2 respectively. However, a small amount of water loss has a significant effect on temperature drop since the loss is accompanied by latent heat removal. In general, water loss is ramping up as heat input to the condenser is increased. This result is in net agreement with the result found by Naik et al. [82] in their study on CT performance assessment. As the temperature increases, so does the partial pressure of water, making water molecules at the water-air interface to be knocked off easily by the air stream. Also from the weather data, the lowest relative humidity coincides with the peak ambient temperature which gives the dry air more water absorption potential. For model 2 and model 3, fan power has been reduced by 67% as stated in table 6.1. This result was expected since fan power drops from 3 kW to 1 kW when air velocity is reduced from 100% to 69% according to fan law.

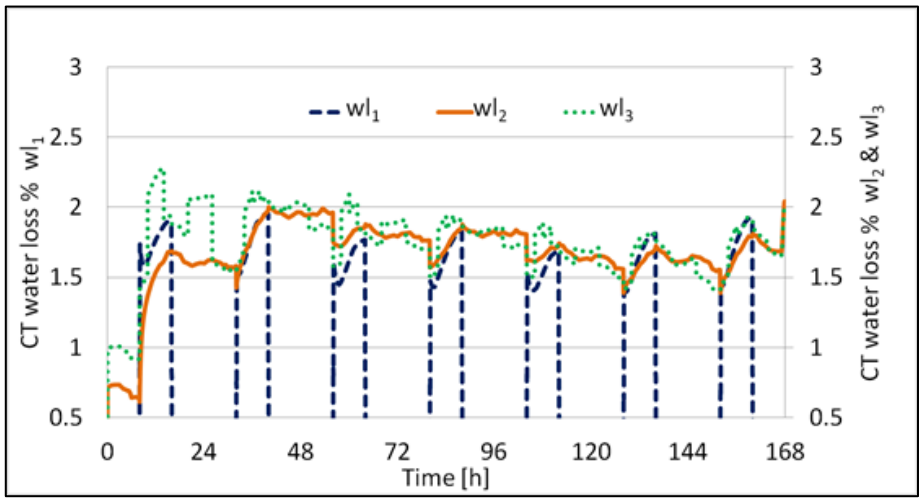

Figure 6.9. Water Loss Rate Percentage

6.3. Case C (Chiller & Chilled Water Storage)

6.3.1. Temperatures

From the temperatures curves in figures 6.10, it appears that the generator temperatures T_g, and the hot storage tanks temperatures T_{st} are lower for Model S_3, followed by Model S_2 then Model S_1. Also, temperatures are at their highest values in

the middle of the cooling season where solar DNI value is the highest. Since S_2 used a cold storage tank to level the cooling load, the heating demand is also leveled, which prevents the temperature from going high at the generator side. S_3 in addition to cold storage tank also used cooling water tanks to further reduce indirectly the generator temperature, by reducing the absorber/condenser temperature. This explains why S_3 has the lowest generator temperature. S_1 and S_2 have closer temperatures profiles which means that the factor that can lower significantly the generator temperature is the cooling water temperature and not the load leveling action using cold tanks. Model S_3 tank temperature dropped by 15°C in average. However, for storage tank temperatures, Model S_1 and Model S_2 are identical while Model S_3 gives a lower temperature. Lower cooling water temperature is what mades Model S_3 gets the lowest hot tank temperature.

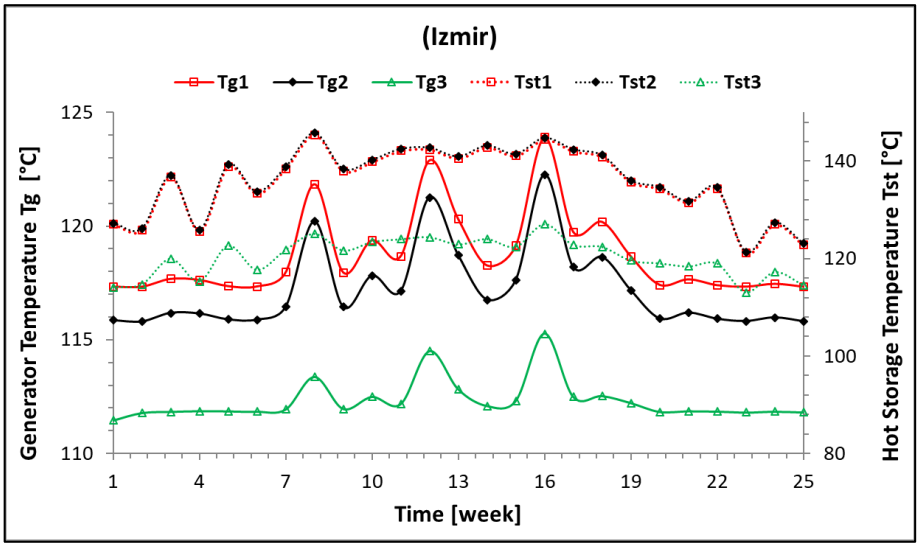

Figure 6.10. Temperature Results

6.3.2. Thermal Power

Solar heat profile Q_s and boiler heat profile Q_b closely follow each other for both systems as it can be seen in figure 6.11. Solar heat in average is 245 kW. For boiler heat, this value is 160 kW. The addition of storage tanks to the proposed systems has a negligible effect on the amount of harvested solar energy. However, when it comes to heat loss Q_{loss}, the reference system S_1 offers the least heat loss compared to the proposed systems as shown in figure 6.12. On average, the losses increase by 57%. This is mainly due to the heat gain of the cold storages; ambient conditions contributing to

set the magnitude of the losses. The higher the ambient-tanks temperature differences, the higher the heat losses.

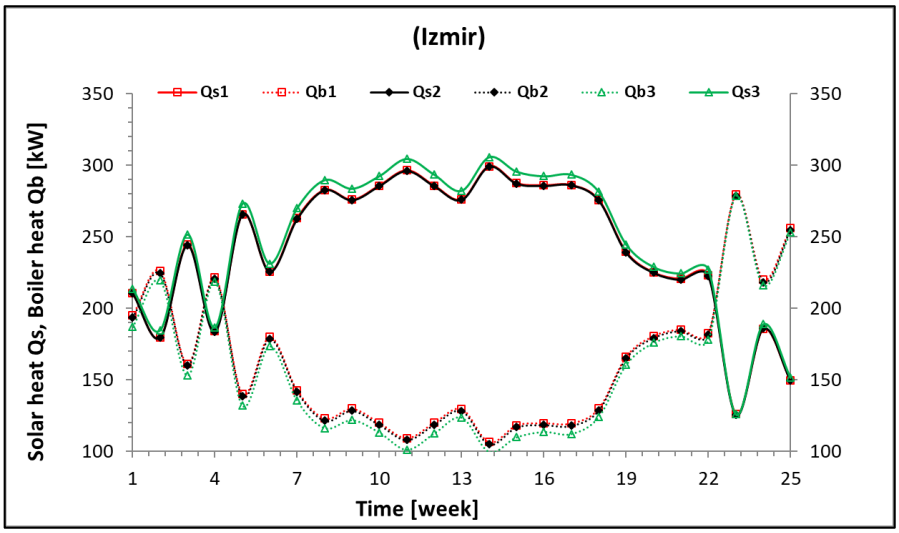

Figure 6.11. Heat Power Results (Solar & Boiler)

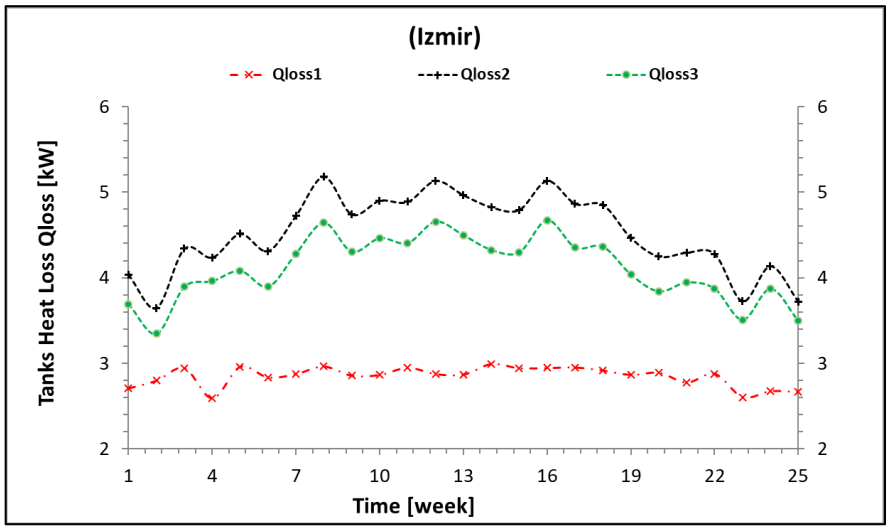

Figure 6.12. Heat Power Results (Heat loss)

6.3.3. Performance Indicators

The collector efficiency, the solar fraction and the system performance ratio shown in figure 6.13 demonstrate that regardless of system modification, the performances are negligibly affected. The average collector efficiencies shown in figure 6.14 is 44%. This result is due to the low value (0.0013) of the second order efficiency curve coefficient which reduces significantly the receiver heat loss. If a flat plate collector which has a higher second order coefficient in its efficiency curve function

was used instead, a much lower efficiency would have been observed. The solar fractions differences are less than 14%. For systems performance ratio which is defined as the "COP" of the systems, the values remained almost the same despite the modifications. This is one of the most significant results as it confirms that in terms of thermal performane, the positive effects and negative effects of adding tanks to the reference system almost cancel each other.

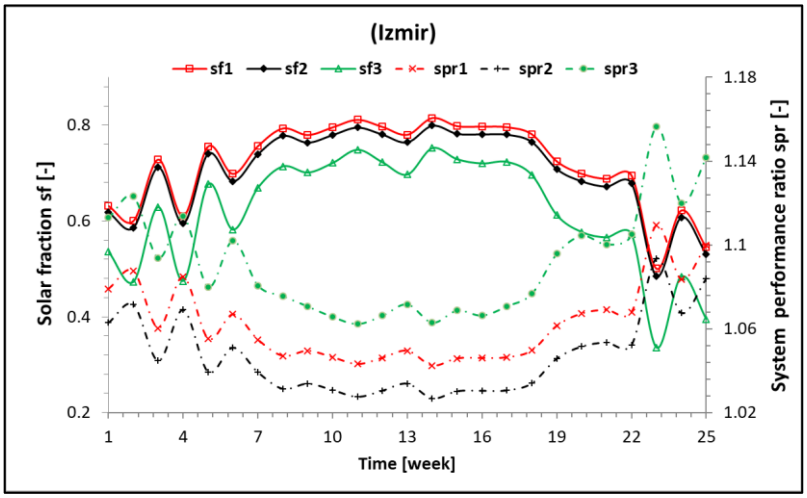

Figure 6.13. Performance Indicators

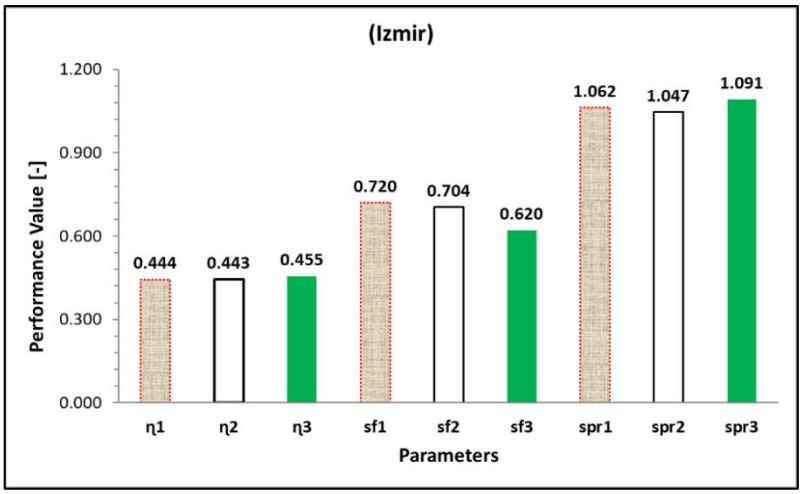

Figure 6.14. Seasonal Performance Indicators

6.3.4. System Sizing Optimization

From the results that have been already mentioned, it appears that all systems achieved nearly the same system performance ratio and solar fraction so system S_2 which has the least modification (least cost) is used for further optimization study. In figure 6.15 and figure 6.16, the operation hour per day of the chiller is varied from

10h/24h to 24h/24h, to study how cold storage size, heat loss, chiller peak power, and its capacity factor are affected. For all operation duration of the chiller, the building load remains the same 14h/day, from 9:00 to 23:00. From 10h/day (9:00-19:00), the operation time is incremented by 2h until midnight; it is extended backward from 9 am to midnight until a full 24h/24h is reached.

It can be deduced from figure 6.15 that the cold storage tank volume is minimum for 14h operation. As the load ON time (14h) is the same with the chiller ON time, there is no need to store chilled water to serve during the OFF time. As chiller ON time is shifted more or less relative to the load time, there is a need to store chilled water for later use which results in increasing storage volume.

In figure 6.15, the cold tank heat gain increases from 10h/day operation time to 12h/day decreases from 12h/day to 14h/day, then increases again from 14h/day to 24h/day. Heat gain is proportional to storage tank size and water storage duration. In the first section of the curve, the effect of tank volume decreases while that of storage duration increases. As heat gain increases it means storage duration is the dominating factor in shaping heat loss profile. In the second section, tank size reduction is the dominating factor. In the last section, both factors are causing heat loss to increase.

For the hot tank, shorter chiller ON time leads to greater heat loss due to higher operating temperature. When operation time is extended, hot water doesn't remain in the hot tank for a long time which reduces heat loss. The total normalized heat loss is highest for shorter operation time, and then slightly increases for longer operation time.

The most significant output of the study is that the required peak power of the chiller decreases almost linearly from 79% at 10h/day to 34% at 24h/day as shown in figure 6.16. The slight nonlinearity is due to the need of the chiller to support the extra heat loss caused by chilled water storage tanks. The capacity factor of the chiller increased from 41% to 96% when ON time goes from 10h to 24h. This result was expected as it is a direct consequence of peak power reduction. Despite the compensation of heat loss caused by storage tanks, Model S_2 solar fraction remained almost equal to that of the reference system, the drops being less than 4%. However, its optimized capacity factor is far better than that of the reference system.

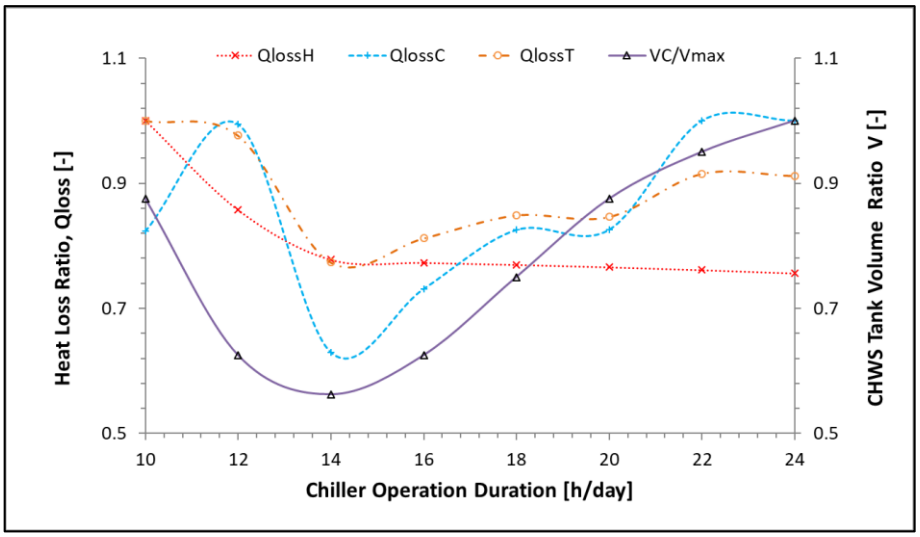

Figure 6.15. Model S_2 System Optimization (Tank Volume & Heat Loss).

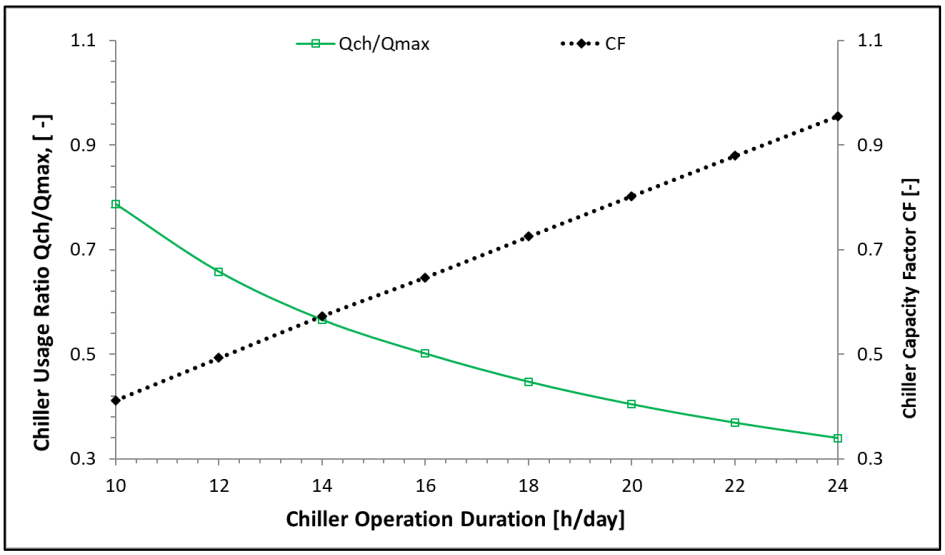

Figure 6.16. Model S_2 System Optimization (Chiller Size & Capacity Factor)

6.4. Economic Considerations

The Case A model 3 showed the best technical performance. However, due to the high cost of borehole energy storage, it is not worth considering economically. Also, the addition of hot tank to the system increased the temperature but did not improve significantly the thermal performance. For this reason, the reference model of case A or Case C model 1 is retained as the best solution for heating.

Case C model 3 showed the best system performance ratio for cooling. However, model 2 with only chilled water tanks showed a performance ratio only 4.4% less than model 3.

Due to the lower cost of Case C model 2, it is retained as the best configuration for cooling.

6.4.1. Time Value of Things

Our daily possessions such as money, real estate, car, have value which increases or decreases as a function of time. For things that depreciate such as a car, it is easy to understand why their value starts to decrease from the newly purchase date. For money however, it is not straightforward to figure out why its value decreases without using less common economic terms such as inflation. People experience that the cost of living is increasing daily because the same rent they use to pay for an amount "x" 10 years ago became expensive by 5% to 100% or even more today. The factor that increased the price is the inflation or price escalation "e" to keep it simple. The future value FV of the rent can be written in terms of the present value as and the price escalation e:

$$FV = PV(1 + e)^n \tag{6.1}$$

where $FV[\$]$ is the future value, $PV[\$]$ the present value, $e[\%]$ the price escalation or inflation rate, $n[years]$ the number of years in the future. Equation 6.1 can be used to calculate the present value of a future value. As inflation is often positive, it tells us that 1000$ now will be worth less next years.

6.4.2 Levelized Cost of Energy

In order to compare two investments that may have different future values, that are done in different markets with different inflations, or that have different life cycles "n" years, the expenditure and the cash generated by the investments in the future are all converted to their present value and added up to calculate the net present values of the projects. In this case, the escalation e is called the discount rate "d". It is a variable that depends on the investor profit generation capability. If an investor expects to have 100% profit in a year with her/his current investment, he/she will not be willing to deposit it at a bank for 3-7% interest rate tor even lend that fund for a 50% interest rate to another person. In this case her discount rate is 100%. For a person that has a reserve fund in a bank at 3% interest rate, he or she will be willing to move the fund at another

bank that offers 6% interest rate; that is, her discount rate is just 3%. The discount rate can also be seen as the weighted average cost of capital WACC, or simply the borrowing cost. If a bank or a lender imposes a WACC of 10% to finance a project, the profit of the project must be at least 10% otherwise it is not viable. Generally, WACC is taken as 8% for rich countries and 10% for poor countries although this number can vary greatly depending on the country, the nature of the project, the loan payment time and so on. The riskier a project is the higher the WACC will be.

Like money others, quantifiable things such as energy can be discounted from the future to the present to see their real value. The Levelized Cost of Electricity LCOE or the levelized cost of heating LCOH or the levelized cost of cooling LCOC are calculated by taking the ratio of the discounted future expenditures over the discounted future energy. The general equation is

$$LCOX = \frac{\sum_0^n \frac{Expenditure_n}{(1+d)^n}}{\sum_0^n \frac{Energy_n}{(1+d)^n}} \tag{6.2}$$

where $LCOX\left[\frac{\$}{kWh}\right]$ is the leveilzed cost of energy, $n[year]$ the year of the expenditure done or energy used, $d[\%]$ the discount rate or the WACC of the project. For a cooling system project, the expenditures are the initial capital expenditures (CAPEX) and the yearly operation cost (OPEX) which includes the fuel cost and the maintenance cost.

$$LCOCH = \frac{I_0 + \sum_1^n \frac{F_n + M_n}{(1+d)^n}}{\sum_1^n \frac{CL_n + HL_n}{(1+d)^n}} \tag{6.3}$$

where $LCOCH[\$kWh]$ the levelized cost of cooling/heating, $I_0[\$]$ the initial CAPEX, $F_n[\$]$ the fuel cost at year n, $M_n[\$]$ the maintenance cost at year n, $CL_n/HL_n[kWh]$ cooling/heating load at year n.

The levelized cost of cooling/Heating has been calculated with the CAPEX OPEX assumptions in the table 6.2 below. The fuel cost is based on the local natural gas price [83]. The collector cost is based on a study made by NREL in the USA [84], while the chiller cost is based on numbers published by USA energy information agency [10]. The storage cost is set from a quotation obtained from a private company while the insulation price has been taken from online retail store [85]. The CAPEX of the

proposed system option 2 is 38% less compared to the reference system option1. In terms of OPEX, option 2 costs 14% less than option 1. The cost calculations show that adding chilled water storage to the reference system Case C Model 1, reduces the LCOCH by 29%.

Table 1. Levelized Cost of Cooling/Heating Calculations

Option 1		**Case A Model 1 for Cooling, Case C Model 1 for Heating**		
Option 2		**Case C Model 2 for Cooling, Case C Model 1 for Heating**		
Parameter		**Cooling**		**Heating**
		Case A Model 1	**Case C Model2**	**Case C Model 1**
Building Load	[kWh]	1,468,800	1,468,800	1,073,520
spr	[-]	1.062	1.047	0.83
Heat Energy	[kWh]	1,383,051	1,402,865	1,293,398
sf	[-]	0.72	0.704	0.44
Boiler Heat	[kWh]	387,254	415,248	724,303
Heat cost	[$/kwh]	0.026	0.026	0.026
Heat OPEX	[$/year]	$ 10,023	$ 10,748	$ 18,747
Collector Cost	[$/m2]	250	250	
Collector maintenance cost	[$/m2]	5	5	
Collector size	[m2]	1000	1000	
Collector CAPEX	[$]	250000	250000	
Collector OPEX	[$/year]	5000	5000	
Chiller cost	[$/kW]	572	572	
Chiller maintenance cost	[$/Kw]	11.44	11.44	
chiller size	[kW]	1020	347	
Chiller CAPEX	[$]	583440	198369.6	
Chiller OPEX	[$/year]	11,668.80	3,967.39	
Storage cost	[$/m3]	68	68	
Storage maintenance cost	[$/m3]	2.04	0.68	
Storage volume	[m3]		1008	
Storage CAPEX	[$]		68544	
Storage OPEX	[$]		685	
Total CAPEX	[$]	$ 833,440	$ 516,914	
Total OPEX	[$/year]	$ 45,439	$ 39,147	
Discount rate	[%]	0.08	0.08	
LCOCH	[$/kWh]	0.049	0.034	
LCOCH Change	**[%]**	**-29%**		

6.4.3 Levelized Cost of Energy Sensitivity Analysis

The sensitivity analysis of LCOCH as a function of the discount rate, fuel cost, and chiller cost is summarized in figure 6.17. As the discount rate change from 6% to 12% the LCOCH reduction changed from 28% to 31%. As fuel cost increases from

0.026$/kWh to 0.06$/kWh, the LCOCH reduction goes from 29% to 22%. When the chiller cost drops to 50% of its current price, the LCOCH reduction gets down to 16%. It can be deduced from these results that the chiller cost has the strongest effect on the LCOCH, followed by the fuel cost and the discount rate. This result was expected since the proposed system is built around the idea of reducing the size/cost of the chiller by using much cheaper storage tanks.

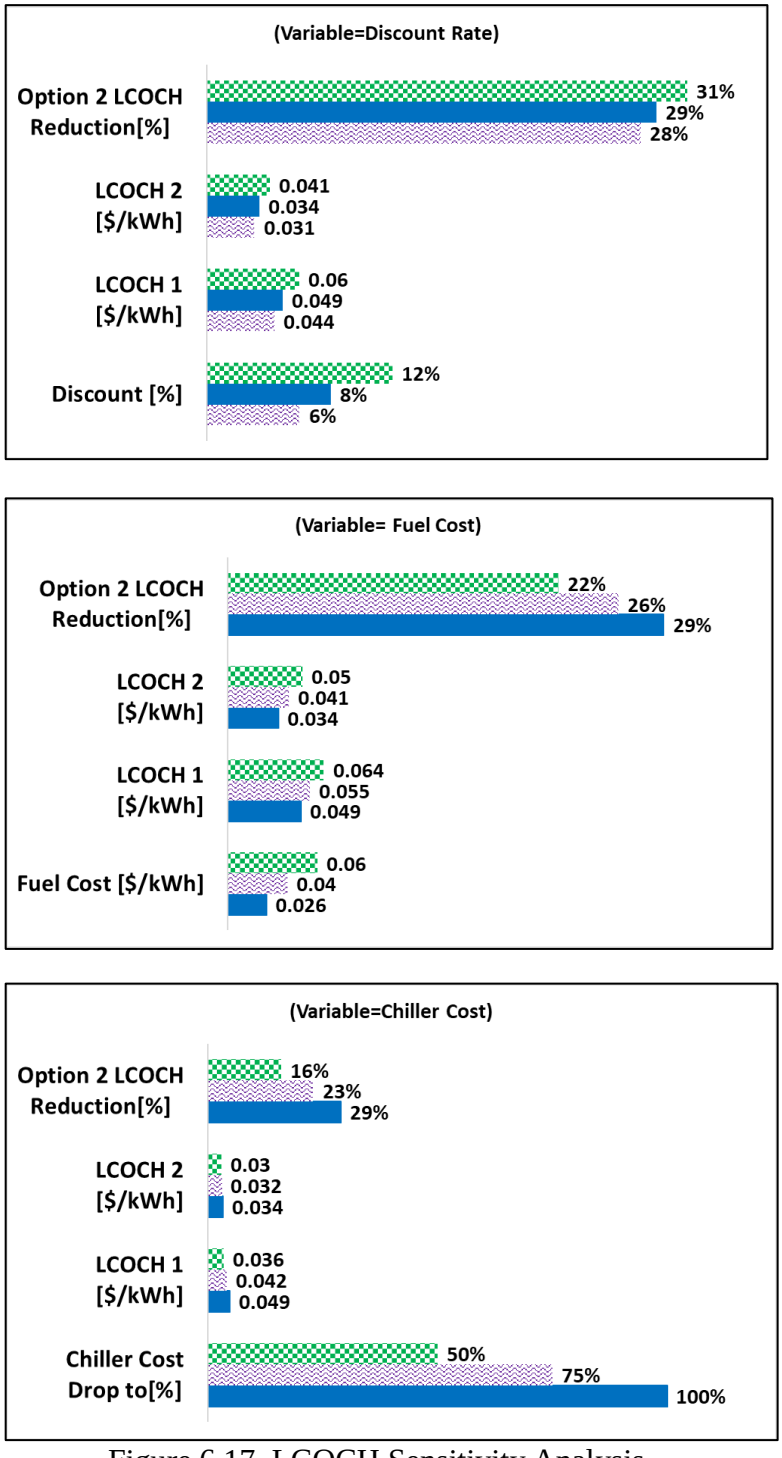

Figure 6.17. LCOCH Sensitivity Analysis

CHAPTER 7

CONCLUSION

CASE A (Chiller & Boreholes)

From the results obtained for case A, it appears that using a double hot tanks increases the storage tanks temperature when the system is operating at over 130°C. For low-temperature operation below 60°C, a second tank does not give significant hot source temperature rise. The system performance ratio which represents the thermal performance of the model remains unaffected by the tank addition. The solar fraction which can be regarded as an economic measure of the fossil fuel expenses is also unaffected by the second tank. Therefore, It can be deduced that a double hot storage tank is not necessary for application where the temperature is less than 200°C or where the heat inlet/outlet temperature difference is not high (10°C-30°C). In concentrated solar power application for example, the turbine inlet may be steam at high-pressure high temperature of 450°C-550°C, while the outlet is low-pressure low temperature less than 100°C. In this case, using two separate tanks to store inlet/outlet fluid is useful in conserving the exergy of solar heat.

The borehole showed a real performance boost capability by increasing the solar fraction up to 40% in winter and the system performance ratio by 110%. This means that the low solar radiation available in winter can be well complemented by including borehole field in the design of the system. Even with a low efficiency of the borehole (37%), the heat that would have been discharged in the atmosphere is converted to useful energy for winter use. If solar heat was directly used to charge the borehole, the low efficiency would have been an unfavorable factor. Also, the cost of the borehole should be taken into account to determine whether it is beneficial to include it in the system or simply increase the size of the collector field.

CASE B (Night Cooling of Water)

The cooling performance of a regular cooling tower that switches ON/OFF simultaneously with a condenser has been compared with that of a LCF cooling system.

From the two tanks operation, the required storage volume can be reduced up to 50% by using multiple smaller tanks and a control mechanism that alternately fills/drains tanks. As the number of tank increases, they become smaller and may represent handling or economical drawbacks. For 12 tanks, storage capacity becomes 40% lower than the initial 2 tanks model. This can be a good arbitrary cut off number for the flow rate in this study if practical implementation is sought. The number of tanks appears not to have an impact on the thermal response of the system.

The most significant outcome of the case B study is the reduction of condenser inlet temperature by 5°C or 20%. For a heat driven engine, this translates into a system overall efficiency improvement as the heat source and the heat sink temperature gap gets wider. Therefore, using low night temperature is an efficient way to boost the performance of thermal devices. This is done at no penalty of water loss which is nearly the same for both systems. Both sensible heat and latent heat can be removed from the water at night while only latent heat can be significantly removed on daytime because of the high ambient temperature. From the power side, delayed cooling has the advantage of running at 33% of the regular CT fan power. For a big cooling tower, this can represent a saving in power demand charge. From an energy point of view, there is no saving since fans in Model 2 and Model 3 are running 24h. However, fan in the proposed models can be replaced by a smaller one to save money and improve electrical performance.

The disadvantage of delayed cooling is the requirement for storage tanks. The working principle can be used for others applications where storage is freely available or where the condenser heat has value for evening usage. Cogeneration system which outputs cool water for the condenser and thermal energy for domestic hot water production can fit such application. In overall, the suggested system is positive as it effectively reduces the condenser working temperature and fan power at once while keeping water loss negligible.

CASE C (Chiller & Chilled Water Storage)

The study revealed that the overall performance of the cooling system including solar fraction, system performance ratio, remain nearly unchanged when storage tanks are added to level the load or to better cool the condenser. From this result, it is concluded that system S_2 which has the least modification is the most valuable

economically. The peak power of the chiller is reduced to 34% of its current value, driving up the capacity factor from 41% to 95%. This is an enormous saving in the chiller cost since absorption chiller is 3 times more expensive than electric chiller. Also, with a much smaller chiller, the operation cost including the electricity cost and the maintenance cost will be much reduced. The study showed that renewable energy cooling system's economic performance can be improved by using only storage tanks without affecting badly the thermal performance of the system. In addition to the traditional peak load shifting, baseload can be shifted as well to get the maximum work out of a smaller chiller.

The preliminary economic analysis showed that the levelized cost of cooling/heating is lowered by 29% by using chilled water storage tanks to reduce the size of the chiller. A more detailed economic analysis is recommended to quantify the benefit of the proposed system S2.

Future Works

As renewable energy share in the energy mix continue to increase, grid instability issues will become more and more important. To alleviate the problems, storage systems including batteries, thermal storage tanks, and demand-side management prooved to be handful for the future. The economy of scale may lead to the development of more efficient solar driven absorption chillers which will open doors for applications such as data centers cooling, greenhouses cooling, districts cooling and so on. An experimental design of a triple or quadruple effects absorption chiller powered by PTC, LFC or heliostats, followed by a deep economic analysis is recommended to explore the future of green cooling.

REFERENCES

[1] Morna, I., and Vuuren, D., 2009, "Modeling Global Residential Sector Energy Demand for Heating and Air Conditioning in the Context of Climate Change," Energy Policy, **37**(2), pp. 507–521.

[2] Cao, X., Dai, X., and Liu, J., 2016, "Building Energy-Consumption Status Worldwide and the State-of-the-Art Technologies for Zero-Energy Buildings during the Past Decade," Energy Build., **128**, pp. 198–213.

[3] Balta, M. T., Dincer, I., and Hepbasli, A., 2010, "Performance and Sustainability Assessment of Energy Options for Building HVAC Applications," Energy Build., **42**(8), pp. 1320–1328.

[4] Cetin, K. S., and Kallus, C., 2016, "Data-Driven Methodology for Energy and Peak Load Reduction of Residential HVAC Systems," Procedia Eng., **145**, pp. 852–859.

[5] Demirbas, A., and Bakhsh, A., 2017, "The Cost Analysis of Electric Power Generation in Saudi Arabia," Energy Sources, Part B Econ. Planning, Policy, **12**.

[6] Cetinay, H., Kuipers, F. A., and Guven, A. N., 2017, "Optimal Siting and Sizing of Wind Farms," Renew. Energy, **101**, pp. 51–58.

[7] U.S. Energy Information Administration, 2018, *Electric Power Monthly with Data for July 2018*.

[8] International Renewable Energy Agency, 2017, *Renewable Power Generation Costs in 2017*.

[9] Sharma, C., Sharma, A. K., Mullick, S. C., and Kandpal, T. C., 2018, "Cost Reduction Potential of Parabolic Trough Based Concentrating Solar Power Plants in India," Energy Sustain. Dev., **42**, pp. 121–128.

[10] U.S. DOE, 2016, *Combined Heat and Power Technology Fact Sheet Series. Reciprocating Engines*.

[11] Oró, E., de Gracia, A., Castell, A., Farid, M. M., and Cabeza, L. F., 2012, "Review on Phase Change Materials (PCMs) for Cold Thermal Energy Storage Applications," Appl. Energy, **99**, pp. 513–533.

[12] Helm, M., and Hagel, K., 2014, "Solar Heating and Cooling System with Absorption Chiller and Latent Heat Storage – A Research Project Summary," Energy Procedia, **48**, pp. 837–849.

[13] University of Illinois, 2011, "Thermal Energy Storage" [Online]. Available: http://www.fs.illinois.edu/docs/default-source/Utilities-Energy/thermal-energy-storage-%28tes%29.pdf?sfvrsn=0. [Accessed: 01-Feb-2018].

[14] Micah J. Somarriba, 2018, “Chilled Water Thermal Energy Storage Tank Overview,” DNTANKS [Online]. Available: https://www.districtenergy.org. [Accessed: 01-Oct-2018].

[15] Allen, K., and Theodor von Backström, 2016, “Rock Bed Thermal Storage: Concepts and Costs.”

[16] Barber, S., 2012, *History of Passive Solar Energy*.

[17] Bureau-International-des-Expositions, 2017, “Expo 1878 Paris: The Revelation of Sun Power” [Online]. Available: https://www.bie-paris.org/site/en/blog/entry/expo-1878-paris-the-revelation-of-sun-power. [Accessed: 20-Aug-2010].

[18] Chung, K.-M., Chen, C.-C., and Chang, K.-C., 2018, “Effect of Diffuse Solar Radiation on the Thermal Performance of Solar Collectors,” Case Stud. Therm. Eng., **12**, pp. 759–764.

[19] Bhowmik, H., and Amin, R., 2017, “Efficiency Improvement of Flat Plate Solar Collector Using Reflector,” Energy Reports, **3**, p. 119.

[20] Mousa, W., and Shomran, A., 2018, “Case Study on Solar Water Heating for Flat Plate Collector,” Case Stud. Therm. Eng., **12**, pp. 666–671.

[21] Chen, Z., and Furbo, S., 2012, “Efficiencies of Flat Plate Solar Collectors at Different Flow Rates,” Energy Procedia, **30**, pp. 65–72.

[22] Morrison, G., and White, S., 2016, “Multi-Effect Absorption Chillers Powered by the Sun: Reality or Reverie,” Energy Procedia, **91**, pp. 844–856.

[23] Rodriguez-Sanchez, D., 2016, “Enhancing Concentration Ratio of Solar Concentrators,” RMIT University.

[24] Bellos, E., and Tsimpoukis, D., 2018, “Optimum Number of Internal Fins in Parabolic Trough Collectors,” Appl. Therm. Eng., **137**, pp. 669–677.

[25] Akbarzadeh, S., and Valipour, M. S., 2018, “Heat Transfer Enhancement in Parabolic Trough Collectors: A Comprehensive Review,” Renew. Sustain. Energy Rev., **92**, pp. 198–218.

[26] Bellos, E., and Tzivanidis, C., 2018, “Thermal Analysis of Parabolic Trough Collector Operating with Mono and Hybrid Nanofluids,” Sustain. Energy Technol. Assessments, **26**, pp. 105–115.

[27] Hafez, A. Z., Attia, A. M., Eltwab, H. S., ElKousy, A. O., Afifi, A. A., AbdElhamid, A. G., AbdElqader, A. N., Fateen, S.-E. K., El-Metwally, K. A., Soliman, A., and Ismail, I. M., 2018, “Design Analysis of Solar Parabolic Trough Thermal Collectors,” Renew. Sustain. Energy Rev., **82**, pp. 1215–1260.

[28] Marc, O., and Sinama, F., 2015, “Dynamic Modeling and Experimental Validation Elements of a 30 KW LiBr/H2O Single Effect Absorption Chiller for Solar Application,” Appl. Therm. Eng., **90**, pp. 980–993.

[29] Ochoa, A. A. V., Dutra, J. C. C., Henríquez, J. R. G., and dos Santos, C. A. C., 2016, “Dynamic Study of a Single Effect Absorption Chiller Using the Pair LiBr/H2O,” Energy Convers. Manag., **108**, pp. 30–42.

[30] Prasartkaew, B., 2013, “Mathematical Modeling of an Absorption Chiller System Energized by a Hybrid Thermal System: Model Validation,” Energy Procedia, **34**, pp. 159–172.

[31] Mansouri, R., Boukholda, I., Bourouis, M., and Bellagi, A., 2015, “Modelling and Testing the Performance of a Commercial Ammonia/Water Absorption Chiller Using Aspen-Plus Platform,” Energy, **93**, pp. 2374–2383.

[32] Zhang, Y., Xu, S., and Xiao, Y., 2016, “Modeling the Dynamic Simulation and Control of a Single Effect LiBr–H2O Absorption Chiller,” Appl. Therm. Eng., **107**, pp. 1183–1191.

[33] U.S.-Department-of-Energy, 2017, “Absorption Chillers for CHP Systems.”

[34] Gomri, R., 2009, “Second Law Comparison of Single Effect and Double Effect Vapour Absorption Refrigeration Systems,” Energy Convers. Manag., **50**(5), pp. 1279–1287.

[35] Avanessian, T., and Ameri, M., 2014, “Energy, Exergy, and Economic Analysis of Single and Double Effect LiBr–H2O Absorption Chillers,” Energy Build., **73**, pp. 26–36.

[36] Winston, R., Jiang, L., and Widyolar, B., 2013, “Performance of a 23KW Solar Thermal Cooling System Employing a Double Effect Absorption Chiller and Thermodynamically Efficient Non-Tracking Concentrators.”

[37] Vasilescu, C., and Ferreira Carlos, 2014, “Solar Driven Double-Effect Absorption Cycles for Sub-Zero Temperatures,” Int. J. Refrig., **39**, pp. 86–94.

[38] Lubis, A., Jeong, J., Saito, K., Giannetti, N., Yabase, H., Idrus Alhamid, M., and Nasruddin, 2016, “Solar-Assisted Single-Double-Effect Absorption Chiller for Use in Asian Tropical Climates,” Renew. Energy, **99**, pp. 825–835.

[39] Sun, H., Xu, Z., Wang, H., and Wang, R., 2015, “A Solar/Gas Fired Absorption System for Cooling and Heating in a Commercial Building,” Energy Procedia, **70**, pp. 518–528.

[40] Mastropietro, J., 2005, “Geothermal Geoexchange Heating & Cooling System.”

[41] Tarnawski, V. R., Leong, W. H., Momose, T., and Hamada, Y., 2009, “Analysis of Ground Source Heat Pumps with Horizontal Ground Heat Exchangers for Northern Japan,” Renew. Energy, **34**(1), pp. 127–134.

[42] Pulat, E., Coskun, S., Unlu, K., and Yamankaradeniz, N., 2009, "Experimental Study of Horizontal Ground Source Heat Pump Performance for Mild Climate in Turkey," Energy, **34**(9), pp. 1284–1295.

[43] Thorshaug Andresen, H., and Li, Y., 2015, "Modelling the Heating of the Green Energy Lab in Shanghai by the Geothermal Heat Pump Combined with the Solar Thermal Energy and Ground Energy Storage," Energy Procedia, **70**, pp. 155–162.

[44] Bär, K., Rühaak, W., Welsch, B., Schulte, D., Homuth, S., and Sass, I., 2015, "Seasonal High Temperature Heat Storage with Medium Deep Borehole Heat Exchangers," Energy Procedia, **76**, pp. 351–360.

[45] Rehman, H. ur, Hirvonen, J., and Sirén, K., 2016, "Design of a Simple Control Strategy for a Community-Size Solar Heating System with a Seasonal Storage," Energy Procedia, **91**, pp. 486–495.

[46] Gao, L., Zhao, J., and Tang, Z., 2015, "A Review on Borehole Seasonal Solar Thermal Energy Storage," Energy Procedia, **70**, pp. 209–218.

[47] Flynn, C., and Sirén, K., 2015, "Influence of Location and Design on the Performance of a Solar District Heating System Equipped with Borehole Seasonal Storage," Renew. Energy, **81**, pp. 377–388.

[48] Wang, E., Fung, A. S., Qi, C., and Leong, W. H., 2012, "Performance Prediction of a Hybrid Solar Ground-Source Heat Pump System," Energy Build., **47**, pp. 600–611.

[49] Lança, M., Coelho, P. J., and Viegas, J., 2019, "Enhancement of Heat Transfer in Office Buildings during Night Cooling − Reduced Scale Experimentation," Build. Environ., **148**, pp. 653–667.

[50] Jiang, L., and Tang, M., 2017, "Thermal Analysis of Extensive Green Roofs Combined with Night Ventilation for Space Cooling," Energy Build., **156**, pp. 238–249.

[51] Ali, H., 2007, "Passive Cooling of Water at Night in Uninsulated Open Tank in Hot Arid Areas," Energy Convers. Manag., **48**(1), pp. 93–100.

[52] Dyreson, A., and Miller, F., 2016, "Night Sky Cooling for Concentrating Solar Power Plants," Appl. Energy, **180**, pp. 276–286.

[53] Rosiek, S., and Batlles Garrido, F. J., 2012, "Performance Evaluation of Solar-Assisted Air-Conditioning System with Chilled Water Storage (CIESOL Building)," Energy Convers. Manag., **55**, pp. 81–92.

[54] Rosiek, S., and Batlles, F. J., 2013, "Reducing a Solar-Assisted Air-Conditioning System's Energy Consumption by Applying Real-Time Occupancy Sensors and Chilled Water Storage Tanks throughout the Summer: A Case Study," Energy Convers. Manag., **76**, pp. 1029–1042.

[55] Lin, H., Li, X., Cheng, P., and Xu, B., 2014, "Study on Chilled Energy Storage of Air-Conditioning System with Energy Saving," Energy Build., **79**, pp. 41–46.

[56] "Pluto and the Solar System | IAU" [Online]. Available: https://www.iau.org/public/themes/pluto/. [Accessed: 29-Jan-2019].

[57] Duffie, J. A., and Beckman, W. A., 1991, *Solar Engineering of Thermal Processes*.

[58] Maria Isabel Roldán Serrano, 2017, *Concentrating Solar Thermal Technologies*.

[59] Goswami, D. Y., 2015, *Principle of Solar Engineering*.

[60] Weiss, W., 2010, *Collectors Suitable for Industrial Applications*.

[61] "Adsorption Chillers Bryair" [Online]. Available: https://www.bryair.com/products-solutions/adsorption-chillers/. [Accessed: 30-Jan-2019].

[62] Melody Baglione, "Building Sustainability into Chillers Control Systems" [Online]. Available: https://engfac.cooper.edu/melody/411. [Accessed: 30-Jan-2019].

[63] B.C. Chung, "Trend and Applications of Absorption Chiller" [Online]. Available: http://www.eurocooling.com/public_html/articleseagroup.htm. [Accessed: 30-Jan-2019].

[64] Herold, K. E., and Klein, S. A., 1995, *Absorption Chillers and Heat Pumps*.

[65] Senseware Company, "Back to Basics: Cooling Towers 101" [Online]. Available: https://blog.senseware.co/2018/02/06/back-basics-cooling-towers-101. [Accessed: 30-Jan-2019].

[66] Kumar, P., 2005, "Cooling Tower," *India Bureau of Energy Efficiency Guide Book, Chap.7*.

[67] Liu, N., Zhang, L., and Jia, X., 2017, "The Effect of the Air Water Ratio on Counter Flow Cooling Tower," Procedia Eng., **205**, pp. 3550–3556.

[68] Khamis Mansour, M., and Hassab, M. A., 2014, "Innovative Correlation for Calculating Thermal Performance of Counterflow Wet-Cooling Tower," Energy, **74**, pp. 855–862.

[69] Yumrutas, R., and Kanoglu, M., 2005, "Computational Model for a Ground Coupled Space Cooling System with an Underground Energy Storage Tank," Energy Build., **37**(4), pp. 353–360.

[70] Canbay, Ç. S., 2003, "Optimization of HVAC Control Strategies By Building Management Systems Case Study: Özdilek Shopping Center."

[71] Weiss, W., and Rommel, M., 2005, “Solar Heat for Industrial Processes,” IEA SHC - TASK 33.

[72] Static Rockwool, 2014, “Rockwool” [Online]. Available: https://static.rockwool.com/globalassets/rockwool-in/downloads/brochures/prorox-product-catalogue-in.pdf. [Accessed: 10-Oct-2018].

[73] TRNSYS, 2006, “Mathematical Reference Volume 5.”

[74] Navarro-Esbrí, J., Molés, F., Peris, B., Barragán-Cervera, Á., Mendoza-Miranda, J. M., Mota-Babiloni, A., and Belman, J. M., 2014, “Shell-and-Tube Evaporator Model Performance with Different Two-Phase Flow Heat Transfer Correlations. Experimental Analysis Using R134a and R1234yf,” Appl. Therm. Eng., **62**(1), pp. 80–89.

[75] Vera-García, F., García-Cascales, J. R., Gonzálvez-Maciá, J., Cabello, R., Llopis, R., Sanchez, D., and Torrella, E., 2010, “A Simplified Model for Shell-and-Tubes Heat Exchangers: Practical Application,” Appl. Therm. Eng., **30**(10), pp. 1231–1241.

[76] Kasumu, A. S., Nassar, N. N., and Mehrotra, A. K., 2017, “A Heat-Transfer Laboratory Experiment with Shell-and-Tube Condenser,” Educ. Chem. Eng., **19**, pp. 38–47.

[77] SPX Company, 2018, “Free Cooling - SPX Cooling Technologies” [Online]. Available: https://spxcooling.com/featured/free-cooling/. [Accessed: 08-Feb-2018].

[78] Fantech Company, 2016, “Fan Laws” [Online]. Available: www.fantech.com.au/images/PDF/Catalogue/fanlaws.pdf. [Accessed: 01-Feb-2018].

[79] Rosiek, S., and Javier, F., 2012, “Performance Evaluation of Solar-Assisted Air-Conditioning System with Chilled Water Storage (CIESOL Building),” Energy Convers. Manag., **55**, pp. 81–92.

[80] Zhua, K., and Campana, E., “Techno-Economic Feasibility of Integrating Energy Storage Systems in Refrigerated Warehouses,” Appl. Energy, **216**, pp. 348–357.

[81] Asadi, I., Shafigh, P., Abu Hassan, Z. F. Bin, and Mahyuddin, N. B., 2018, “Thermal Conductivity of Concrete – A Review,” J. Build. Eng., **20**, pp. 81–93.

[82] Naik, B. K., Choudhary, V., Muthukumar, P., and Somayaji, C., 2017, “Performance Assessment of a Counter Flow Cooling Tower – Unique Approach,” Energy Procedia, **109**, pp. 243–252.

[83] OMV, 2018, “Turkey Natural Gas Price,” 2018 [Online]. Available: http://www.omv.com.tr/portal/01/tr/omv_tr/omv/gas-and-power/natural-gas/tariffs. [Accessed: 12-Jan-2018].

[84] Kurup, P., and Turchi, C. S., 2015, *Parabolic Trough Collector Cost Update for the System Advisor Model (SAM)*.

[85] "Rockwool Thermal Roll 100mm (Twin) X 1200mm X 2750mm" [Online]. Available: http://www.builderdepot.co.uk/rockwool-insulation-td-roll-100mm-twin-x-1200mm-x-2750mm.html. [Accessed: 09-Dec-2018].

APPENDIX A

LEVELIZED COST OF HEATING/COOLING

The financial analysis of the project is summarized in table A1. For 25 years life cycle, the cooling/heating load and their associated net cash flow are listed. The cash flow at year 0 correspond to the amount of investment made.The load energy and the cash flow are discounted then summed up to find the net present value of each parameters. The levelized cost of energy is then calculated by taking the ratio of the dollars amount net present value over the net present value of the cooling/heating load.

Table A1: Project Financial Analysis

			Option 1		Option 2	
SUM		27,138,697		$ 1,318,486		$ 934,800
Year	Cooling/Heating load [kWh]	Discount Load [kWh]	Cash Flow [$]	Discounted Cash Flow [$]	Cash Flow [$]	Discounted Cash Flow [$]
0	-	-	$ 833,440	$ 833,440	$ 516,914	$ 516,914
1	2,542,320	2,354,000	$ 45,439	$ 42,073	$ 39,147	36,247
2	2,542,320	2,179,630	$ 45,439	$ 38,956	$ 39,147	33,562
3	2,542,320	2,018,176	$ 45,439	$ 36,071	$ 39,147	31,076
4	2,542,320	1,868,681	$ 45,439	$ 33,399	$ 39,147	28,774
5	2,542,320	1,730,260	$ 45,439	$ 30,925	$ 39,147	26,643
6	2,542,320	1,602,093	$ 45,439	$ 28,634	$ 39,147	24,669
7	2,542,320	1,483,419	$ 45,439	$ 26,513	$ 39,147	22,842
8	2,542,320	1,373,536	$ 45,439	$ 24,549	$ 39,147	21,150
9	2,542,320	1,271,793	$ 45,439	$ 22,731	$ 39,147	19,583
10	2,542,320	1,177,586	$ 45,439	$ 21,047	$ 39,147	18,133
11	2,542,320	1,090,357	$ 45,439	$ 19,488	$ 39,147	16,790
12	2,542,320	1,009,590	$ 45,439	$ 18,044	$ 39,147	15,546
13	2,542,320	934,806	$ 45,439	$ 16,708	$ 39,147	14,394
14	2,542,320	865,561	$ 45,439	$ 15,470	$ 39,147	13,328
15	2,542,320	801,445	$ 45,439	$ 14,324	$ 39,147	12,341
16	2,542,320	742,079	$ 45,439	$ 13,263	$ 39,147	11,427
17	2,542,320	687,110	$ 45,439	$ 12,281	$ 39,147	10,580
18	2,542,320	636,213	$ 45,439	$ 11,371	$ 39,147	9,797
19	2,542,320	589,086	$ 45,439	$ 10,529	$ 39,147	9,071
20	2,542,320	545,450	$ 45,439	$ 9,749	$ 39,147	8,399
21	2,542,320	505,046	$ 45,439	$ 9,027	$ 39,147	7,777
22	2,542,320	467,636	$ 45,439	$ 8,358	$ 39,147	7,201
23	2,542,320	432,996	$ 45,439	$ 7,739	$ 39,147	6,667
24	2,542,320	400,922	$ 45,439	$ 7,166	$ 39,147	6,173
25	2,542,320	371,224	$ 45,439	$ 6,635	$ 39,147	5,716